

Northumbria Research Link

Citation: Chan, Hsung-Hung (1998) Indoor infrared wireless PPM systems. Doctoral thesis, University of Northumbria.

This version was downloaded from Northumbria Research Link:
<https://nrl.northumbria.ac.uk/id/eprint/15689/>

Northumbria University has developed Northumbria Research Link (NRL) to enable users to access the University's research output. Copyright © and moral rights for items on NRL are retained by the individual author(s) and/or other copyright owners. Single copies of full items can be reproduced, displayed or performed, and given to third parties in any format or medium for personal research or study, educational, or not-for-profit purposes without prior permission or charge, provided the authors, title and full bibliographic details are given, as well as a hyperlink and/or URL to the original metadata page. The content must not be changed in any way. Full items must not be sold commercially in any format or medium without formal permission of the copyright holder. The full policy is available online: <http://nrl.northumbria.ac.uk/policies.html>

Some theses deposited to NRL up to and including 2006 were digitised by the British Library and made available online through the [EThOS e-thesis online service](#). These records were added to NRL to maintain a central record of the University's research theses, as well as still appearing through the British Library's service. For more information about Northumbria University research theses, please visit [University Library Online](#).



**Northumbria
University**
NEWCASTLE



UniversityLibrary



INDOOR INFRARED WIRELESS PPM SYSTEMS

A THESIS SUBMITTED IN PARTIAL FULFILMENT OF THE REQUIREMENTS OF THE
UNIVERSITY OF NORTHUMBRIA FOR THE DEGREE OF DOCTOR OF PHILOSOPHY

BY

Hsun-Hung, Chan
BEng(Hons), MSc, MIEEE, AMIEE

Centre for Communication Systems Research
Optical Communications Research Group
School of Engineering
University of Northumbria
December 1998

Dedicated to my parents

獻 給 我 敬 愛 的 父 母

Abstract

Optical wireless communication systems offer several advantages over their radio frequency counterparts. For example, cost, wavelength re-usability and a large unregulated bandwidth are among the advantages. The limitations of this technique include the optical power safety issue, multipath dispersion and interference from ambient light and background radiation. In this project, pulse position modulation is used for receiver sensitivity improvement, and code division multiple access is exploited to provide multiple access facilities. The limitations of an optical wireless system are studied and methods for performance improvement are suggested.

A theoretical model for multipath dispersion based on multi-reflections is outlined. Multipath dispersion results in intersymbol interference (ISI) which affects the signal transmission through the channel. Results are presented demonstrating that the sensitivity is reduced by 5.3 dB (receiver at middle of the room) and by 3.41 dB (receiver at corners) when multipath dispersion effects are taken into account.

The impact of background noise is measured and analysed based on two room configurations. The results show that the effect is more devastating when the receiver is placed directly under an ambient light source. The results also show that ambient noise affects the sensitivity of the PPM format to the same extent as OOK format (about 5.2 dB under the set of conditions considered). Thus PPM still offers superior performance.

A PIN-BJT receiver has been designed for indoor infrared PPM wireless diffuse systems and its performance has been analysed. The results show that the receiver achieves a low noise current of $2.7 \text{ pA}/\sqrt{\text{Hz}}$. Original results are presented demonstrating that the system can achieve a sensitivity of -50.5 dBm at a bit rate of 10 Mbit/s and an error rate of 10^{-9} . This represents a sensitivity improvement of 9.8 dB over a comparable on-off keying PIN-BJT system.

A new equaliser for indoor optical wireless systems has been designed to reduce the impact of channel multipath dispersion. The results show that the system sensitivity can improve by up to 4.2 dB when a fixed equaliser is used. However large ripples at the end of the received pulse can be introduced when a fixed equaliser is employed. The results also show that when a variable equaliser is used (i.e. filter coefficients can be tuned) the system sensitivity improvement can be maintained while eliminating the large ripples at the end of received pulse. From the results, it can therefore be concluded that an adaptive filter is required for the indoor optical wireless system to improve the system performance.

An original theoretical analysis shows that pulse position modulation code division multiple access (PPM CDMA), can offer 5 times the bit rate achievable using OOK CDMA for the same bandwidth requirements over the range of parameters considered. Results are presented for the maximum number of users that can communicate over

the network at a given bit rate and it is shown that there exist an optimum PPM order, at a given number of users, that maximizes the achievable bit rate. Three different orthogonal code families have been examined and analysed in the context of the indoor infrared communication network. The results have shown that extended prime codes offer the best performance when utilised with PPM CDMA.

Acknowledgements

The work presented in this document has been carried out in the centre for communications systems research at the University of Northumbria at Newcastle. I wishes to sincerely thank my academic supervisors Dr. J.M.H. Elmirghani and Professor R.A. Cryan for their invaluable expertise, guidance and encouragement. I would also wish to thank the Committee of Vice-Chancellors and Principals (CVCP) of the Universities of the United Kingdom for offering an Overseas Research Students (ORS) award.

I would like to thank my parents, my wife and all my family members, to whom I dedicate this achievement, for having the belief and confidence in me.

To all my colleagues in the centre for communications Systems Research I would like to express my appreciation for all their assistance and discussions over the course of my studies. The warm and friendly working environment will certainly be missed. I would like to acknowledge the support of all the staff, technicians and secretaries who have assisted me in any way.

CONTENTS

Abstract	i
Acknowledgements	iii
List of Figures	viii
List of Tables	xii
List of Abbreviations	xiii
Glossary of Symbols	xv
Chapter 1: Introduction	1
1.1 Research objectives	5
1.2 Organisation of the thesis	7
1.3 Original Contributions	9
Chapter 2: Review	12
2.1 Introduction	12
2.2 Wireless infrared link configurations	14
2.3 Optical safety	18
2.4 Impairments	20
2.4.1 Photodiode high capacitance	21
2.4.2 Multipath dispersion	22
2.4.3 Background light	23
2.5 Modulation schemes	24
2.5.1 On Off Keying modulation	25
2.5.2Pulse Position Modulation	26

2.5.3 Subcarrier modulation	27
2.6 Multiple access	28
2.6.1 Time division multiple access	28
2.6.2 Frequency division multiple access	30
2.6.3 Code division multiple access	31
2.6.3 Wavelength division multiple access	33
2.7 Current indoor infrared wireless systems	34
2.8 Summary	38
 Chapter 3: Optical Wireless Channel	 39
3.1 Introduction	39
3.2 Test room set-up	41
3.3 Ambient noise	43
3.4 Multipath dispersion	54
3.5 Summary	62
 Chapter 4: Receiver Design	 63
4.1 Introduction	63
4.2 Performance limitations	65
4.3 Receiver noise analysis	67
4.4 Preamplifier structures	71
4.4.1 Low impedance preamplifier	72
4.4.2 High impedance preamplifier	73
4.4.3 Transimpedance impedance preamplifier	74
4.5 Preamplifier design	76
4.6 Summary	80
 Chapter 5: Optical wireless PPM system	 82
5.1 Introduction	82
5.2 The PPM system	84
5.3 Error sources	86
5.3.1 Erasure errors	87

5.3.2 Wrong slot errors	88
5.3.3 False alarm errors	89
5.4 Sensitivity evaluation	90
5.4.1 Receiver performance analysis	91
5.4.2 Analytic results	95
5.4.2.1 LOS system	96
5.4.2.2 Diffuse system	101
5.5 PPM coder design and experimented results	105
5.6 PPM decoder design	108
5.7 Summary	110
Chapter 6: Equalisation	111
6.1 Introduction	111
6.2 Range of received pulse shapes	113
6.3 Filter design	115
6.4 Sensitivity evaluation	121
6.5 Summary	124
Chapter 7: Optical wireless PPM CDMA system	126
7.1 Introduction	126
7.2 PPM CDMA systems	129
7.3 Orthogonal coding schemes	134
7.3.1 Optical orthogonal codes	136
7.3.2 Prime codes and Extended prime codes	140
7.4 PPM CDMA coder design	149
7.6 Summary	152
Chapter 8 : Conclusions	153
Chapter 9: Future work	157
References	159

Appendices	166
1. Background noise measurement results	166
2. PIN-BJT receiver component values and circuit model	167
3. Receiver noise analysis	172
4. Matched filter transfer function	175
5. Derivation of output signal current of matched filter assuming a Gaussian pulse shape	177
6. Noise equivalent bandwidth of the receiver assuming a Gaussian pulse shape	179

List of Figures

Figure 2.1 Configurations of non-directed indoor infrared links	15
Figure 2.2 (a) Channel impulse response (b) Input pulse and received pulse	22
Figure 2.3 Spectral power density of three common ambient light sources	23
Figure 2.4 Modulation Schemes. Transmitter waveforms of (a) OOK with NRZ (b)OOK with RZ (c) 16-PPM (d) BPSK subcarrier with subcarrier frequency $f_o = 1/t_b$	26
Figure 2.5 TDMA scheme where each channel occupies a cyclically repeating time slot	29
Figure 2.6 FDMA where different channels are assigned different frequency bands	30
Figure 2.7 CDMA in which each channel is assigned a unique PN code which is orthogonal to PN codes used by other users.	32
Figure 2.8 WDMA scheme	33
Figure 2.9 Optical wireless diffuse system	36
Figure 3.1 Infrared wireless channel model	39
Figure 3.2 Test room set-up (a) test room A (4m×8m×3m) (b) test room B (5m×5m×3m)	42
Figure 3.3 Optical power spectra of common ambient infrared sources	44
Figure 3.4 Noise reduction using an optical filter	44
Figure 3.5 Optical spectrum of various light sources	45
Figure 3.6 Set-up used to measure the intensity diffusion of artificial light sources	46
Figure 3.7 Measured normalised power distribution versus distance for various light sources	48
Figure 3.8 : Areas used to calculate the constant k (Room A)	50
Figure 3.9 Modelling the noise level received at communication plane (Room A)	50
Figure 3.10 Points where the received noise levels was calculated	52

Figure 3.11 Noise caused by an incandescent spotlight with $n = 36.1$ at Room A	52
Figure 3.12 Noise caused by an incandescent spotlight with $n = 36.1$ at room B	53
Figure 3.13 Reflection elements	55
Figure 3.14: Angle of possible detection	55
Figure 3.15: Transmission path through a reflection	56
Figure 3.16 Channel impulse response (Test room A)	57
Figure 3.17 Channel impulse response (Test room B)	58
Figure 3.18 Pulse response at various locations on the communication plane at room A	59
Figure 3.18 Pulse response at various locations on the communication plane at room B	60
Figure 4.1 Equivalent circuit for an optical receiver.	66
Figure 4.2 Low impedance per-amplifier	71
Figure 4.3 High impedance pre-amplifier	73
Figure 4.4 Transimpedance pre-amplifier	74
Figure 4.5. PIN-BJT transimpedance receiver	77
Figure 4.6 (a) Receiver transimpedance (b) noise performance	78
Figure 5.1 The digital wireless PPM system	83
Figure 5.2 The PPM frame structure	84
Figure 5.3 The erasure error	84
Figure 5.4 The wrong slot error	86
Figure 5.5 The false alarm error	87
Figure 5.6 PIN-BJT PPM and OOK sensitivity	95
Figure 5.7 Bit error rate performance	96
Figure 5.8: PIN-BJT and OOK sensitivity (Test room A) worst and best case scenario	98

Figure 5.9 Sensitivity performance in a semi-dispersive environment (room A)	100
Figure 5.10 Sensitivity performance under highly directive spotlamps (room A)	101
Figure 5.11 Sensitivity performance in a semi-dispersive environment and under highly directive	102
Figure 5.12 Binary source to digital PPM coder, designed to be employed with an optical wireless system	103
Figure 5.13 Frame timing diagram (a) OOK (b) PPM	104
Figure 5.14 Observed PPM stream and the PPM frame at $n=16$ and $m=0.8$.	106
Figure 5.15 Details of the digital 16-PPM decoder	107
Figure 6.1 Transversal filter	110
Figure 6.2 Channel impulse response and received pulse shape	112
Figure 6.3 Frequency response (a) Channel (b) Equaliser (c) Channel and Equaliser	113
Figure 6.4 Z-plane pole-zero configuration	114
Figure 6.5 Frequency response (a) Equaliser (b) Total	115
Figure 6.6 Z-plane pole-zero configuration	115
Figure 6.7 Total frequency response	116
Figure 6.8 Z-plane pole-zero configuration	117
Figure 6.9 Total frequency response	117
Figure 6.10 Received pulse before and after equaliser using fixed equaliser	118
Figure 6.11 Received pulse before and after equaliser using variable equaliser	121
Figure 6.12 System sensitivity	122
Figure 7.1 A schematic of an optical wireless code division multiple-access communication system with	126
Figure 7.2 PPM CDMA system structure 1	127
Figure 7.3 Bit rate enhancement for structure 1	129

Figure 7.4 The PPM CDMA system structure 2	130
Figure 7.5 Bit rate Enhancement for Structure 2	132
Figure 7.6: System bit rate at a given PPM order and number of users	136
Figure 7.7 Optimum PPM order at a given number of user	136
Figure 7.8 The OOC error rate	138
Figure 7.9 Prime Codes (a) Auto-correlation (b) Cross-correlation function	141
Figure 7.10 Extend prime codes (a) Auto-correlation (b) Cross-correlation function	144
Figure 7.11 Probability of error versus number of user for OCs($X=1024$, $k=7$, $Thr=6$) Prime codes ($P=31$) and Extended prime codes ($P=23$)	145
Figure 7.12 The additional PPM CDMA false alarm errors	146
Figure 7.13 Frame timing diagram (a) OOK (b) PPM (c) PPM-CDMA	148
Figure 7.14 32 bit CDMA code-sequences coder, designed to be employed with an optical 16 bit PPM wireless system.	149

List of Tables

Table 1.1 Published Accounts of wireless infrared communication systems research	2
Table 1.2 Comparison between radio and infrared systems for indoor wireless communication	3
Table 2.1 Class 1 MPE levels specified in IEC825	19
Table 3.1 Parameters of multipath simulation	41
Table 3.2 Light sources that have been used in the experimental measurements	47
Table 5.1 The PIN-BJT receiver parameters	88
Table 5.2 Sensitivity performance in s semi-dispersive environment	100
Table 5.3 Sensitivity performance under highly directive spotlamps	101
Table 6.1 Channel frequency response bandwidth and FWHM value	111
Table 6.2 Filter transfer function parameters	119
Table 6.3 System Sensitivity	120
Table 7.1 Family of prime sequences for $p = 5$	139
Table 7.2 Family of prime codes for $p = 5$	140
Table 7.3 Family of extended prime codes for $p = 5$	143
Table App1-1 Ambient noise in test room A	164
Table App1-2 Ambient noise in test room B	164
Table App2-1 Receiver components	165

List of Abbreviations

APD	Avalanche Photodiode
BPSK	Binary Phase Shift Keying
BER	Bit Error Rate
BJT	Bipolar Junction Transistor
CW	Continuous Wave
CDMA	Code Division Multiple Access
CP	Communication
CRB	Channel Receiver Bandwidth
EPC	Extended Prime Code
FOV	Field Of View
FDMA	Frequency Division Multiple Access
FWHM	Full Width Half Maximum
FET	Field Effect Transistor
IR	Infrared
ISI	Intersymbol Interference
IrDA	Infrared Data Association
LOS	Line of Sight
LED	Light Emitting Diode
LAN	Local Area Network
LA	Incandescent Light
MPE	Maximum permissible Exposure
NRZ	Non Return to Zero
OOC	Optical Orthogonal Code
OW	Optical Wireless
OOK	ON OFF Keying
PDD	Proportional Derivative Delay

PRBS	Pseudo Random Binary Sequence
PIN	p-i-n Photodiode
PCM	Pulse Code Modulation
PTM	Pulse Time Modulation
PPM	Pulse Position Modulation
PC	Prime Code
PN	Pseudo Noise
QPSK	Quaternary Phase Shift Keying
RZ	Return to Zero
RF	Radio frequency
RC	Receiver
SNR	Signal to Noise Ratio
SSM	Single Subcarrier Modulation
TDMA	Time Division Multiple Access
TR	Transmitter
WDMA	Wavelength Division Multiple Access

Glossary of Symbols

Symbol	Definition
A_{vcc}	Common collector gain
A_{vcl}	Closed loop gain
$A_1(\omega)$	Preamplifier transfer function
$A_2(\omega)$	Post amplifier transfer function
b	Number of photons in the pulse
c	Speed of light
C_s	Stray capacitance (receiver bias circuit)
C_d	Diode capacitance
C_{bs}	bootstrapping capacitance
C_{in}	Total input capacitance
C_π	Hybrid π model transistor base capacitance
C_{cl}	Hybrid π model transistor collector capacitance
C_1	PIN, stray and feedback capacitance
CRB	Normalisation parameter (channel and receiver bandwidth)
e_k	Threshold crossing error at frame k.
$E(\omega)$	Equaliser transfer function
e_a	Input equivalent series voltage noise generator of preamplifier
f_o	Cut-off frequency
F	PPM CDMA bit rate enhancement factor
f_s	Sampling frequency
$f(\tau)$	Channel impulse response
G	Power gain of optical amplifier
$g(t)$	Signal pulse shape arriving at photodiode
$G(f)$	Fourier transform of g(t)
$H(f)$	Equalisation filter transfer function

h	Planck's constant, 6.63×10^{-34} Js
$h_p(t)$	Input pulse shape to an optical fiber receiver
i_d	Noise from current flowing in photodetector
i_{det}	Receiver signal current at detection threshold
$i_s(t)$	Signal photocurrent
i_l	Bias/feedback resistor noise
i_a	Input equivalent shunt current noise generator of preamplifier
j	$\sqrt{-1}$
k	Number of pulses in a CDMA sequence
m	Modulation index
M	Number of PCM bits in one frame duration
n	Number of PPM slots in one frame duration
$n(t_d)$	Noise at threshold crossing
$\langle n_o(t)^2 \rangle$	Mean square receiver output noise
$n_o(t)$	Receiver output noise voltage
P	Emitted optical power
P_{LA}	Total lamp output power
P_{pd}	Total received power
P_r	Erasur error probability
P_t	Probability of noise sample crossing the threshold during a blank period of a frame
P_s	Wrong slot error probability
P_f	False alarm error probability
P_s	Average signal power incident on the photodiode
$P_{tc}(t)$	unit rectangular pulse of duration T_c
P_e	Binary error probability
$P(t)$	Optical power incident on photodetector
q	Electronic charge, 1.6×10^{-19} C
Q_r	Complimentary error function coefficient for erasures
Q_s	Complimentary error function coefficient for wrong slot errors

Q_t	Complimentary error function coefficient for false alarms
r	Distance from transmitter to receiver
R_c	Maximum chip rate
R_b	PPM CDMA bit rate
R_{in}	Input resistance
R'_b	OOK CDMA bit rate
r	photodiode responsivity coefficient
R_L	Load resistance
R_G	Generator resistance
R_f	feedback resistance
r_i	Tap coefficient
$S(\omega)$	Additive noise PSD
S_o	White part of receiver noise
S_2	Coefficient of parabolic receiver noise
t	Time
T_f	Frame duration
t_d	Detection instant
t_b	One PCM bit time
t_s	One PPM slot time
T_c	Chip duration
Thr	Threshold detection level
t_c	A PPM CDMA chip time
T_{of}	OOK frame duration
T_{pf}	PPM frame duration
T_{pcf}	PPM CDMA frame duration
$v_o(t)$	Receiver output voltage
V_i	Equaliser input voltage
V_o	Equaliser output voltage
$v_o(t)$	Receiver output voltage
v_d	Receiver voltage at detection instant
v_p	Peak receiver output voltage

X	Length of optical orthogonal code sequence
y_i	Received symbol
$y(t)$	Receiver output current
$Y_{in}(\omega)$	Total input admittance
$Y_a(\omega)$	Amplifier input admittance
Z_t	Low frequency transimpedance
$Z(\omega)$	Transimpedance transfer function of receiver channel
λ_a	Autocorrelation value
λ_c	Crosscorrelation value
τ_o	Minimum delay time
r'_{bb}	BJT base spreading resistance
η	Quantum efficiency of photodiode
ω_n	Noise corner frequency
ω_1	Angular frequency
ω_0	Channel frequency response's first lowest frequency
α	PPM pulse variance
τ_r	Time required for autocorrelation function of receiver filter to decay

Chapter 1 Introduction

In the past few years, the growth of data communications has been enormous. Data communication has been established using wired physical connections. These physical connections introduce difficulties in construction and rewiring during the system set up, and expansion phases. An alternative that achieves the same goal for data communication is the wireless network. Traditionally, radio frequency transmission has been used in wireless applications [1,2]. However, the RF spectrum is so congested that it is very difficult to accommodate new high bit rate applications. Optical systems with low implementation complexity and no spectrum license requirements provide a possible solution. The use of infrared light for indoor data communication has been widely studied [3-17]. The first optical wireless data link was demonstrated by Gfeller and Bapst in 1979. This link pioneered the feasibility of an ON OFF Keying (OOK) baseband 125 kbit/s transmission system [3]. Since then, numerous other infrared wireless systems have been demonstrated (see Table 1.1).

Data	Organization	Bit rate	Modulation	Directionality
1979/1981	IBM Zurich	64-125kb/s	Subcarrier BPSK	Diffuse
1983	Fujitsu	19.2kb/s	Subcarrier FSK	LOS, Diffuse
1985	Fujitsu	48kb/s	Subcarrier BPSK	NLOS uplink WLOS downlink
1984	Hitachi	0.25-1 Mb/s	Subcarrier FSK	NLOS uplink WLOS downlink
1985	HP Labs	1Mb/s	Manchester Coding	NLOS
1986	Motorola	50kb/s	RZ OOK	WLOS
1987	Bell Labs	45Mb/s	OOK	NLOS
1988	Matsushita	19.2kb/s	Subcarrier FSK	NLOS uplink WLOS downlink
1993	BT Labs	50Mb/s	-	Cellular
1994	Berkeley	50Mb/s	OOK with DFE	Diffuse
1994	BT Labs	155Mb/s	-	Cellular
1994/96	BT Labs	1Gb/s	-	Tracked
1997/1998	Northumbria University	10Mb/s	PPM CDMA	Diffuse LOS

*NLOS - Narrow Line-of-Sight. WLOS - Wide Line-of-Sight

Table 1.1 Published Accounts of wireless infrared communication systems research

The use of an optical wireless network for indoor applications offers numerous advantages over the equivalent RF wireless network. For example, the optical infrared energy can typically be contained within the room or communication environment, thus virtually eliminating the problems of interference generated by neighbouring users. The same transmission equipment and optical wavelength can be re-used in other parts of the building without posing security violation problems. Infrared has an abundance of bandwidth, and infrared components are small, inexpensive and consume little power. As such, indoor infrared communication has recently received

much attention especially in view of the increased data and mobility requirements of the computing and communications users.

Property of medium	Radio	Infrared
Multiple Fading	Yes	No
Multiple Distortion	Yes	Yes
Bandwidth Limitation	Regulatory	Photodiode/preamplifer, diffuse channel
Bandwidth Regulated	Yes	No
Path Loss	High	High
Noise	Other user	Ambient light
Range/Coverage	High	Low
Security	Low	High
Technology cost	?	Low
Input signal Represents	Amplitude	Power

Table 1.2 Comparison between radio and infrared systems for indoor wireless communication

The infrared wireless communication system is not without disadvantages. An infrared link is suceptible to shadowing caused by objects or people positioned between the transmitter and receiver. Infrared communication between two rooms requires the installation of infrared access points that are interconnected via a wired backbone, that is because infrared cannot penetrate walls. In many indoor environments there exists intense ambient infrared noise, arising from sunlight, incandescent lighting and fluorescent lighting, which induces noise in an infrared receiver. Another disadvantage of infrared wireless communication system is limited range, which is a result of power limits on infrared transmitters imposed by safety

considerations. The characteristics of radio and infrared indoor wireless links are compared in Table 1.2.

Radio and infrared are complementary transmission media, and different applications favour the use of one medium or the other. Radio is favoured in applications where user mobility must be maximized or transmission through walls or over long ranges is required and may be favoured when transmitter power consumption must be minimised. Infrared is favoured for short range applications in which per-link bit rate and aggregate system capacity must be maximized, while keeping the cost minimised, international compatibility is required, or receiver signal processing complexity must be minimised.

An important consideration, is that of providing multiple access facilities over the network. Several multiple access techniques exist such as time division multiple access (TDMA), wavelength division multiple access (WDMA) and code division multiple access (CDMA). TDMA is not desirable over such a network since it is a synchronous technique where common timing must be provided and users cannot communicate independently and concurrently. WDMA calls for each user to have N (where N is the number of users) independent wavelengths together with an optical tuneable reception filter, such a complex structure is generally not desirable and is expensive for multi-user mobile communication. CDMA with a positive $\{0,1\}$ class of optical sequences (Optical Orthogonal Codes (OOC), Prime Codes (PC) and Extended Prime Codes (EPC)) can provide a potential solution suited for application in the optical wireless multiple access environments. In addition the use of pulse position

modulation (PPM) in conjunction with CDMA offers several advantages over comparable On Off Keying (OOK) CDMA in terms of bit rate and co-user interference.

The utilisation of infrared energy to enable indoor communication is a field that has recently attracted much attention. Systems investigated and realised to date can be grouped into optical wireless (OW) line of sight (LOS) and OW diffuse configurations. This project proposes and studies the use of PPM in such an environment. Moreover, it proposes a new hybrid multi-user communication technique (PPM CDMA) that can be utilised to realise the optical wireless network.

1.1 Research objectives

The primary objectives of the work undertaken and presented in this thesis were to:

- Study and identify new communication strategies for the optical wireless multi-user environment. These were to include an evaluation of PPM CDMA.
- Evaluate the effect of noise due to ambient light and its impact on the indoor infrared wireless communication system. Many environments contain intense ambient infrared radiation arising from sunlight, incandescent and fluorescent lamps.

- Develop a mathematical model to simulate the optical wireless channel including impulse response, multipath dispersion and ambient light noise and the effect they have on the optical wireless system (i.e. sensitivity, bit rate).
- Design and simulate an equaliser to reduce Intersymbol interference (ISI) from multipath dispersion. An indoor infrared wireless optical communication system can be categorized as either Line of Sight (LOS) or Diffuse. Diffuse systems have the advantage of being able to support full mobility, however they are prone to multipath dispersion.
- Design and simulate an indoor infrared PPM wireless communication system. PPM is a high sensitivity modulation technique that results in high power efficiency compared to OOK in optical wireless transmission.
- Design and evaluate an optical receiver structure that can be employed in the optical wireless environment (large detector area needed hence capacitance problems) with the proposed PPM format.
- Develop a mathematical model to calculate the performance of indoor infrared PPM CDMA systems using different orthogonal coding schemes (OOC, PC and Extended PC).

1.2 Organisation of the thesis

Following the introduction in Chapter 1, the rest of the thesis is organised as follows:

Chapter two presents a review of indoor infrared wireless communication systems. The different possible indoor optical wireless link configuration are presented and discussed. Optical safety and the three major obstacles to achieving high speed indoor optical communication are also presented. Modulation and multiple access techniques are introduced.

Chapter three evaluates and models the noise from background light. It also considers the selection of suitable optical filters that can reduce the associated background noise. In indoor optical wireless communication, most of the noise comes from background light (sun light, fluorescent light and incandescent light). Using an optical longpass or bandpass filter would reject most of background light.

Multipath dispersion together with its impact on transmitted pulses is also presented in Chapter three and its effect on indoor optical wireless communication is discussed. It is shown that diffuse infrared propagation alleviates the need for physical alignment between the transmitter and receiver. A major drawback of this approach however is the signal distortion caused by reflections from ceiling, walls, and other objects. The need for equalisation is therefore established, however consideration is first given in Chapters four and five for receiver design and PPM signalling in order to establish the pre-equalisation performance.

Chapter four reviews the area of optical receiver design. The performance limitations and receiver noise analysis carried out by Personick are detailed. A PIN-BJT common collector common emitter bootstrapped receiver design is then presented and its performance is analysed in the context of the indoor optical wireless system.

Chapter five introduces the PPM model and the three error sources associated with this format. The performance of optical wireless PPM systems is analysed for LOS and Diffuse links. A 16-PPM coder and decoder were designed and constructed. Details of these are also given in Chapter five.

Chapter six considers the design of an equaliser to reduce the effects of multipath dispersion. Multipath dispersion is a major limitation for indoor infrared high speed communication networks which reduces the system sensitivity between 3.5 to 5 dB. A new equaliser was designed to reduce the impact of multipath dispersion.

Chapter seven focuses on optical CDMA systems. An analysis of a PPM CDMA system using different orthogonal codes is presented in this Chapter and the system performance is evaluated under the various coding schemes.

Chapter eight summarises the major contributions and conclusions of this thesis.

Chapter nine highlights the areas of further investigation.

1.3 Original Contributions

The author has

1. Developed a new mathematical approach to model the optical wireless channel characteristics which include background noise and impulse response. Analysed multipath dispersion and presented a new equalisation technique to reduce ISI.
2. Presented new results based on measurement of background noise power spectra for sources including fluorescent, incandescent and halogen lights. The halogen light optical spectrum measurement is a new result which shows that halogen light possesses a spectrum similar to sun light. Therefore appropriate optical filters were selected and their characteristics were measured. Measured and produced theoretical models for the radiation patterns of these sources.
3. Presented a complete theoretical analysis of a bootstrapped PIN-BJT receiver and demonstrated close agreement between the analytic results and circuit simulations. Due to the careful design and approach adopted, the simulation result show that the receiver noise is the lowest reported so far ($2.7 \text{ pA}/\sqrt{\text{Hz}}$) in a 10 Mbit/s optical PPM wireless system.
4. Evaluated the performance of PPM PIN-BJT optical wireless LOS systems demonstrating that such systems can offer up to 9.8 dB sensitivity improvement over equivalent OOK systems at 10 Mbit/s.

5. Evaluated the performance of PPM PIN-BJT optical wireless diffuse systems demonstrating that such systems can offer up to 6.8 dB sensitivity improvement over equivalent OOK systems also at 10 Mbit/s.
6. Presented a theoretical analysis of pulse position modulation code division multiple access in the context of the indoor infrared channel and evaluated different orthogonal coding schemes (optical orthogonal code, prime code and extended prime code).

These original contributions are supported by the following publications:

1. H.H. Chan, J.M.H. Elmirghani, and R.A. Cryan, "Simulation of IR Channel Impulse Response for PPM-CDMA Indoor Wireless LANs," IEEE Second Communication Networks Symposium, pp. 182-185, Manchester, 10-11 July 1995.
2. H.H Chan, J.M.H. Elmirghani, and R.A. Cryan, "An Equalisation Technique for Indoor IR Wireless LANs," **Microwave and Optical Technology Letters**, Vol. 10, No. 4, pp.235-238, NOV. 1995.
3. H.H. Chan, J.M.H. Elmirghani, and R.A. Cryan, "Equalization Techniques for Indoor Infrared Channels," The International Society for Optical Engineering (SPIE) Wireless Data Transmission Conferences, pp. 274-279, Philadelphia,USA , 22-26 Oct. 1995.
4. A. Hussain, H.H Chan, J.M.H. Elmirghani, and R.A. Cryan, "Matched Filter Realisation for Diffuse Indoor Infrared Wireless Systems," The International Society for Optical Engineering (SPIE) Wireless Data Transmission Conferences, pp. 238-246, Philadelphia,USA , 22-26 Oct. 1995.
5. H.H. Chan, A. Hussain, J.M.H. Elmirghani, and R.A. Cryan, "Channel Equalisation for Optical Wireless Multi-user Systems Utilising Orthogonal Codes," IEE Colloquium on Optical Free Space Communication Links, pp. 1/1-1/7, London, 19 Feb. 1996.

6. H.H. Chan, J.M.H. Elmirghani, and R.A. Cryan, "Performance Analysis of Indoor Infrared Wireless Networks Utilising PPM CDMA," Proc. IEEE The International Conference on Communications Systems, vol 3, pp. 1467-1471, Dallas, Texas USA, June 1996 (ICC'96).
7. H.H. Chan, J.M.H. Elmirghani, and R.A. Cryan, "Indoor Infrared Wireless PPM Systems" IEEE Third Communication Networks Symposium, pp. 206-209, Manchester, 8-9 July 1996.
8. H.H. Chan, J.M.H. Elmirghani, and R.A. Cryan, "Performance analysis of OOK and PPM over wireless channels using PIN-BJT receiver," The International Society for Optical Engineering (SPIE) All-Optical Communication Systems Symposium, pp. 50-58, Boston, 18-22 November 1996.
9. J.M.H. Elmirghani, H.H. Chan, and R.A. Cryan, "Sensitivity evaluation of optical wireless PPM systems utilising PIN-BJT receivers," **IEE Proc. -Optoelectron**, Vol. 143, No. 6, pp. 355-259, December 1996.
10. H.H. Chan, J.M.H. Elmirghani, and R.A. Cryan, "Indoor Optical Wireless Systems using PPM Signaling," The International Society for Optical Engineering (SPIE) Voice, Video, and Data Communications Symposium, pp. 68-78, Dallas, 2-7 November 1997.
11. H.H. Chan, J.M.H. Elmirghani, and R.A. Cryan, "Performance Evaluation of PPM CDMA under different orthogonal coding schemes," Proc. IEEE The International Conference on Communications Systems, vol.3, pp.1284-1288, 7-11 June, 1998 (ICC'98).
12. H.H. Chan, J.M.H. Elmirghani, and R.A. Cryan, "Optical Wireless PPM CDMA Networks Employing OC and PC Signature Codes," Accepted by **Journal of Optical Communications**, 1998.
13. H.H. Chan, K.L. Sterckx, J.M.H. Elmirghani and R.A. Cryan, "Performance of optical wireless OOK and PPM systems under the constraints of ambient noise and multipath dispersion," **IEEE Communication Magazine**, vol. 36, No. 12, pp. 83-87, Dec. 1998.

Chapter 2 Review

2.1 Introduction

Using light to transmit data is not a new idea. Greeks used fire signals in the 8th century BC. More famously, hill-top beacons warned of the approaching Spanish Armada. People have long used sunlight to send messages, by flashing the sunlight with a shiny object. Alexander Graham Bell extended this idea in 1880, with his photophone [18]. In 1895 Marconi succeeded in free space communication using long radio waves. Interest in light communication waned, as sending a message was comparatively slow and cumbersome and also subjected to the vagaries of the weather. Indeed, in 1995 radio has celebrated 100 incredibly successful years. It has helped to satisfy our human desire to communicate further and faster. Now our need for communications has grown to such an extent that radio is struggling to meet it. It is time to re-examine free space communication using light waves. There are two principal reasons for re-examining optical wireless: increasing demand for bandwidth and increasing complexity of radio regulations [19].

Over the last two decades, the growth of computer based terminal stations, such as PCs, workstations, etc., has been enormous. Also the computer industry, over the recent years, has focused on producing laptop portable computers. Subnotebook PC portable workstations currently available are small in size but with high performance. Concurrent with these developments, the industry has recently been faced with a growing demand for networking. This demand is mostly noted in the data communication sector. Traditionally, data communication was achieved by wired physical connections. These physical connections introduce difficulties in construction and rewiring during the system set up, maintenance, and expansion. An alternative that achieves the same goal for portable stations is the wireless network. The first wireless LAN using infrared radiation was developed over nineteen years ago by the IBM Zurich Laboratory [3]. Since then, numerous other infrared LANs have been demonstrated [12], [20-27]. These systems seek to exploit the many advantages enjoyed by infrared over radio as a medium for wireless networks. For example, infrared has an abundance of bandwidth, infrared is immune to radio interference, and infrared components are small, inexpensive, and consume little power. Infrared and visible light, being near in wavelength, behave similarly; infrared is absorbed by dark objects, diffusively reflected by light objects, and directionally reflected by mirrors and shiny metals. Infrared light penetrates glass, but not walls, which is an important advantage over radio, because it allows neighbouring cells, separated by a wall, to coexist without interference. It also makes infrared radiation a secure medium, confining data to the room in which it originates.

The following sections introduce the link configuration and optical safety for the indoor environment. The three impairments for the high speed indoor infrared wireless network are then presented. Next , three modulation and four multiple access techniques will be discussed. Their effect on indoor infrared systems are then presented. The chapter concludes by describing current indoor infrared wireless systems.

2.2 Wireless infrared link configurations:

A wireless optical communication link can take a number of forms and we adopt the following notation. A directed transmitter has a narrow-beam radiation pattern, and a directed receiver has a narrow field of view. Likewise, a non-directed transmitter has a broad-beam radiation pattern, nearly omnidirectional, and a non-directed receiver has a wide field of view.

Wireless infrared links may be deployed in the following ways:

1. Directed: An infrared link is considered to be a directed link when both transmitter and receiver are directed.
2. Non-directed: When a non-directed transmitter and a non-directed receiver are used the infrared link is considered to be arranged as a non-directed link.

3. Hybrid: A hybrid link is implemented when the system consists of either a directed transmitter and a non-directed receiver or a non-directed transmitter and a directed receiver.

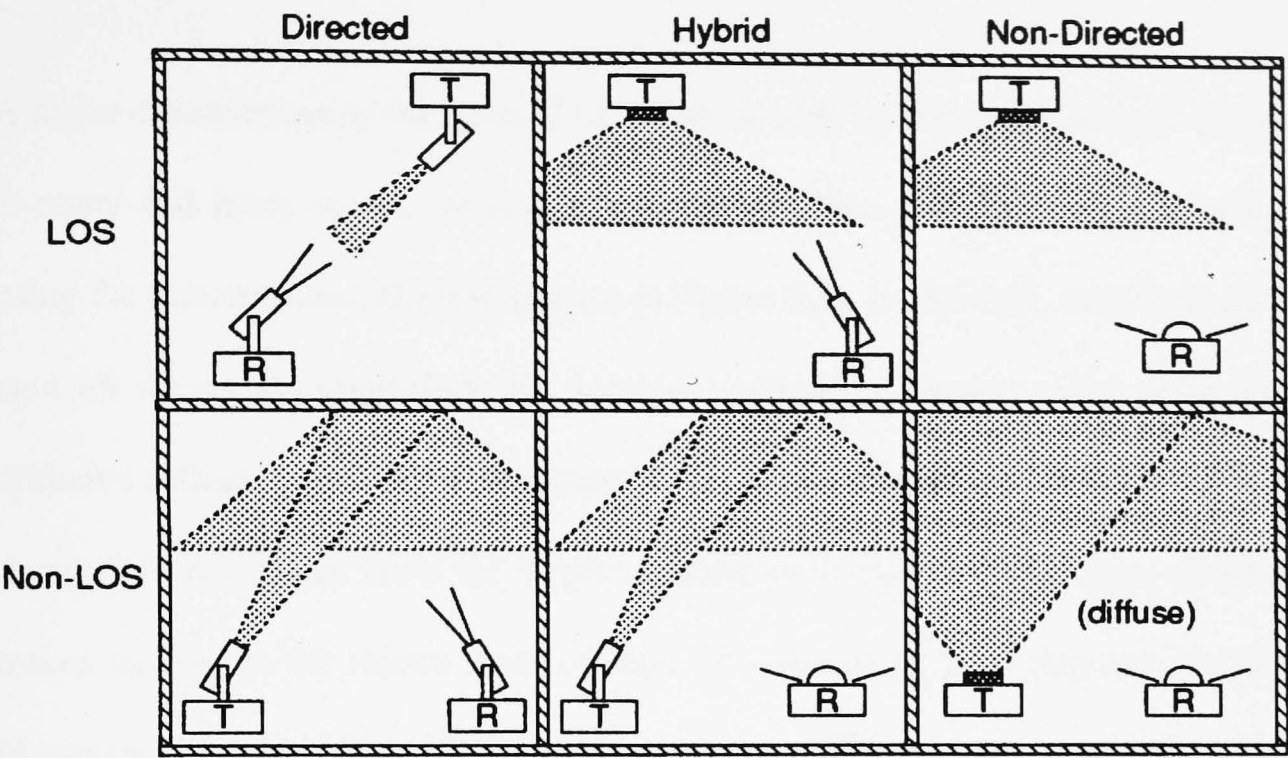


Figure 2.1. Configurations of non-directed indoor infrared links [17].

All the links described can be categorised as either line-of-sight (LOS) or Non-LOS (see Figure 2.1). There are six possible link configurations, as shown in Figure 2.1. Next, each configuration will be explained and the related works by other researchers reviewed.

The directed LOS configuration is shown in Figure 2.1. It makes efficient use of optical power because the signal energy is concentrated into narrow optical beams, and most of the ambient background light is rejected by the narrow field of view of the receiver. A directed LOS link does not suffer from multipath dispersion because the narrow field of view rejects reflections from the walls. In 1985, Yen and

Crawford [5] reported a 1 Mb/s directed LOS wireless link to connect multiple terminals to a centrally located base station. This network uses different wavelengths to provide full duplex transmission without interference.

A major disadvantage of the directed LOS links is their inability to cope with the one-to-many and many-to-one communication modes. This problem can be solved by using the directed non-LOS link (shown in Figure 2.1). In this link, each node in the network directs its transmitter and receiver towards a common target point on a diffusive reflecting surface in the room. With this configuration, energy from each terminal is re-radiated from the target reflector in every direction, some of which makes its way to the narrow field of view of receivers on each terminal. In 1985, Photonics Corp. used this configuration in their Photolink product, which operates at 230 kb/s with a range of about 22 m [28,29].

By replacing the passive reflector in the directed non-LOS links with an active repeater or base station, we arrive at the hybrid LOS configuration of Figure 2.1. Like directed non-LOS links, this link can also support the one to many and many to one modes. There have been a number of systems based on the hybrid LOS configuration [30-32]. Minami et al [30] reported a 19.2 kb/s system which was operated over 10 m with LOS intact and 5m with LOS obstructed. With the LOS obstructed, the configuration falls under the hybrid non-LOS category, as show in Figure 2.1. Takashi and Touge [31] extended Minami's work by increasing the transmitter power and changing the modulation secheme from subcarrier frequency shift keying to subcarrier phase shift keying, achieving 48 kb/s over the same range.

Unfortunately, none of the directed or hybrid configurations shown in Figure 2.1 are appropriate for portable computers and other mobile platforms, because they all require alignment between transmitter and receiver. Wireless links for portable terminals must be non-directed links.

Consider next the diffuse configuration of Figure 2.1. The first diffuse link was proposed by Gfeller and Bapst in 1979 [3], in which the transmitter emits infrared energy into a broad optical beam, and the receiver has a wide field of view. The system bit rate was 125 kb/s and the range was 10-20 m, depending on the severity of the ambient light noise. From Figure 2.1 it is clear that the diffuse configuration is the most convenient from the user's standpoint, because the user does not have to worry about alignment or maintaining a LOS path. Unfortunately, diffuse links suffer multipath dispersion and more noise from background light. Therefore the diffuse system is the most challenging from a design standpoint.

As a compromise, the non-directed LOS configuration of Figure 2.1 makes better use of signal power than the diffuse link, but it requires that the LOS path be unobstructed. This configuration may be used in very high speed applications and long distance applications. A recent multichannel public access telephone system was proposed by Poulin et al [33,34], which is based on the non-directed LOS configuration. In this system, the base station consists of an array of moderately narrow directed beams, each pointing in a different direction, so that the combined effect is a wide optical beam. The range was about 20 m and the data rate was 230 kb/s.

2.3 Optical safety

One of the most important issues concerning the development of optical wireless systems is optical safety. Optical radiation can present a hazard to the eye and skin if the exposure is high enough. The degree of hazard depends on a number of factors, including exposure level, exposure time and wavelength. The size of the optical source is also an important factor, since the lens of the eye may focus the energy from a point source to a small intense spot on the retina. The same optical energy from a large source would give a much larger spot on the retina and would thus result in less risk for the eye.

Various National and International Standards on the safety of laser, such as IEC 825, specify the levels of optical emissions from lasers considered to be safe [35,36]. In these standards, lasers are classified according to the potential hazard, with class 1 being defined as inherently safe, even when viewed with optical instruments such as binoculars. It will be essential that all infrared wireless systems must fall into this category. Some LEDs now have similar output power to Laser Diodes, and therefore it is planned that they will also be included in the next amendment to the safety standard IEC825. The natural focusing properties of the eye may concentrate the optical radiation (400-1400 nm) and create exposure conditions which could damage the retina. The retina is the most sensitive part of the eye, and most vulnerable to thermal burns. The wavelength, exposure duration, pulse characteristics, distance from the eye and image size are all factors relating to the maximum safe exposure limits.

Wavelength (nm)	Actual MPE (mW)	Proposed MPE (mW)
850	0.24	0.4
1300	0.60	8.0
1480-1550	0.80	10.0

Table 2.1 Class 1 MPE levels specified in IEC825

The relevant wavelengths in optical wireless systems are 850nm, 1300nm, 1480nm and 1550nm where suitable sources and detectors are available. In general, the maximum safe power levels are relatively low at the shorter wavelengths near the visible part of the spectrum. This is because the eye is particularly efficient at focusing and absorbing radiation at those wavelengths. For wavelengths greater than 1400nm the retina is not at risk, but skin damage at sufficiently high power is possible. Proposed changes, in amendment 2 of IEC825, will incorporate relaxation to some maximum permissible exposure (MPE) limits at these wavelengths. The class 1 MPE levels for each wavelength, together with the proposed increases are summarised in Table 2.1; the values quoted in this table have been compiled from Smyth et al [9].

The use of large area sources reduces significantly the risk of retinal damage. For larger area sources, the power density on the retina, and thus the hazard, will depend on the power density incident on the cornea and the size of source in terms of the angle subtended by the optical source at the eye. A more appropriate measure of radiation for safety purpose irradiance (W/m^2 /ster) of the source. For the wavelength 850nm, the maximum safe irradiance for continuous viewing (IEC825) is 12.8 kW/m^2 /ster. If a large area Lambertian source is assumed, which is the power distribution

expected from a perfect diffuser, the radiance L ($\text{W/m}^2 \text{ /ster}$) is related to the power density on the emitting surface H (W/m^2) by

$$L = \frac{H}{\pi} \tag{2.1}$$

Hence the maximum safe power density will be 41 kW/m^2 for a Lambertian source. For sources which give distributions of power different from Lambertian this power density will be scaled according to the total solid angle covered. A power density of 41 kW/m^2 appears to be too large to be considered as eye safe, especially considering that it exceeds the MPE level for skin damage, 2 kW/m^2 . New proposals for dealing with larger area sources will appear in amendment 2, and are likely to reduce this value considerably. Initial proposals indicate that the maximum safe power density from a Lambertian source for continuous viewing at a wavelength of 850nm could be 0.37 kW/m^2 .

2.4 Impairments

The three major obstacles to achieving high-speed indoor infrared communication are noise from ambient light, high capacitance of large area photodiodes, and multipath dispersion.

2.4.1 Photodetector Capacitance and f^2 Noise

There are three primary sources of noise in the electrical signal that follows the photodetector of an indoor infrared system: shot noise from background light, thermal noise from the bias resistance of the detector and from the preamplifier, and so-called “amplifier” or f^2 noise [12]. There are other sources of noise, such as photodiode dark-current noise and shot noise from the received signal, but they are negligible in comparison. An unfortunate by-product of communicating with nondirected optical beams is a small signal irradiance at the receiver. However there are a few methods which can be used to obtain sufficient signal power, for example using a concentrator, an optical lens or a large area receiver photodetector. In this project a large area photodiode is employed because it is the simplest method to collect the optical signal. Unfortunately, the capacitance of a photodetector is proportional to its area, and a large capacitance at the input to an amplifier acts as a low-pass filter, attenuating the high-frequency components of the received signal. This low pass filter results in a noise penalty, because although the received signal is attenuated by it, any noise that follows the input stage, such as the channel thermal noise of a Field-Effect Transistor based preamplifier is not attenuated. When a white noise process following a first-order low pass filter is referred back to the input of the filter, its power-spectral density becomes quadratic in frequency. For this reason, it is often called f^2 noise.

2.4.2 Multipath Dispersion

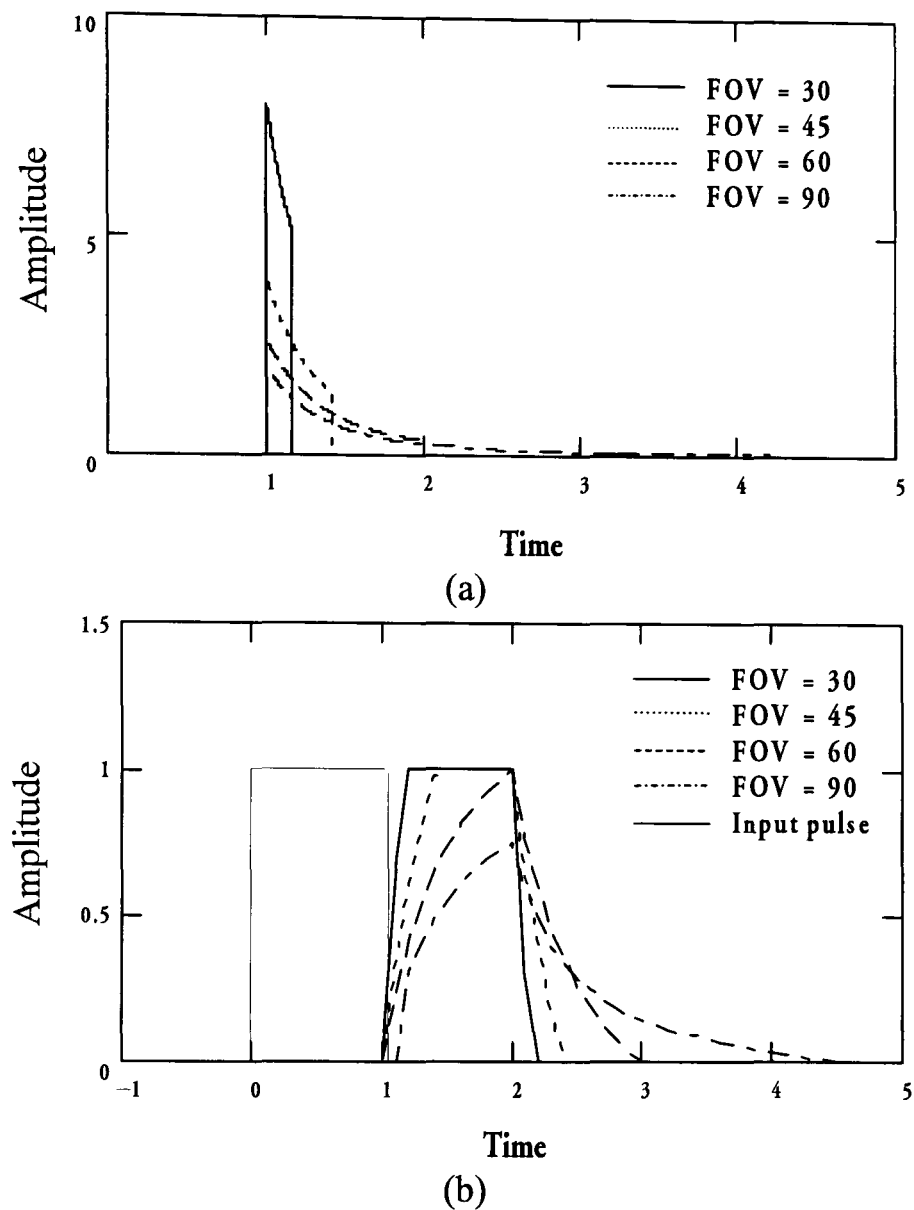


Figure 2.2 (a) Channel impulse response (b) Input pulse and received pulse

In an indoor environment, an optical signal from the transmitter to the receiver undergoes temporal dispersion due to reflections from walls and other reflectors. The dispersed signal can be modelled as the resultant signal in a multipath propagation environment. Diffusive systems are more prone to multipath effects than directed beam systems, because their larger beamwidths result in more light hitting potential reflectors, and the large fields of view of their detectors mean more reflected light is detected. In Figure 2.2 , we show the channel impulse response and also the received signal after multipath dispersion [3]. From Figure 2.2 (b) we can see that multipath

dispersion can cause “Intersymbol Interference (ISI)”. To mitigate ISI, the receiver must equalise the channel. The details of multipath dispersion and the equalisation technique will be discussed in the Chapters 3 and 6.

2.4.3 Ambient light

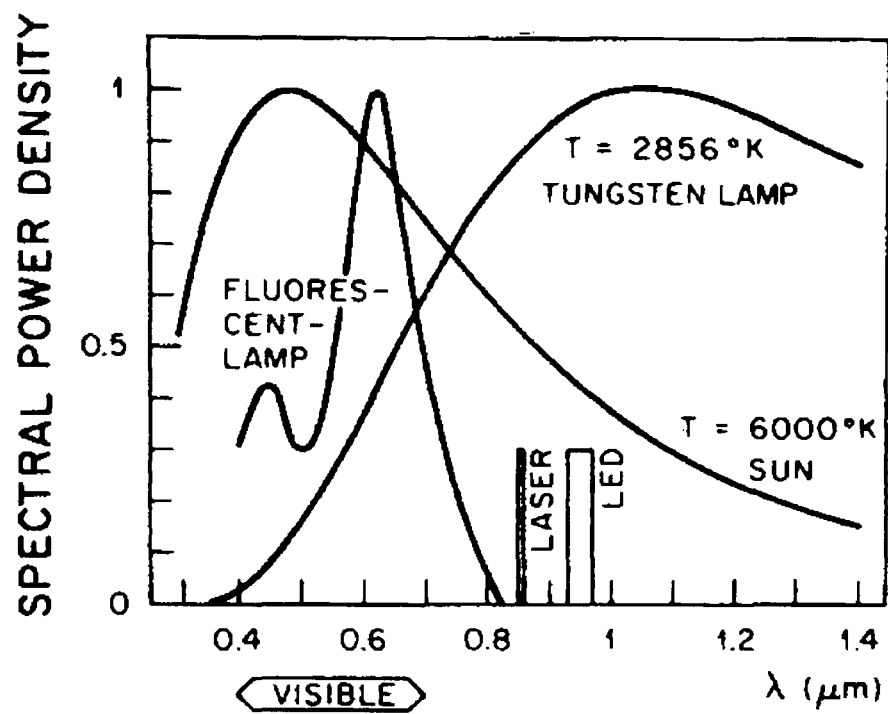


Figure 2.3 Spectral power density of three common ambient light sources [3]

In a diffuse optical channel, the photodiode is exposed to the ambient light, introducing additional noise to the input circuit of the receiver amplifier. This is in contrast to fiber optic receivers. The most commonly encountered ambient light sources are daylight, tungsten, and fluorescent lamps. Their relative spectral power densities are shown in Figure 2.3 [3]. In general, there is high level of stationary or slowly fluctuating ambient light generating shot noise in the photodiode. In addition, artificial-light sources also emit rapidly fluctuating components associated with higher harmonics of mains frequency. There are two ways to mitigate the effects of

background light; the first is to use a narrow band optical source, such as a single or near single frequency laser diode, in combination with a narrow band optical filter to reject out-of-band ambient light. The second way is to introduce electrical postdetection filtering to remove the low frequency ambient noise. The latter approach cannot always be used since such filtering can distort the wanted signal. Moreover signal and noise will usually have overlapping spectral components. Therefore the first approach is preferred. An optical concentrator can be introduced between the transmitter and receiver to provide optical gain. Together, the concentrator and filter make up the optical front end. Ideally, we would like the front end to act as an ideal optical band pass filter, providing a large optical gain G across a narrow passband of width $\Delta\lambda$, and rejecting all other wavelengths. The detail of ambient light noise and filter selection will be presented in Chapter 3.

2.5 Modulation Schemes

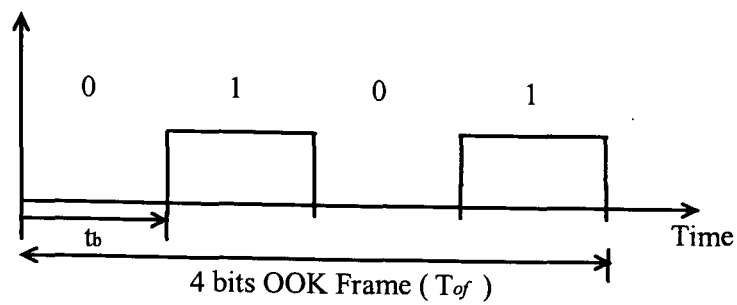
Optical bit modulation can be classified as either pulse or continuous wave (CW). In a pulse system, the bits are transmitted by pulsing the light source (Laser or LED). In a CW system the bits are modulated so that the laser source is continuously emitting. Usually, Pulse modulation is used with direct detection, whereas CW modulation may involve either direct detection or heterodyning systems.

The most common forms of pulse modulation in binary direct detection receivers are On-Off-Keying (OOK) and Pulse Position Modulation (PPM). In OOK, each bit is

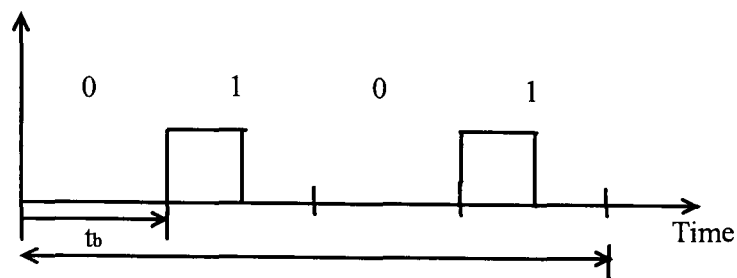
transmitted by pulsing the light source on or off during each bit time. This represents the most basic type of optical signal and corresponds to merely blinking the light source for digital encoding. In PPM an optical pulse is placed in one of M adjacent time slots to represent the data. The common form of CW encoding uses subcarrier modulation of the light source for direct detection.

2.5.1 ON OFF Keying Modulation

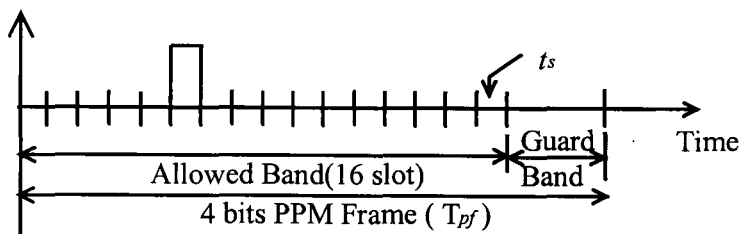
Among all modulation techniques suitable for wireless infrared links, OOK is the simplest to implement. The waveforms of OOK using Non-Return-to-Zero (NRZ) pulses and using Return-to-Zero (RZ) pulses of duty cycle equal to 0.5 are shown in Figure 2.4 (a) and (b). Each 'one' bit is encoded into an optical pulse and each 'zero' bit is encoded into an off bit. Clearly, the maximum source bit rate is directly related to the rate at which the source can be switched on and off. Since lasers and LEDs can be switched at rates up to hundreds of megahertz, OOK modulation represents a simple procedure for producing relatively high bit rates. The light pulses of the OOK bit sequence are then transmitted as a pulse laser beam in a wireless channel. NRZ OOK offers an excellent bandwidth efficiency and its simplicity makes it the easiest scheme to implement. The main disadvantage of OOK is that it uses a relatively high optical power.



(a)



(b)



(c)



(d)

Figure 2.4 Modulation Schemes. Transmitter waveforms of (a) OOK with NRZ (b) OOK with RZ (c) 16-PPM (d) BPSK subcarrier with subcarrier frequency $f_o = 1/t_b$

2.5.2 Pulse Position Modulation

PPM is an orthogonal modulation scheme that offers a decrease in average power requirement compared to OOK, at the expense of an increased bandwidth. Instead of

sending a light pulse according to the level of signal, bits of data are conveyed by a signal pulse in one of $n = 2^M$ positions. The n positions are called time slots. The transmission signal for 16-PPM is shown in Figure 2.4(c). The n slots constitute a PPM frame (T_{pf}). The location of the pulse in the frame, therefore, determines the data word. Furthermore, a guard band of duration $(1-m)T_{pf}$ (where $0 < m < 1$ is the modulation index) serves to eliminate interframe interference (IFI). Compared with NRZ-OOK, PPM requires less optical power but a larger bandwidth.

2.5.3 Subcarrier Modulation

In single-subcarrier modulation (SSM), a bit stream is modulated onto a radio frequency subcarrier, and this modulated subcarrier is modulated onto $X(t)$, the instantaneous power of the infrared transmitter. Because the subcarrier is typically a sinusoid taking on negative or positive values, a dc bias must be added to it to satisfy the requirement that $X(t)$ be non-negative. The transmitted waveforms of a BPSK subcarrier are shown in Figure 2.4(d) assuming a subcarrier frequency equal to the bit rate. Such a BPSK subcarrier requires twice the bandwidth of an OOK signal, while a QPSK subcarrier requires the same bandwidth as OOK [16]. After optical-to-electrical conversion at the receiver, the subcarrier can be demodulated and detected using a standard BPSK or QPSK receiver. In distortionless channels, a single BPSK or QPSK subcarrier requires 1.5 dB more optical power than OOK. This can be explained by observing the BPSK and transmission of average power which are equivalent to binary antipodal signals plus a dc bias carrying no information [17].

2.6 Multiple Access

Multiple access schemes are used to allow many mobile users to share simultaneously a finite amount of spectrum. The sharing of spectrum is required to achieve high capacity by simultaneously allocating the available bandwidth (or the available amount of channels) to multiple users. For high quality communications, this must be done without severe degradation in the performance of the system. Time division multiple access (TDMA), frequency division multiple access (FDMA), wavelength division multiple access (WDMA), and code division multiple access (CDMA) are the four major access techniques used to share the available bandwidth in an optical communication system.

2.6.1 Time division multiple access

Time division multiple access systems divide the time domain into slots, and in each slot only one user is allowed to either transmit or receive. It can be seen from Figure 2.5 that each user occupies a cyclically repeating time slot, so a channel may be thought of as particular time slot that re-occurs every frame, where N time slots comprise a frame. The characteristic features of TDMA include the following:

1. TDMA shares a single carrier frequency with several users, where each user makes use of non-overlapping time slots. The number of time slots per frame

depends on several factors, such as modulation technique, available bandwidth, etc.

2. Data transmission for users of a TDMA system is not continuous, but occurs in bursts. This results in low battery consumption, since the subscriber transmitter can be turned off when not in use.
3. Adaptive equalization is usually necessary in TDMA systems, since the transmission rates are generally very high compared to FDMA channels.
4. High synchronization overhead is required in TDMA systems because of burst transmissions. TDMA transmission is slotted, and this requires the receivers to be synchronized for each data burst. In addition, guard slots are necessary to separate users, and this results in TDMA systems having larger overheads as compared to FDMA.
5. TDMA can allocate different numbers of time slots per frame to different users. Thus bandwidth can be supplied on demand to different users by concatenating or reassigning time slots based on priority.

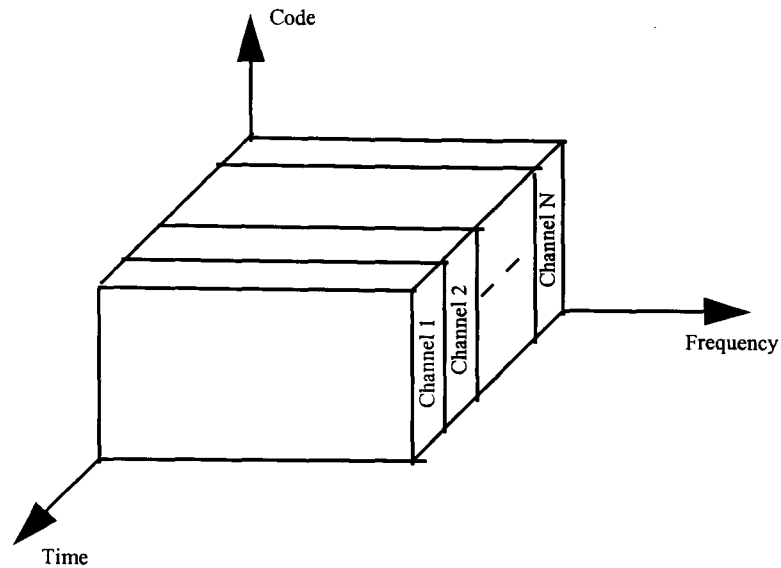


Figure 2.5 TDMA scheme where each channel occupies a cyclically repeating time slot

2.6.2 Frequency division multiple access

Frequency division multiple access assigns individual frequency bands ‘channels’ to individual users. It can be seen from Figure 2.6 that each user is allocated a unique frequency band or channel. These channels are assigned on demand to users who require service. The features of FDMA are as follows:

1. The FDMA channel carries only one communication circuit at any one time.
2. If an FDMA channel is not used, then it sits idle and cannot be used by other users to increase or share capacity. It is essentially a waste of resources unless each user can transmit in any of the N channel frequencies which in turn is waste of hardware.

- 3. The bandwidths of FDMA channels is relatively narrow (30 kHz) as each channel supports only one circuit per carrier. This means that FDMA is usually implemented in narrowband systems.
- 4. The symbol time is large compared to the typical channel average delay spread. This implies that the amount of intersymbol interference is low and thus little or no equalisation is required in FDMA narrowband systems.
- 5. FDMA systems have higher ‘cell’ costs as compared to TDMA systems because of the single channel per carrier design.

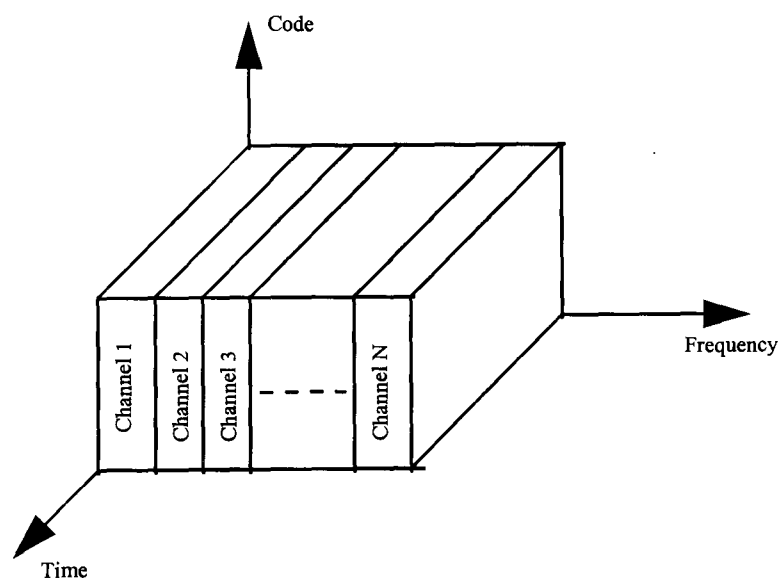


Figure 2.6 FDMA where different channels are assigned different frequency bands.

2.6.3 Code division multiple access

In code division multiple access systems, the narrowband message signal is multiplied by a very large bandwidth signal called the spreading signal. The spreading signal is a

pseudo-noise sequence that has a chip rate which is several orders of magnitudes greater than the data rate of the message. All users in a CDMA system, as seen from Figure 2.7 , use the same carrier frequency and may transmit simultaneously. Each user has its own pseudorandom codeword which is approximately orthogonal to all other codewords. The receiver performs a time correlation operation to detect only the specific desired codeword. All other codewords appear as noise due to decorrelation. For detection of the message signal, the receiver needs to know the codeword used by the transmitter. Each user operates independently with no knowledge of the other users. The characteristic features of CDMA include the following:

1. Users of a CDMA system share the same frequency
2. Unlike TDMA or FDMA, CDMA has a soft capacity limit. Increasing the number of users in a CDMA system raises the noise floor in a linear manner.
3. Channel data rates are very high in CDMA systems. Consequently, the symbol duration is very short and usually much less than the channel delay spread. Since PN sequences have low crosscorrelation, multipath dispersion effects which are delayed by more than a chip will appear as noise.

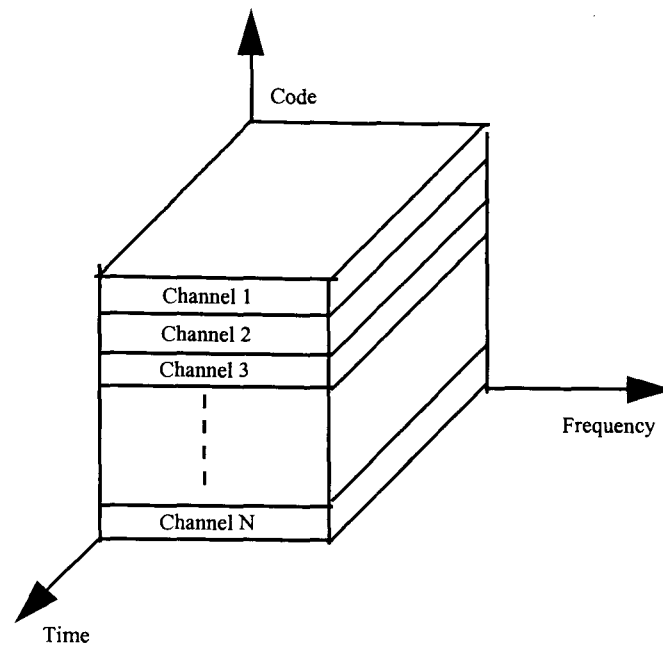


Figure 2.7 CDMA in which each channel is assigned a unique PN code which is orthogonal to PN codes used by other users.

2.6.4 Wavelength Division Multiple Access

In wavelength division multiple access (WDMA), different users transmit at different infrared wavelengths using narrow spectrum sources and a receiver employs a bandpass optical filter to select the desired channel. The characteristics of WDMA include the following:

1. Wavelength tunable optical transmitters are currently expensive, and fairly sophisticated techniques are required to tune them to a precisely defined wavelength.
2. Tunable bandpass filters are costly.

3. Because the transceiver is to have multiwavelength capability, it must probably include multiple transmitters and receivers, which are likely to be too costly for indoor optical wireless applications.

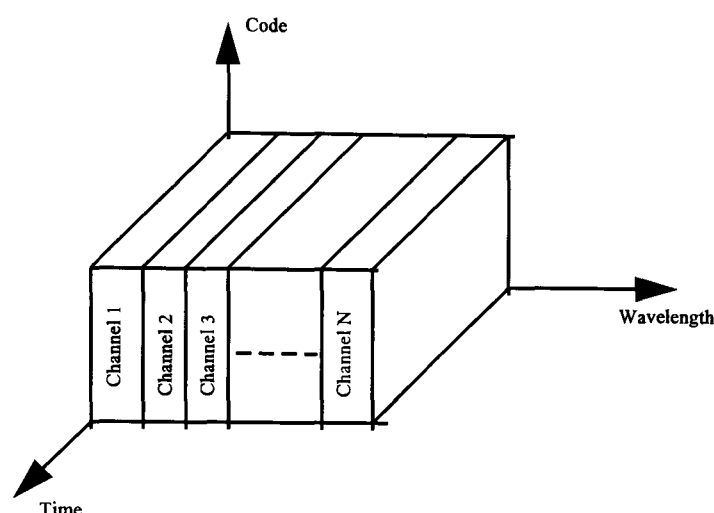


Figure 2.8 WDMA scheme

2.7 Current indoor infrared wireless systems

In the past few years, a variety of infrared wireless systems have been launched in the communication market (incorporated in portable computer, printer, and LAN). At present, most infrared links are of the directed-LOS or hybrid-LOS designs. The low path loss of these designs minimises the transmitter power requirements and permits the use of a simple, low-cost receiver. Typically, these links transmit using a single light-emitting diode (LED), which emits an average power of several tens of mW that is concentrated within a semiangle of 15°-30°. Typically the LED emission wavelength lies between 850 and 950 nm. This wavelength matches the responsivity peak of the silicon positive-intrinsic-negative (PIN) photodiode. Those systems are meant to eliminate the physical connection between the network terminals.

Hybrid-LOS links are relatively free from multipath distortion, sometimes permitting them to achieve bit rates above 100 Mb/s [22] while maintaining a very simple design. These link designs are well suited for point-to-point or point-to-multipoint applications, but are not suited for multiple-access networks, as they are unable to support full bidirectional connectivity between more than two transceivers.

Directed-LOS and hybrid-LOS links have been used for many years in remote-control units and other unidirectional, low bit rate applications. Over the past five years, the Infrared Data Association (IrDA) has established standards for short-range, half-duplex LOS links operating at bit rates up to 4 Mb/s [37,38]. 4Mb/s links employ four-pulse-position modulation (4-PPM), while 1.152 Mb/s links utilize on-off keying (OOK) with return-to-zero (RZ) pulses having a duty cycle of 0.25. Links operating at bit rates of 115.2 kb/s and below employ OOK with RZ pulse having a duty cycle of 0.1875. IrDA-compliant transmitters must emit at a wavelength between 850 and 900 nm into a semiangle of 15°-30°. Compliant receivers must have a FOV of at least 15°. Most IrDA receivers have a much larger FOV, thus most IrDA links are of the hybrid-LOS type. IrDA links are required to achieve a bit error rate (BER) not exceeding 10^{-9} (10^{-8} for 4 Mb/s links) over a range of at least 1 m, but many links achieve a range as long as 3 m. Two of the key features of IrDA transceivers are low cost and low power consumption. At present, more than 160 companies worldwide are members of IrDA.

As mentioned previously, among all infrared link designs, diffuse links are the most easy to use and robust, since no aiming of transmitter or receiver is required, and since no LOS path between the transmitter and receiver is required. However, diffuse links

have a higher path loss than their LOS counterparts, requiring high transmitter power and a receiver having a larger light collection area. Typical diffuse transmitters employ several 850-900 nm LED's which are sometimes oriented in different directions, to provide a diversity of propagation paths. When transmitting, they typically emit an average power in the range of 100-500 mW, making their power consumption higher than a typical IrDA transmitter. Diffuse receivers typically employ silicon p-i-n detectors encapsulated in hemispherical or plain cylindrical lenses, which provide some light concentration while maintaining a wide FOV. Often they employ several detectors, in which case each of them is oriented in a different direction. Wireless communication systems using diffuse infrared can be formed in two different ways, which are illustrated in Figure 2.9.

In the first technique, diffuse infrared links are used to achieve access to resources on a wired LAN. Clearly, this architecture also permits communication among the portable terminals via the wired backbone. This wireless LAN architecture is well suited for wireless data communication in offices, hospital, schools, or other heavily used environments, in which the cost of installing a backbone and wireless access points can be justified. An example of this type of wireless LAN is SpectrixLite™ [39], made by the Spectrix Corporation. This system utilises a base station to connect together up to 16 wireless access points, forming a LAN having an aggregate capacity of 4 Mb/s.

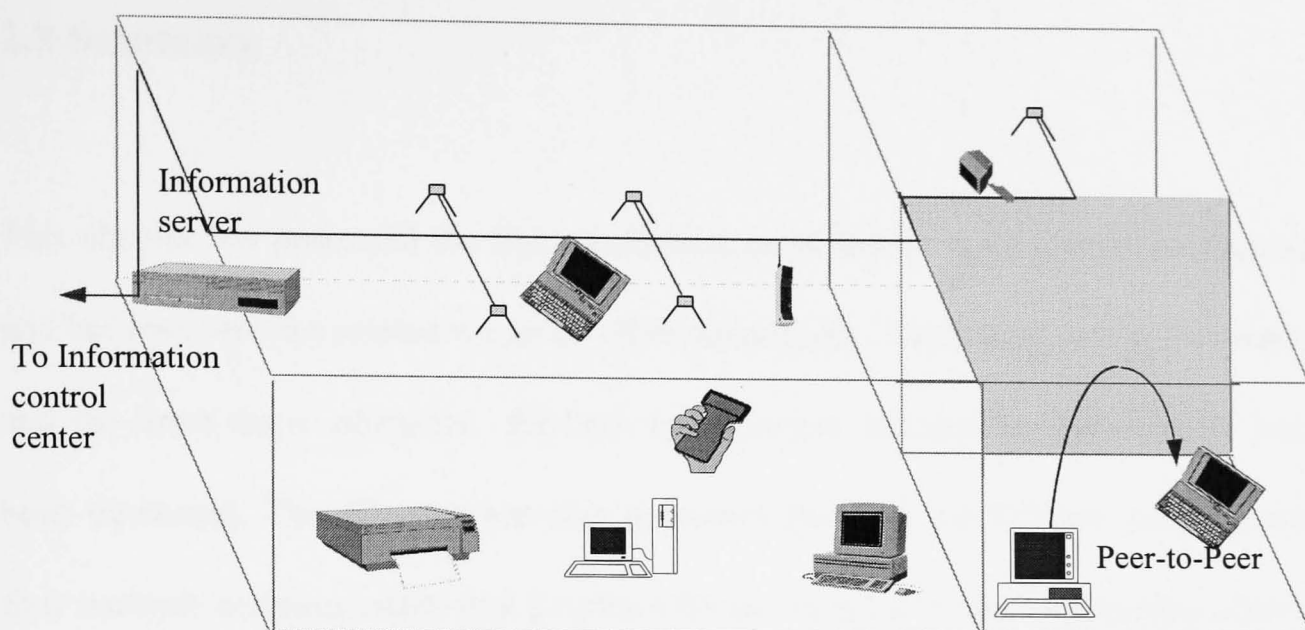


Figure 2.9 Optical wireless diffuse system

In the second technique, diffuse infrared links are employed to achieve direct, peer-to-peer communication between a number of portable and/or fixed terminals. This type of ad hoc interconnection is well suited to new or temporary work groups, for collaboration while travelling or at off-site meetings in which all nodes are located within a single room. IBM supplies a diffuse infrared ad hoc LAN operating at 1 Mb/s using 16-PPM. It is intended to achieve coverage of a 10 m × 10 m region [40].

Through judicious use of the technologies employed in currently available systems, it is possible to enhance the performance of wireless infrared systems significantly. It appears likely that 10 Mb/s diffuse links and low cost LOS links operating at tens of Mb/s can be achieved. Low cost can be achieved in the diffuse environment (where this thesis focuses) once standards emerge and are adopted. This will lead to mass production which will cause a reduction in output cost. It is worth noting that the current IrDA standard deals only with LOS links.

2.8 Summary

This chapter has presented the link configurations of indoor optical wireless systems and has reviewed the related works by other researchers. The optical safety limitations and the three major obstacles for high speed indoor infrared communication have been discussed. This Chapter has also presented the three modulation schemes and four multiple accesses techniques proposed for use in infrared communication. Finally we have reviewed the current indoor infrared wireless systems (including the communication market and Lab. research)

Chapter 3 Optical Wireless Channel

3.1 Introduction

The diffuse optical channel can be visualised as a completely connected network. Optical radiation from the base reaches every terminal within the room. A diffuse link exploits the excellent reflective properties of most indoor environments. Gfeller [3] measured the reflectivities of typical office materials such as painted surfaces, wood, carpets, and plaster walls, and found that the fraction of infrared power reflected from their surface falls between 40% and 90%. Thus, the optical signal in a diffuse link can undergo many reflections and still have appreciable energy. Gfeller also found that these surfaces are well approximated by an ideal Lambertian reflector, so that the incident infrared energy will re-radiate in all directions. This provides multiple redundant paths between the transmitter and receiver that makes the diffuse channel difficult to interrupt by shadowing.

A basic ideal wireless channel is shown Figure 3.1. There are two major impairments that influence the wireless link. These are multipath dispersion and shot noise from

background light. The shot noise from background is typically composed of a combination of fluorescent light, sunlight, and incandescent light. The background light can be quite intense, especially near windows, with a power that often exceeds the desired signal power by 25 dB or more [16]. Background light induces a high intensity shot noise in the photodetector, so that the additive noise $n(t)$ in Figure 3.1 is accurately modelled as white and Gaussian. Compared to this shot noise, the electronic thermal noise in a well designed preamplifier will be negligible.

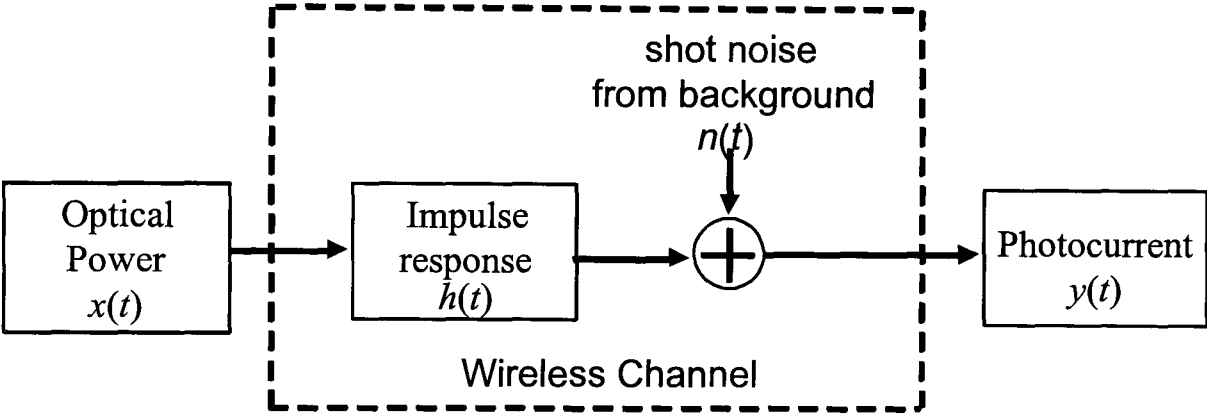


Figure 3.1 Infrared wireless channel model

Noise from ambient lights can be suppressed by inserting a bandpass optical filter before the photodetector, which ideally would transmit only light whose wavelength is near that of the laser source and reject all other wavelengths.

In some ways, the effect of multipath propagation on an infrared signal is similar to that on a radio signal. The optical signal in transit from the transmitter to the receiver undergoes temporal dispersion (i.e. multipath dispersion) due to reflections from walls and other reflectors. The intersymbol interference (ISI) that results is a primary impediment to communication at high speeds. Multipath dispersion, is modelled by a

linear baseband impulse response $h(t)$. The channel can be modelled as a baseband linear system, with input power $x(t)$, output current $y(t)$, an impulse response $h(t)$ and background noise $n(t)$ (see Figure 3.1). The channel model can be written as

$$y(t) = Rx(t) \otimes h(t) + n(t) \quad (3.1)$$

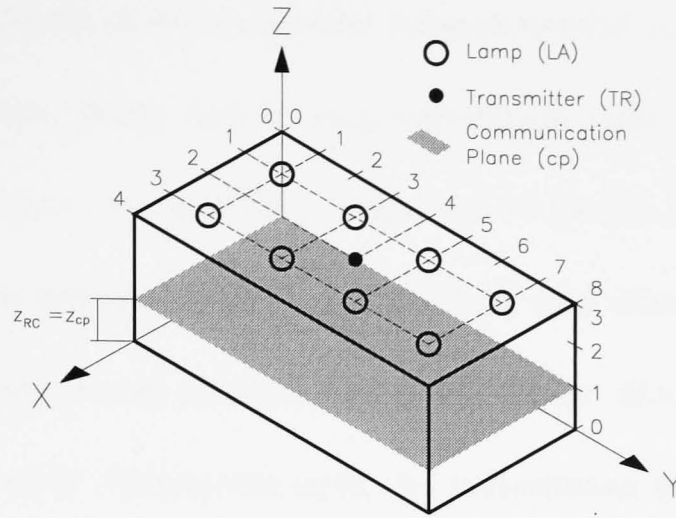
where the ' \otimes ' symbol denotes convolution and R is the detector responsivity (A/W). In this chapter we present a method for calculating the impulse response and background noise of a room with an arbitrarily placed transmitter and a mobile receiver (i.e. different receiver locations). Once calculated, the impulse response and noise level can be used to analyse the effects of multipath dispersion and noise on the performance of indoor optical communications systems. The impact of multipath dispersion and noise effects on a typical system will be discussed in Chapter 5.

3.2 Test room set-up

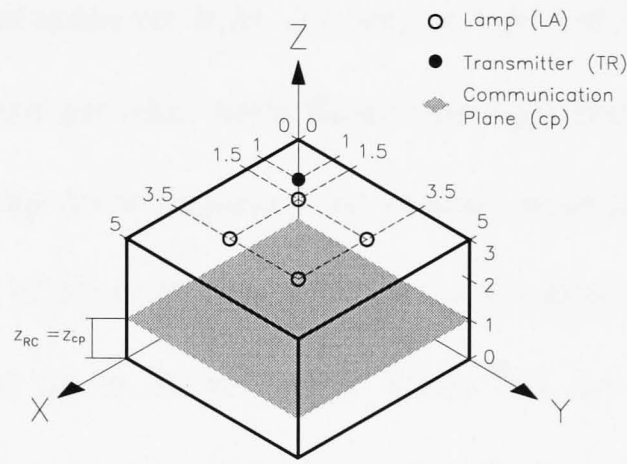
To accommodate the calculation of ambient noise and multipath dispersion, two test room configurations have been considered which represent typical office room dimensions. The various parameters of the test rooms are listed in Table 3.1 (also see Figure 3.2):

Parameter	Test room A	Test room B
Room		
Length (x)	4 m	5 m
Width (y)	8 m	5 m
Height (z)	3 m	3 m
ρ (walls and ceiling)	0.8	0.8
Transmitter		
mode	1	1
x	2 m	1 m
y	4 m	1 m
z	3 m	3 m
Receiver		
area	5 mm ²	5 mm ²
FOV	90°	90°
x	1,2,3 m	1,2,3,4 m
y	1,2,3,4,5,6,7 m	1,2,3,4 m
z	1 m	1m
Background noise	8 lamps (LAs) have been placed at the following locations.	4 lamps (LAs) have been placed at the following locations.
Incandescent Light	LA1 (1 , 1 , 3) LA2 (1 , 3 , 3) LA3 (1 , 5 , 3) LA4 (1 , 7 , 3) LA5 (3 , 1 , 3) LA6 (3 , 3 , 3) LA7 (3 , 5 , 3) LA8 (3 , 7 , 3)	LA1 (1.5 , 1.5 , 3) LA2 (3.5 , 1.5 , 3) LA3 (1.5 , 3.5 , 3) LA4 (3.5 , 3.5 , 3)

Table 3.1 Parameters of multipath simulation



(a)



(b)

Figure 3.2 Test room set-up (a) test room A (4m×8m×3m) (b) test room B (5m×5m×3m)

3.3 Ambient noise

Many environments contain intense ambient infrared radiation arising from sunlight, skylight, incandescent and fluorescent lamps and other sources [41]. Ambient light is the main source of noise in wireless optical communications. The infrared content of ambient light interferes with the reception of IR radiation and, if extensive, can overload the receiver photodiode and drive it beyond its operating point.

The optical power spectra of some common infrared sources are shown in Figure 3.3 [3]. Incandescent light, being rich in long wavelength light, has the worst effect because its spectral peak overlaps that of GaAs and Si diodes. Daylight contains less IR radiation than incandescent light, but if sunlight falls directly onto the receiver lens, the DC component can saturate the photosensitive diode, preventing proper operation of the receiver. Fluorescent light, the predominant type of illumination in office environments, contains a relatively small amount of IR radiation. However, unlike sunlight and incandescent light, fluorescent light induces interference that is nearly deterministic and periodic, since fluorescent light flickers at a constant rate determined by the lamp drive frequency. At present, most lamps are driven at the power line frequency of 50 or 60 Hz, and they induce interference at harmonics of power line frequency, up to 50 kHz [41]. While this interference is potentially detrimental to IR links, it can usually be easily eliminated by careful choice of modulation scheme, and through electrical highpass filtering [43].

The noise from ambient light can be suppressed by an optical filter in front of photodetector. Figure 3.4 shows a typical response for such a filter [3]. It has been shown that, in case an inexpensive daylight filter is placed in front of the photodetector, incandescent lamps introduce a much higher level of ambient noise than low and high frequency fluorescent lamps [43]. Optical spectral measurements carried out within this investigation (Figure 3.5) confirm this fact and, furthermore, show that also halogen lamps inject a considerable amount of their spectral energy into the passband of the photo detector with daylight filter.

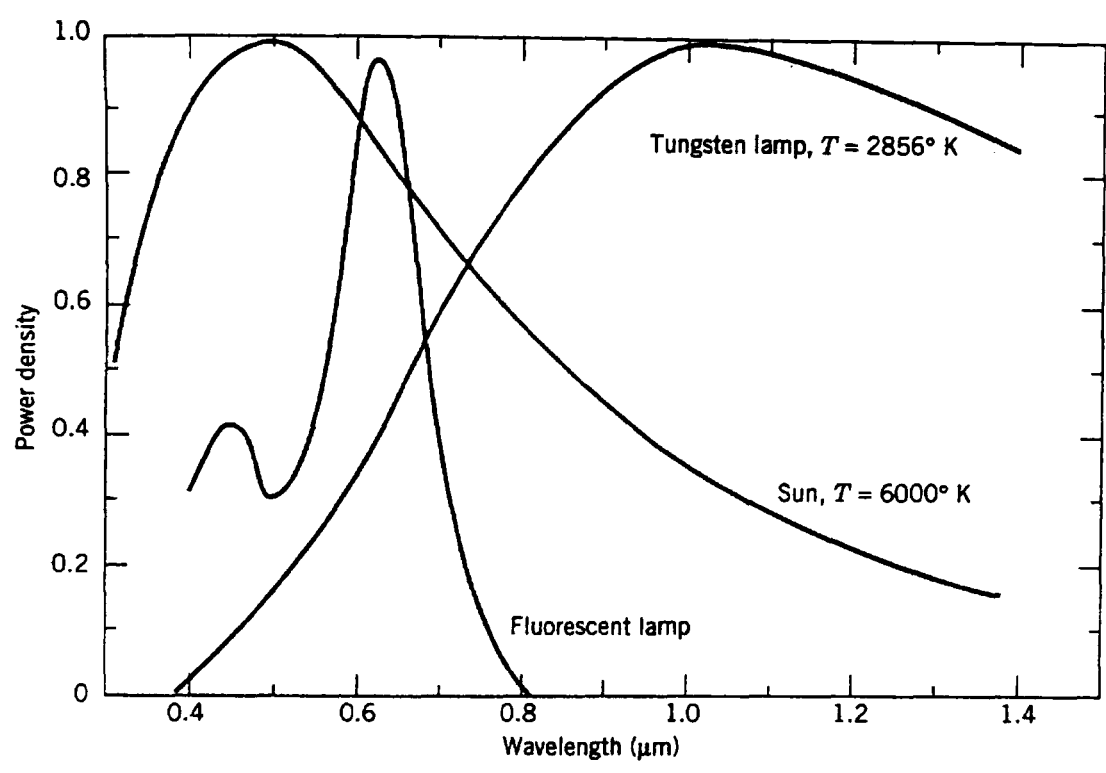


Figure 3.3 Optical power spectra of common ambient infrared sources [3]

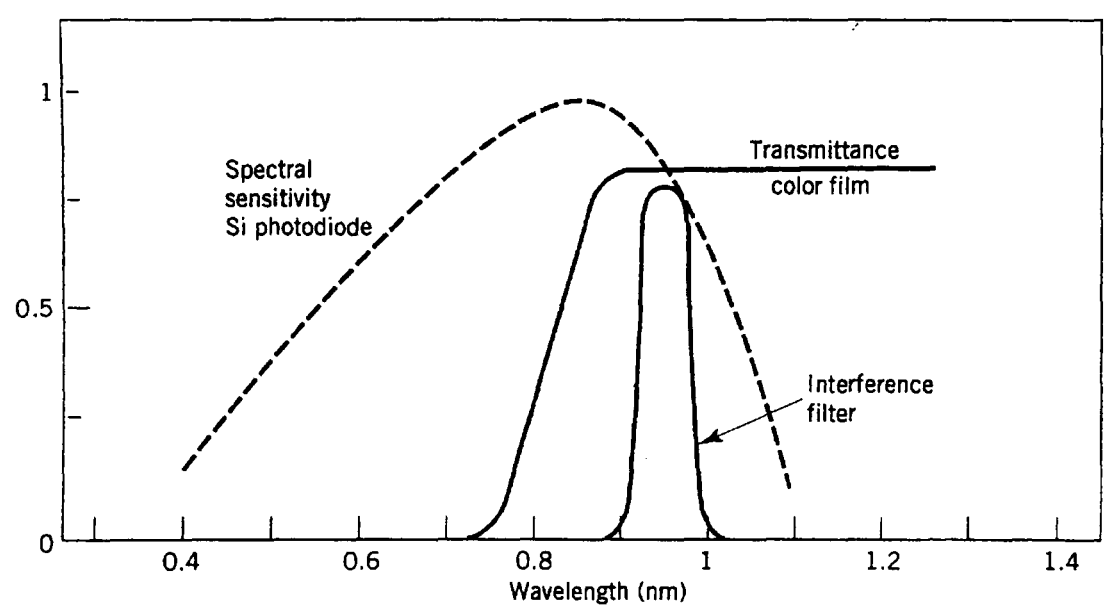
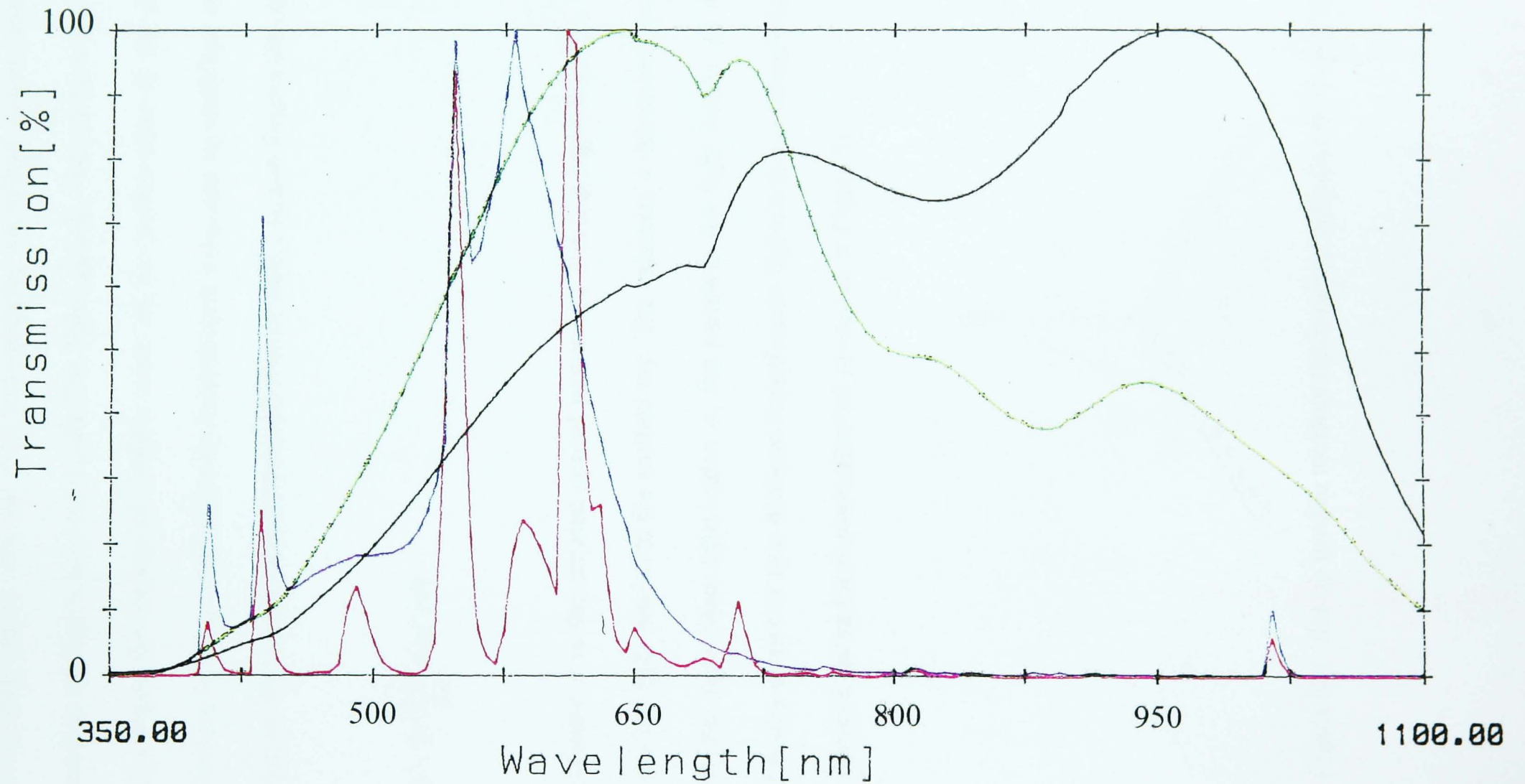


Figure 3.4 Noise reduction using an optical filter

Legend

- Red: OSRAM Dulux EL 41-827 20W 220-240V 50/60Hz (HF fluorescent light)
Blue: Philips fluorescent lamp 240V (LF fluorescent light)
Green: Power Letric PLI 5551 220V/240V 50W ES Dichroic reflector Halogen lamp
Black: Crompton Lighting ES-E27240V 75W Reflector Spot R95 Diffused



Incandescent and halogen spotlights are highly directive, suggesting a burn-out effect of the data signal underneath the lamps. Because of the substantial amount of ambient noise they cause, and the high concentration of optical power, incandescent and halogen spotlights have been modelled. Subsequently, these models have been used to investigate the impact of ambient noise on the performance of the photo detector. Tavares [44] has shown that an incandescent lamp can be modelled as a lambertian source. The angular intensity distribution of such a source follows the equation

$$I = P \frac{n+1}{2\pi} \cos^n(\theta) \tag{3.2}$$

whereby P is the emitted optical power and θ is the angle from the normal of the emitting light source to the emitted ray. The exponent n determines the spread of the emitted light beam (the higher n , the narrower the light beam). In this study, the intensity spread of four different incandescent lights and one halogen lamp have been measured, using the measurement set-up shown in Figure 3.6.

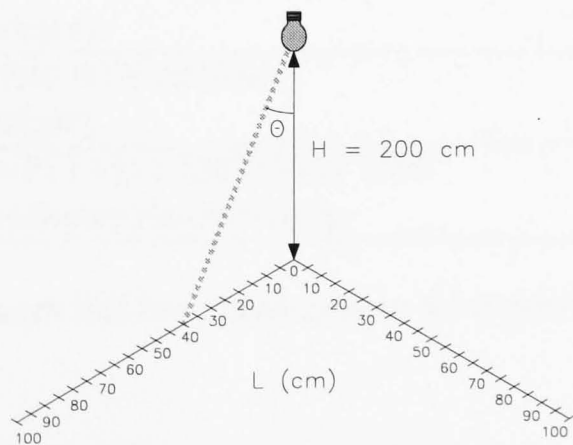


Figure 3.6 : Set-up used to measure the intensity diffusion of artificial light sources

Measurements of the received optical power levels were taken along both axes, in steps of 5 cm and over a distance of 1 m. Measurements were carried out by means of a high speed, medium area silicon photodiode, and United Detector Technology Inc. optical meter. As expected, results were equal along both axes. Since power levels were measured using the same optical detection area, they do represent the intensity. In order to obtain a platform of comparison within one graph, the measurements were converted into percentages. A curve-fit was carried out using the formula

$$P(\%) = a(n + 1)(\cos(\theta))^n \tag{3.3}$$

where θ is the angle from lamp to photodetector. The values of a and n were calculated by curve-fit and displayed in Table 3.2.

Lamp	Reference	n	a
A	Philips PAR 38 Economy (spotlight with diffuser)	36.1	2.64
B	Crompton Lighting 75W Reflector Spot R95 Diffused ES-E27240V	31.8	4.41
C	GE Lighting R80 60W reflector (reflector spotlight)	5.64	15.3
D	GE Lighting R63 60W reflector (reflector spotlight)	12.7	7.27
E	Power Letric PLI 5551 220V/240V 50W ES Dichroic reflector Halogen lamp	13.4	6.87

Table 3.2: Light sources that have been used in the experimental measurements

The radiation measurement results and curve fit values are displayed in Figure 3.7 and show that incandescent spot lights are indeed lambertian and that also halogen lamps have this characteristic.

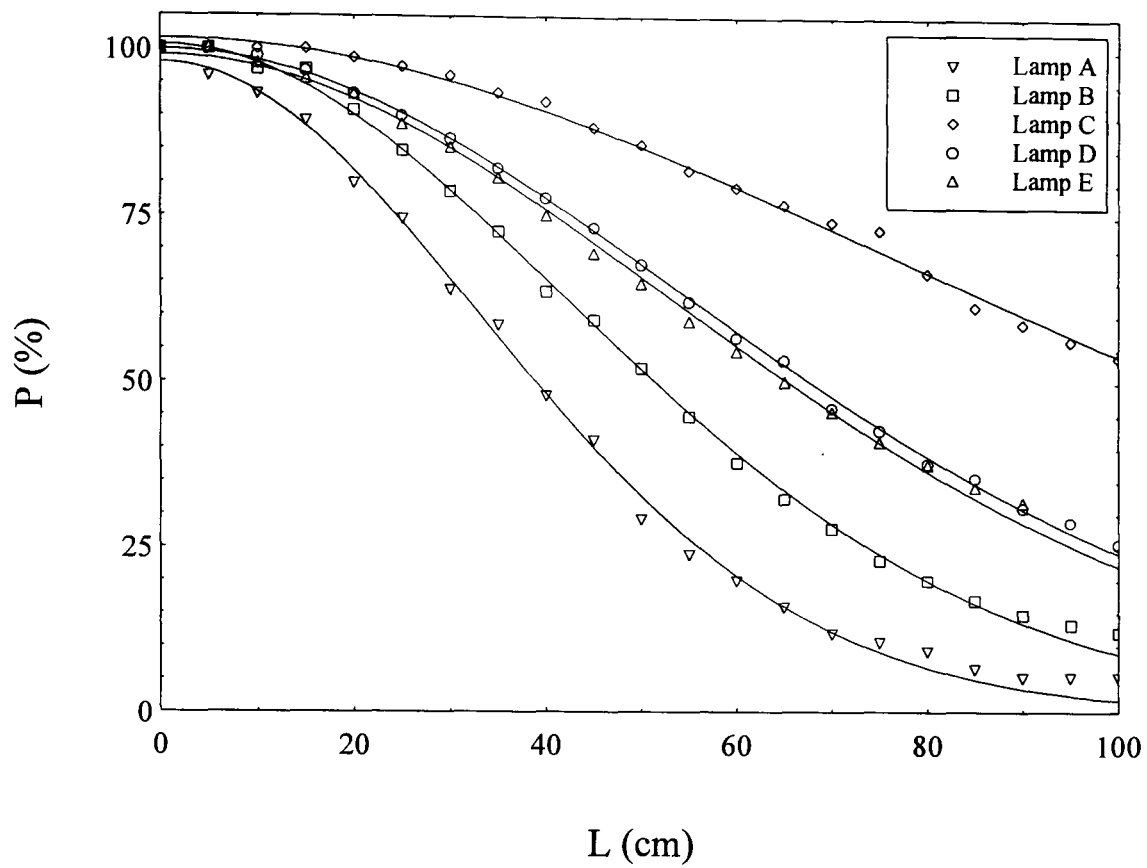


Figure 3.7 Measured normalised power distribution versus distance for various light sources

To accommodate the investigation of the receiver's performance with regard to ambient noise, the spotlight with the highest n -factor (36.1) has been chosen. The intensity spread is an important characteristic of a light source; however, it does not account for propagation losses that are associated with an optical wave. As with any other electromagnetic wave, the propagation loss is inversely proportional to the squared distance. With P_{LA} being the total optical power emitted by the lamp, the optical power received by an optical detector (P_{pd}) at a distance r from the lamp may be written as

$$P_{pd} = \frac{P_{LA}}{k \cdot r^2} \cos^n(\theta) \quad (3.4)$$

where k is a constant. P_{LA} and k are unknown but k can be obtained by assuming unity optical lamp power. Hence equation 3.4 becomes

$$P_{pd} = \frac{\cos^n(\theta)}{k \cdot r^2} \quad (3.5)$$

The constant k can be calculated using the fact that the amount of emitted optical power must equal the amount of received optical power. As the emitted power has been assumed unity, so k can be written as

$$k = \sum_{\forall_i} \frac{\cos^n(\theta_i)}{r_i^2} \quad (3.6)$$

To enhance the accuracy of the calculation of k ; test room A, above the communication plane, has been divided in small, equal squares. Figure 3.8 shows the configuration for a square with a side (d) of 1 m. For the calculation of k , however, d has been taken as 1 mm. Distances (r_i) and angles (θ_i) from the lamps to the various elements have been calculated to the centre of each square. The value of k was found from equation 3.6.

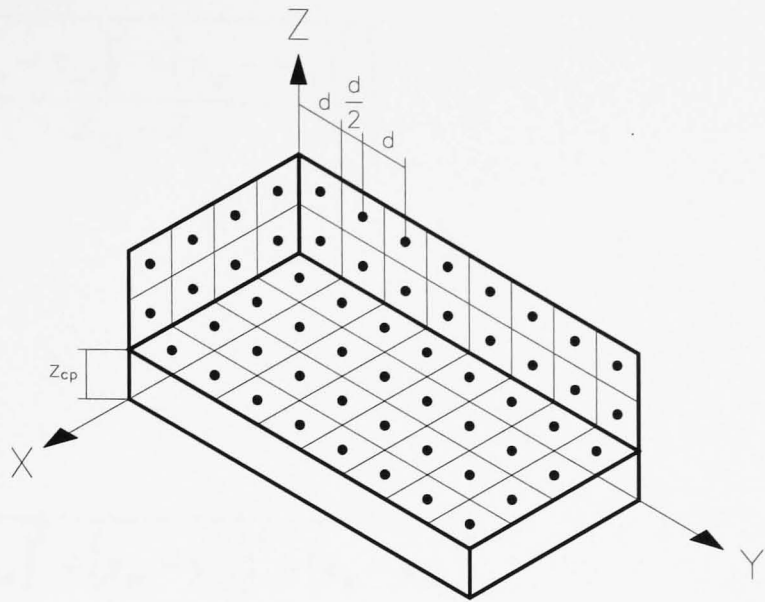


Figure 3.8 : Areas used to calculate the constant k (Room A)

The distance (r_{LAcp}) and angle (θ_{LA}) from a lamp to a single point can be calculated by equation 3.7 and 3.8. Figure 3.9 shows the set-up of test room A used for calculating the noise level.

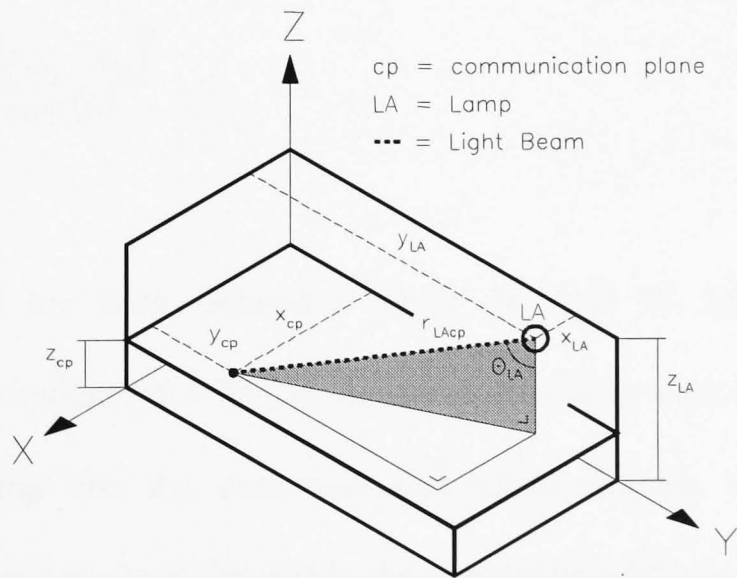


Figure 3.9 Modelling the noise level received at communication plane (Room A)

$$\theta_{LA} = \tan^{-1} \left(\frac{\sqrt{(x_{cp} - x_{LA})^2 + (y_{cp} - y_{LA})^2}}{Z_{LA} - Z_{cp}} \right) \quad (3.7)$$

and

$$r_{LAcp} = \sqrt{(x_{cp} - x_{LA})^2 + (y_{cp} - y_{LA})^2 + (z_{cp} - z_{LA})^2} \quad (3.8)$$

In order to determine the power emitted by the lamp p , P_{LA} , the received power 2 meters directly below the lamp was determined. The measured optical power immediately under the lamp equalled 3.75 mW. Knowing that the active detection area of the photodetector (A_{pd}), used to measure P_{pd} , was 41.3 mm², and the size of the areas to calculate k was taken as $d = 1$ mm, equation 3.4 can be written as

$$P_{LA} = \frac{P_{pd}}{A_{pd}} \cdot d^2 \cdot \frac{k \cdot (z_{LA} - z_{cp})^2}{\cos^n(0)} \quad (3.9)$$

It was found that the lamp radiated a power of 68.54 W. Moreover, given the directionality of the source ($n = 36$), it was found that more than 98% of the ambient noise of each lamp hits the communication plane directly. Contributions from reflections therefore have been ignored in the calculation of the impact of the ambient noise.

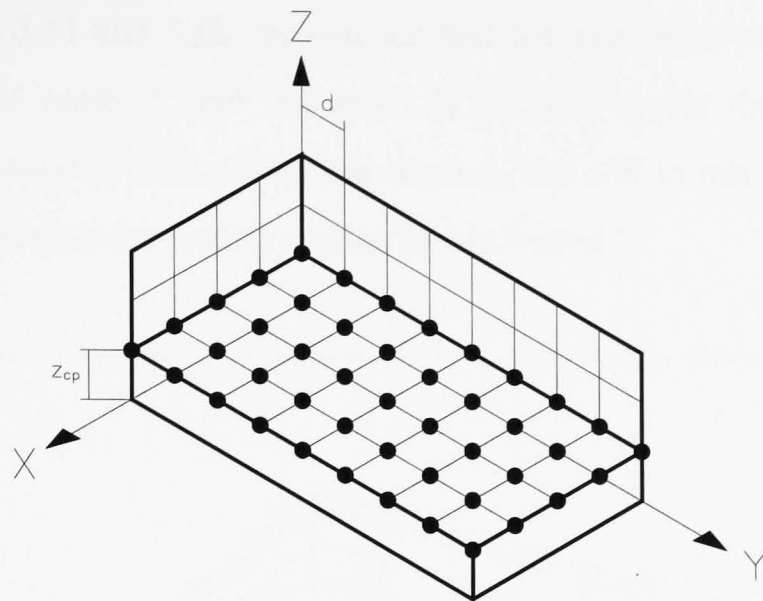


Figure 3.10 Points where the received noise levels was calculated

Figure 3.10 displays the points at which the received noise levels have been calculated. The distance d between these points was taken to be 10 cm and power levels were calculated for a photo detector with an active area of 5 mm^2 . Figures 3.11 and 3.12 show the results (details also shown in appendix 1).

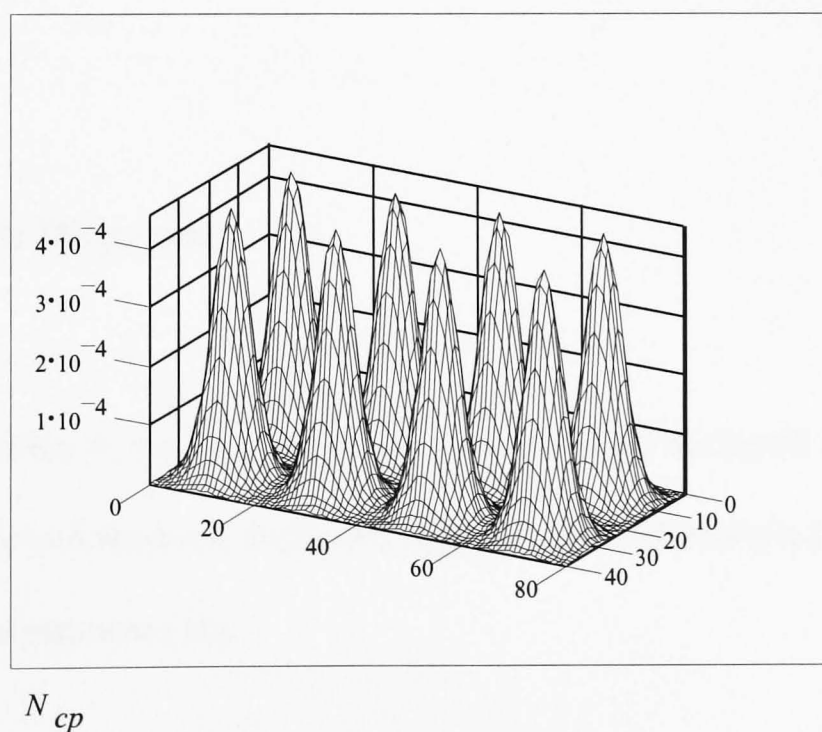


Figure 3.11 Noise caused by an incandescent spotlight with $n = 36.1$ at Room A

From the Figures 3.11 and 3.12, we can see that the maximum background noise is 0.454 mW in test room A and test room B (directly under the spot light). The minimum noise power is 1.42 μ W in test room A, 0.2 μ W in test room B. This data will be used to calculate the system sensitivity in Chapter 5.

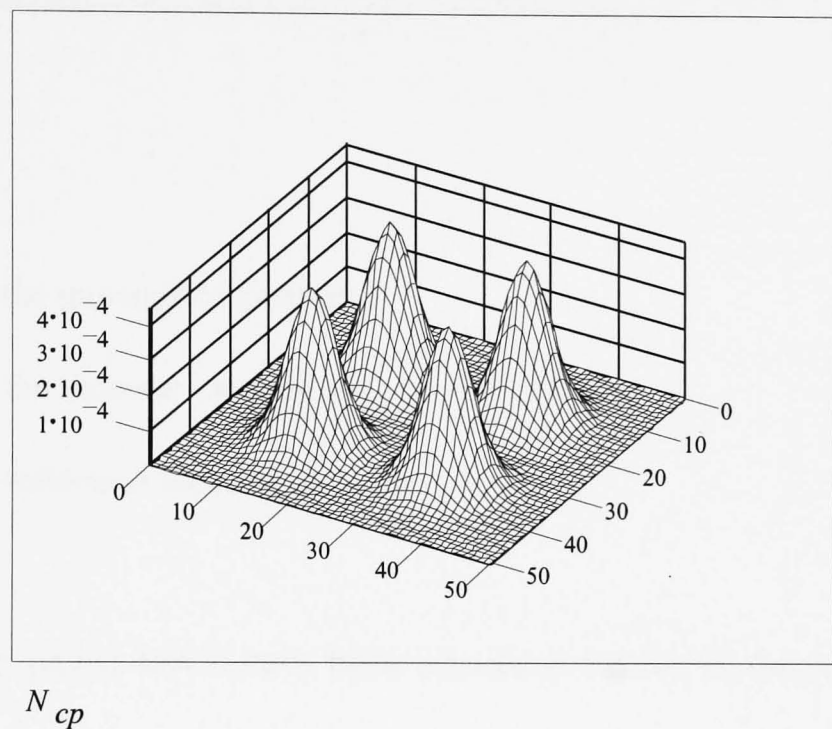


Figure 3.12 Noise caused by an incandescent spotlight with $n = 36.1$ at room B

3.4 Multipath Dispersion

In Chapter 2 section 4, we have introduced and discussed multipath dispersion. For a fixed transmitter and receiver, multipath dispersion can be modelled by using a fixed channel impulse response [10].

Multipath dispersion has been modelled by calculating the time a light ray travels on its way from transmitter to receiver and the power level that is associated with each particular light ray. The time it takes to travel a transmission path is simply calculated

by dividing the path's distance by the velocity of light ($3 \times 10^8 \text{ ms}^{-1}$). The transmission delay time can be written as

$$T_d = \frac{\sqrt{(X_{TR} - X_n)^2 + (Y_{TR} - Y_n)^2 + (Z_{TR} - Z_n)^2} + \sqrt{(X_n - X_{RX})^2 + (Y_n - Y_{RX})^2 + (Z_n - Z_{RX})^2}}{c} \quad (3.10)$$

where

X_{TR}, Y_{TR}, Z_{TR} , is the transmitter location

X_{RX}, Y_{RX}, Z_{RX} , is the receiver location

X_n, Y_n, Z_n is the reflection element location

Received signal power levels have been calculated similar to the levels of ambient noise in section 3.3. The transmitter has been taken to be highly diffuse, emitting the signal as a lambertian source with $n = 1$. Being highly disperse, reflections cannot be ignored. In order to account for the influence of reflections on the detected OW signal; the ceiling and the walls above the communication plane have been divided into square-shaped reflection elements of $10 \times 10 \text{ cm}^2$ for first order reflections, and $50 \times 50 \text{ cm}^2$ for second order reflections. A configuration with reflection elements of $1 \times 1 \text{ m}^2$ is shown in Figure 3.13. The light rays are considered to hit the reflection elements in their centre.

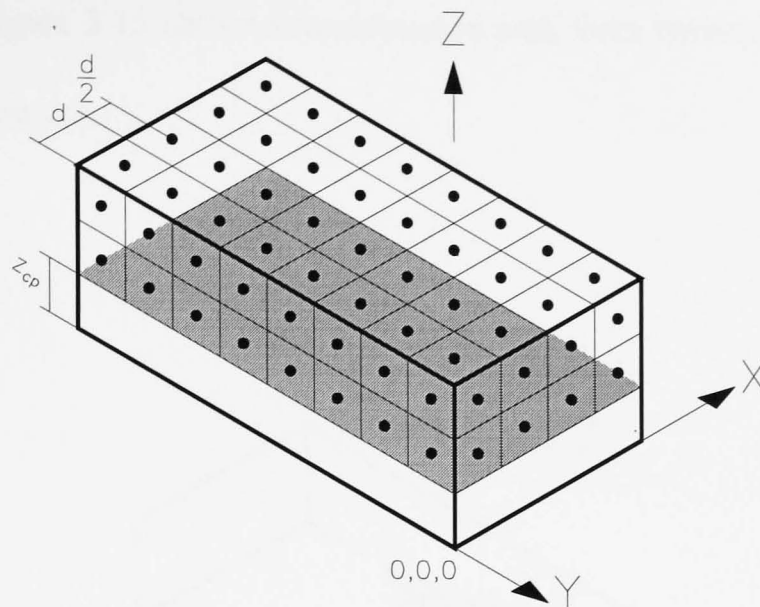


Figure 3.13 Reflection elements

As shown in Figure 3.14 the receiver has been considered to have an all-round detection angle of 180° (ie. $\text{FOV} = 90^\circ$) pointed towards the ceiling.

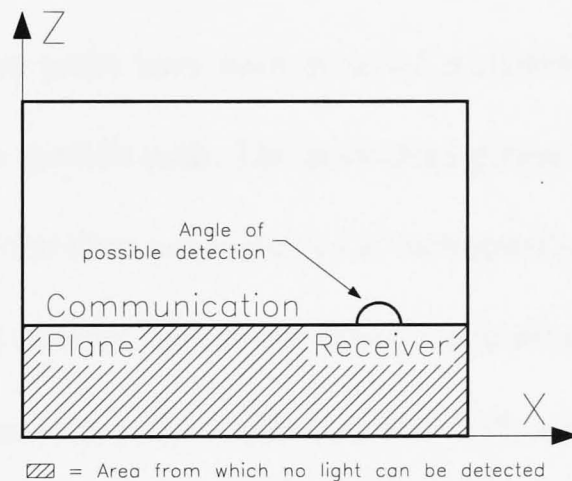


Figure 3.14: Angle of possible detection

Reflections from the ceiling and walls can be considered as small, Lambertian optical power sources with $n=1$. Hence, to account for the power levels associated with the paths that hit the receiver from a reflection, calculations have been conducted in a similar fashion as power levels associated with rays that hit the receiver directly from

the transmitter. Figure 3.15 shows a transmission path from transmitter to the receiver via a reflection element.

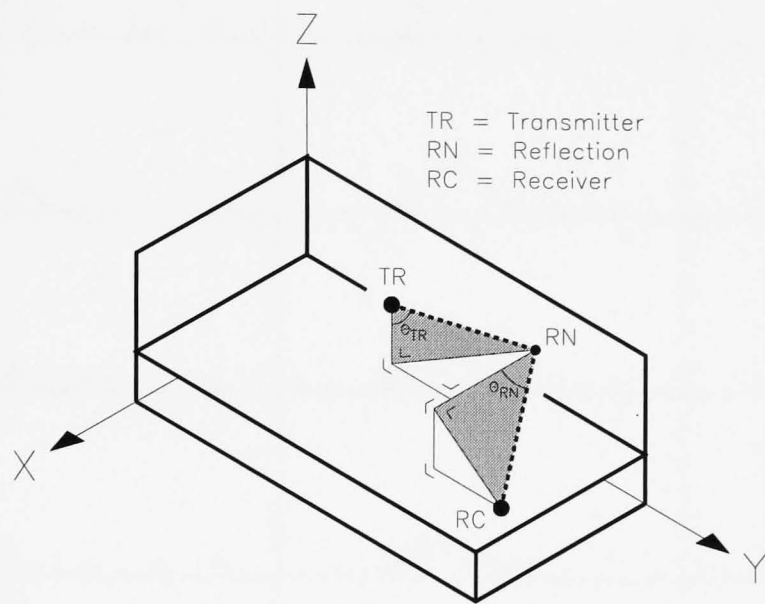


Figure 3.15: Transmission path through a reflection

The various transmission paths have been grouped according to the time it takes the emitted light to travel a specific path. The associated power levels within each group have been summed and the time associated with each specific group was taken as, the time in the middle of its interval. The above described method calculates the multipath dispersion of an instantaneous pulse (delta function) with a magnitude that equals the maximum optical power of the transmitter. The response to a block shaped pulse can be found by convolving the results for the instantaneous pulse with the block pulse. The impulse responses simulated are shown in Figure 3.16 for test room A and in Figure 3.17 for test room B.

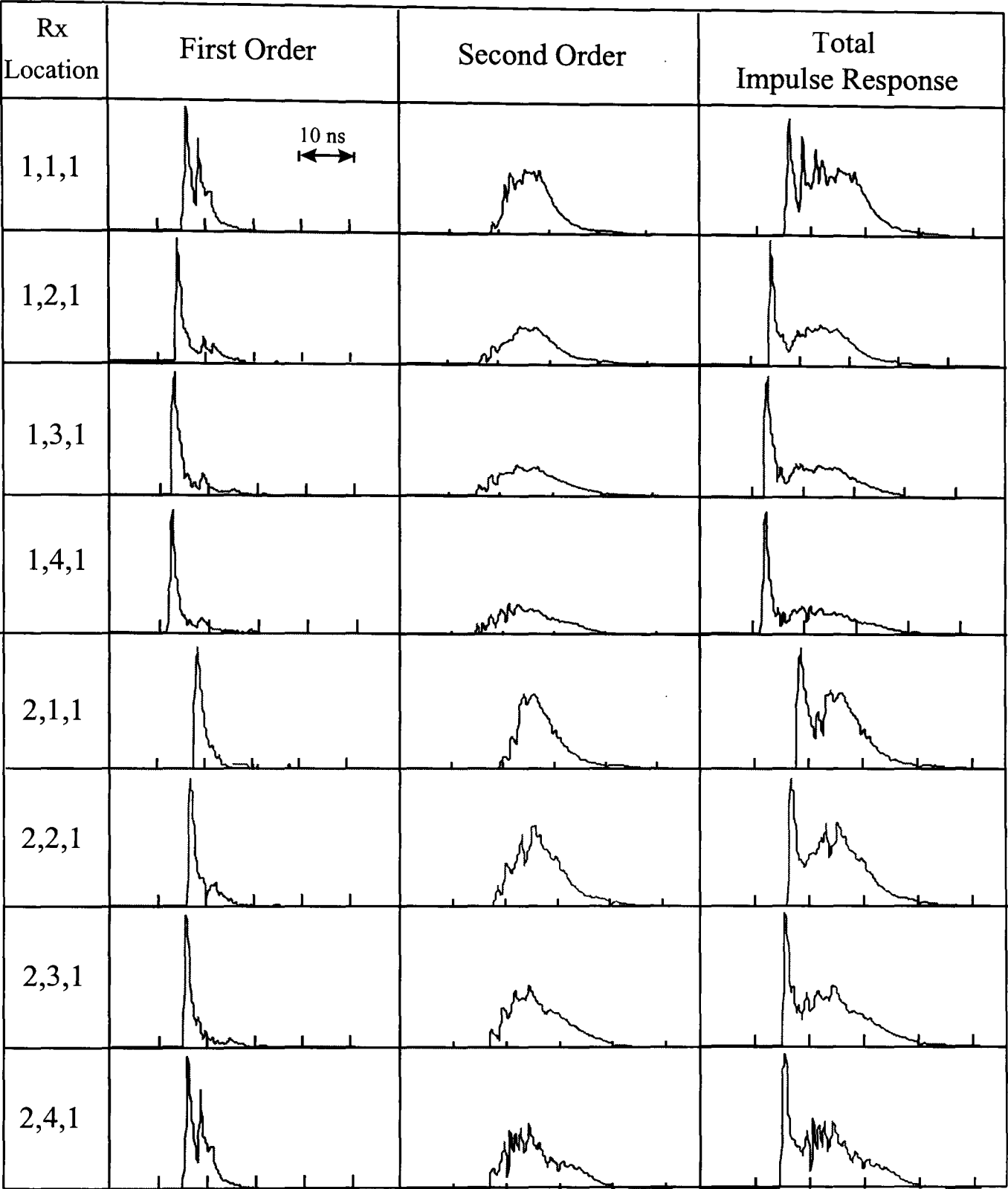


Figure 3.16 Channel impulse response (Test room A)

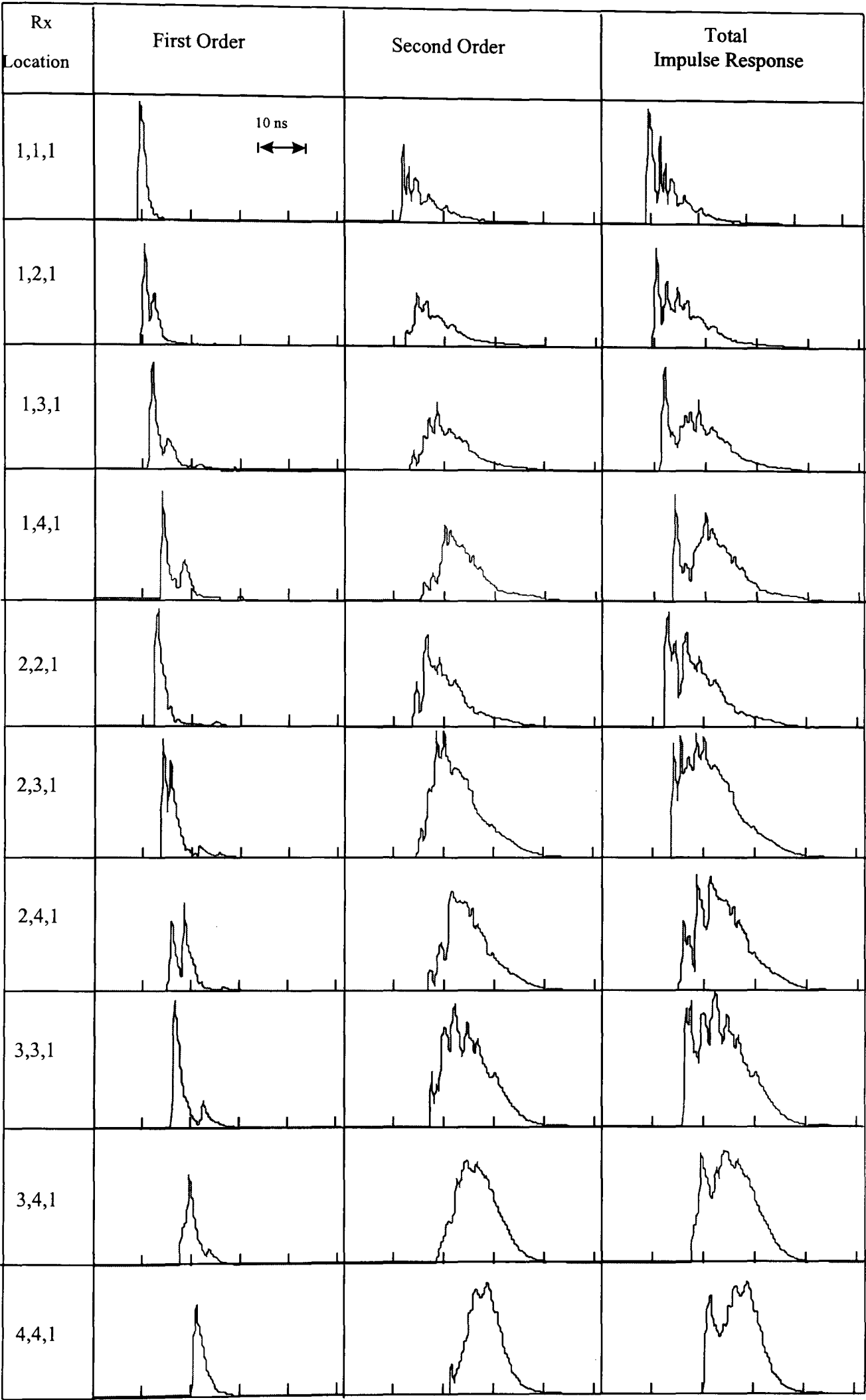


Figure 3.17 Channel impulse response (Test room B)

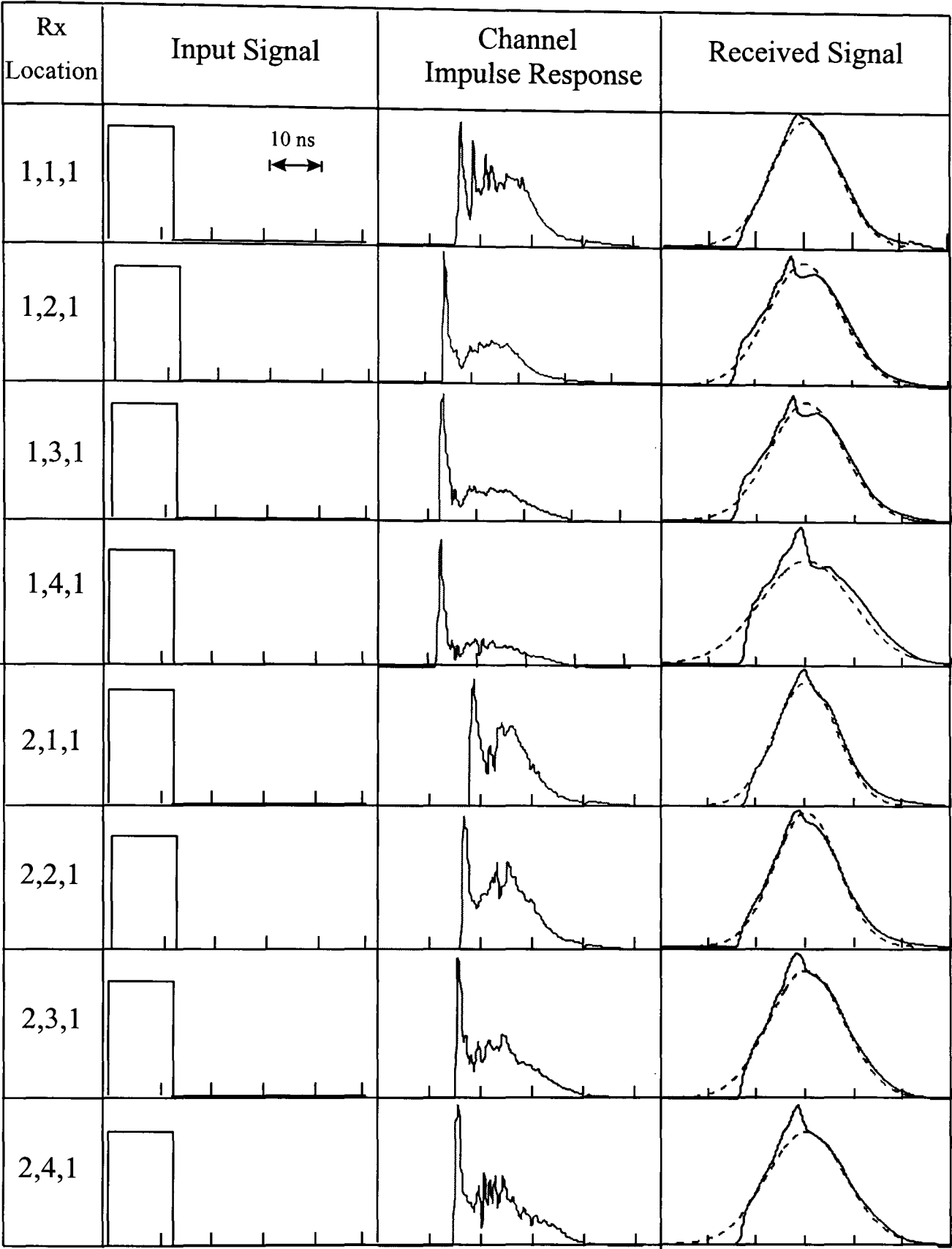


Figure 3.18 Pulse response at various locations on the communication plane at room A

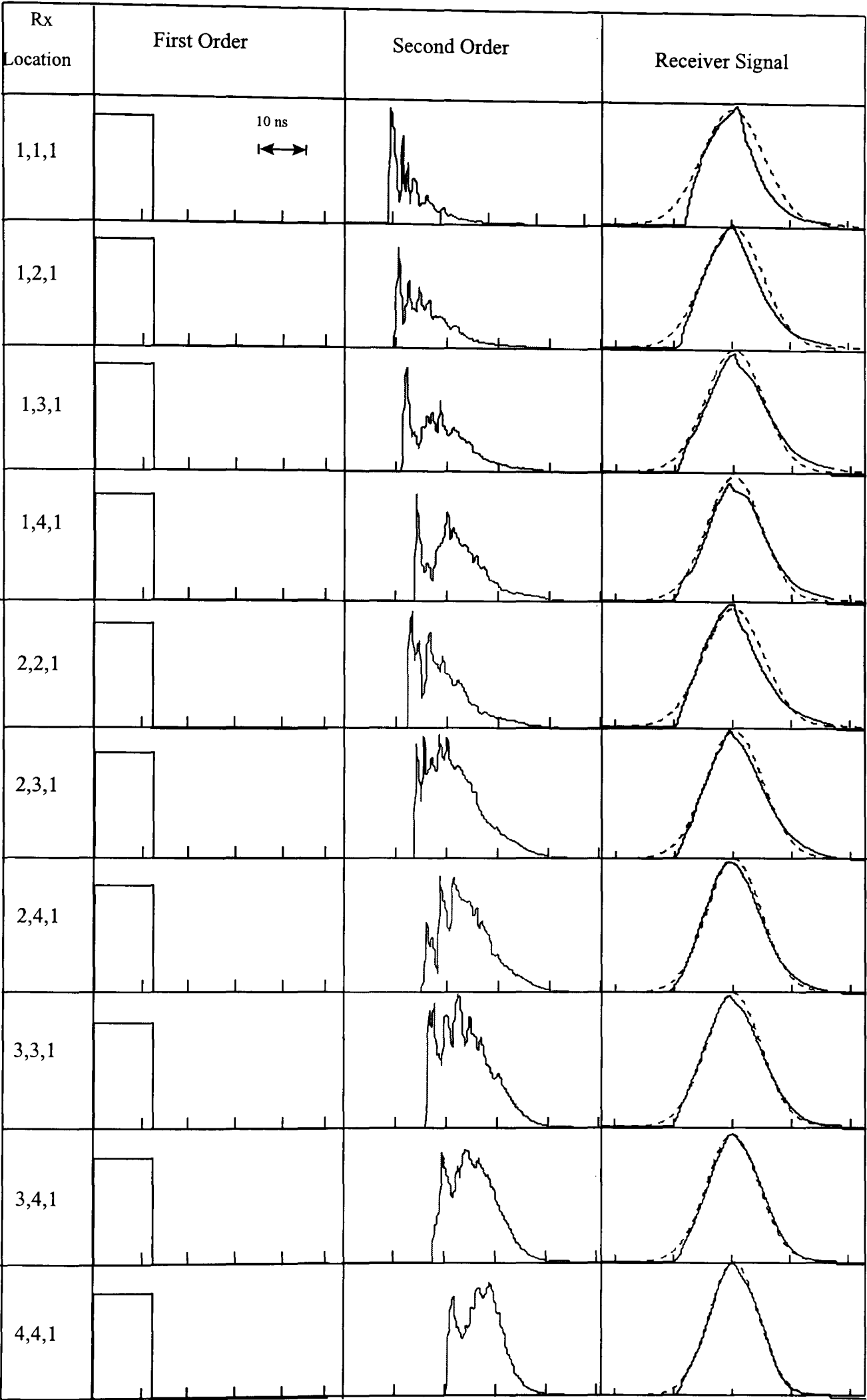


Figure 3.19 Pulse response at various locations on the communication plane at room B

Figures 3.18 and 3.19 display the results at various locations on the communication plane. The received pulses correspond to transmitted pulses with a duration equal to 12.5 ns. This pulse duration has been selected as it corresponds to a 10 Mbit/s PPM system with a coding level $M = 5$ and modulation index $m = 0.8$. This system will be described in Chapter 5. Also shown is the best Gaussian fit for the received pulses. The Gaussian estimation has subsequently been used to calculate the impact of multipath dispersion on the sensitivity performance of the receiver. The result of multipath effect will be shown in Chapter 5. It is to be observed here that approximating the received pulses with a Gaussian shape, has resulted in a close fit in the majority of the cases. This makes the analytic treatment of Chapter 5 more tractable.

3.6 Summary

This chapter has presented the optical wireless channel characteristics. The background light noise and multipath dispersion effects have been introduced. This chapter has also presented a mathematical model for calculating background noise level and channel impulse response. The results have shown that the received signal can be matched to a Gaussian pulse using different pulse variances. The results will be used to evaluate the performance of the optical wireless PPM system to be studied in Chapter 5.

Chapter 4 Optical receiver design

4.1 Introduction

The receiver is a critical part of an optical communication system since it often dictates the overall system performance. The function of the receiver is to detect the incident optical power (by a photodetector) and extract from it the information that is being transmitted. In a digital communication system the receiver output consists of the regenerated data and normally the recovered clock as well. In an analog transmission system the receiver must also demodulate the detected signal to obtain the original transmitted message.

Of most importance to the optical receiver are the photodetector and the following low noise preamplifier. Together, these two elements dictate many of the receiver characteristics as well as its performance. The receiver must achieve the above function under a number of requirements that relate to system performance. Of primary importance is the receiver sensitivity, which determines the minimum incident optical power required at the receiver in order to satisfy a specified value of

bit error rate (for digital systems) or signal-to-noise ratio and signal-to-distortion ratio (for analog systems). A complete understanding of the optical receiver and system impairments including noise and other degradation sources is necessary to examine all the trade-offs involved in the receiver design because of the conflicting requirements.

The photodetector used in optical communication systems can either be a PIN or avalanche photodiode (APD). The important requirements to be met by the photodiodes for optical wireless diffuse systems include a fast response time (for high speed transmission), a low capacitance (for wide bandwidth), and a large area (for maximum signal collection). Unfortunately, a large area photodiode will have a high capacitance, which will limit the bandwidth. In this project, we will use bootstrapping techniques to reduce the photodiode capacitance.

Receiver design for optical wireless communication systems has been addressed in various papers [45-47]. McCullagh and Wisely have designed an APD receiver for a 155 Mbit/s optical wireless link [45]. Nichols and Unwin have employed bootstrapping techniques to minimise the effects that the large photodiode capacitance has on the receiver bandwidth [46]. Yun and Kavehrad have proposed a new approach: diffuse multi-line-of-sight configuration, which is an approach that tries to reduce the required power level of a diffused infrared system [47]. In this chapter we examine the current receiver design strategies and identify their limitations. We will also present a PIN-BJT receiver which employs bootstrapping and evaluate its sensitivity.

4.2. Performance limitations

The receiver-sensitivity analysis of optical receivers is more involved than traditional communication theory, which mainly treats signal detection with additive Gaussian noise. The complication is due to the quantum nature of the photodetection effect, creating a signal-dependent and time-variant Poissonian noise process. Thus there exists an upper limit for the receiver sensitivity even in the theoretical case of perfect transmission medium and noiseless receiver. The problem is much further complicated by the non-Gaussian distribution of the avalanche gain.

Receiver design for optical communication systems has been addressed in various papers [48-51], mostly by Personick, who in his pioneering work formulated the theoretical analysis. In his work, Personick [48,49] formulated the theoretical sensitivity analysis for digital optical receivers, which has been used extensively to date. To simplify the analysis, the Gaussian approximation for the APD gain distribution was used. Muoi and Hullet [51] later extended Personick's analysis to multilevel operation. A simplified form of Personick's theory was also developed by Smith and Garrett [50]. The validity of the Gaussian approximation was checked with various exhaustive and more exact calculations by Personick and coworkers [52].

The function of the optical receiver is to extract the optical signal from various noise sources (both signal dependent and signal independent) and reconstruct the information correctly. The major noise sources associated with signal detection are:

- **Thermal noise:** This is associated with the preamplifier/detector bias and feedback resistances as well as active device parameters such as the BJT base spreading resistance, r'_{bb} .
- **Shot noise:** Associated with the bias currents for the BJT devices or gate leakage current for FET devices.
- **Photodetector noise:** The detector leakage current acts as a shot noise source and there is an 'excess' noise associated with the avalanche process in APD's.
- **Quantum noise:** Even when all the other noise sources are zero, there will be a fundamental noise source associated with the random photon arrival. This leads to a fundamental receiver sensitivity design target of 10.5 photons/bit at a bit error rate of 10^{-9} . Under normal circumstances, this intrinsic noise source is negligible compared to the previous noise sources and so is normally ignored.

The main criteria for the design of optical pre-amplifiers is to select appropriate detector and active devices in order to minimise the noise for a given receiver bandwidth. This can only be done after having gained an understanding of the basic receiver noise model.

4.3 Receiver noise analysis

In this section we consider the noise analysis of optical receivers for use in digital optical communication systems.

The optical receiver can be modelled by an equivalent circuit [49] as shown in Figure 4.1. The photodiode is represented by a signal current source $i_s(t)$ and a dark current source i_d which represents the noise contribution from the current flowing in the photodetector. i_l is the noise associated with the bias and feedback resistors. The input equivalent noise sources of the preamplifier are represented by the shunt current noise generator, i_a , and the series voltage noise generator, e_a . The diode capacitance is represented by C_d while C_s represents the stray capacitance (receiver bias circuit).

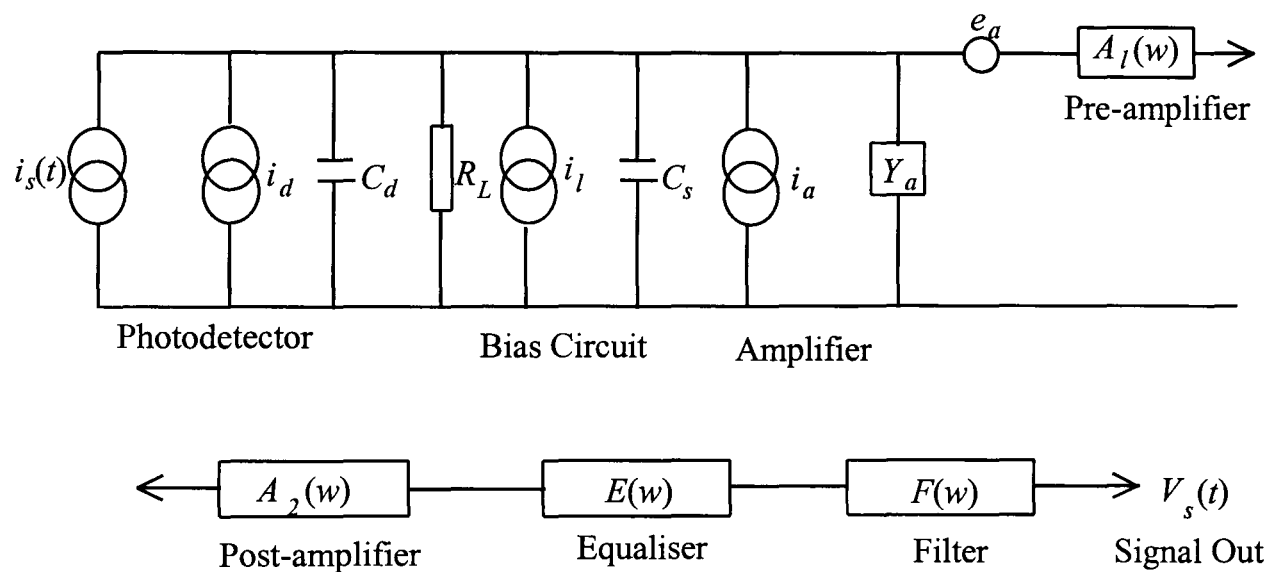


Figure 4.1 Equivalent circuit for an optical receiver.

The photodiode is followed by a linear channel, which consists of the amplifier chain and the shaping filter. The shunt current source, $i_s(t)$, represents the signal current due

to an optical power $P(t)$ incident on the photodetector. For a PIN photodiode this is given by

$$i_s(t) = \left(\frac{\eta q}{h\nu} \right) P(t) \quad (4.1)$$

where η is the quantum efficiency and $(h\nu/q)$ is the photon energy in electron volts.

Following Smith and Personick [48], the total input admittance is

$$\begin{aligned} Y_{in}(\omega) &= Y_a(\omega) + \frac{1}{R_L} + j\omega(C_d + C_s) \\ &= G + jB \end{aligned} \quad (4.2)$$

where $G=1/R_{in}$ represents the total input conductance and $B=\omega C_T$ is the total input susceptance, including contributions from the detector, amplifier and parasitics.

From the equivalent circuit, it follows that the transimpedance of the receiver will be given by

$$Z_T(\omega) = \frac{A_1(\omega)A_2(\omega)E(\omega)F(\omega)}{Y_{in}(\omega)} \quad (4.3)$$

where $A_1(\omega)$ and $A_2(\omega)$ are the pre-amplifier and post amplifier transfer functions respectively, $E(\omega)$ the transfer function of the equaliser and $F(\omega)$ the transfer function of the filter. The resulting output voltage due to the signal current $i_s(t)$ becomes

$$v_o(t) = \frac{1}{2\pi} \int_{-\infty}^{\infty} I_s(\omega) Z_T(\omega) e^{j\omega t} d\omega \quad (4.4)$$

The shunt current noise generators associated with the amplifier and bias circuit are all connected to the same node and so may be combined to give one equivalent shunt current generator with a noise spectral density, S_I (assuming all the noise generators are white over the frequency range of interest). The resulting output noise contribution due to S_I is then given by

$$\langle n^2(t) \rangle_{shunt} = \frac{1}{2\pi} \int_{-\infty}^{\infty} S_I |Z_T(\omega)|^2 d\omega \quad (4.5)$$

The output noise due to the amplifier series voltage generator e_a , with noise spectral density S_E is given by

$$\langle n^2(t) \rangle_{series} = \frac{1}{2\pi} \int_{-\infty}^{\infty} S_E |Y_{in}(\omega)|^2 |Z_T(\omega)|^2 d\omega \quad (4.6)$$

Making the substitution for $Y_{in}(\omega)$ this becomes

$$\langle n^2(t) \rangle_{series} = \frac{1}{2\pi} \int_{-\infty}^{\infty} S_E \left(\frac{1}{R_{in}^2} + (\omega C_T)^2 \right) |Z_T(\omega)|^2 d\omega \quad (4.7)$$

Combining the contributions from the shunt current and series noise generators, the total amplifier mean square output noise, assuming the noise sources are uncorrelated becomes

$$\langle n_o(t)^2 \rangle = \frac{1}{2\pi} \int_{-\infty}^{\infty} \left[S_I + S_E \left(\frac{1}{R_{in}^2} + (\omega C_T)^2 \right) \right] |Z_T(\omega)|^2 d\omega \quad (4.8)$$

which is of the form

$$\langle n_o(t)^2 \rangle = \frac{1}{2\pi} \int_{-\infty}^{\infty} [S_O + S_2(\omega)^2] |Z_T(\omega)|^2 d\omega \quad (4.9)$$

and so the equivalent input noise density has a white term, S_O and a frequency squared term, S_2 . It is this latter term, associated with the series noise voltage source, that ultimately limits performance at high frequencies. In order to get an indication as to what frequencies the S_2 term becomes important equation 4.9 can be expressed as

$$\langle n_o(t)^2 \rangle = \frac{1}{2\pi} \int_{-\infty}^{\infty} S_O \left[1 + \left(\frac{\omega}{\omega_n} \right)^2 \right] |Z_T(\omega)|^2 d\omega \quad (4.10)$$

where $\omega_n = \sqrt{\frac{S_O}{S_2}}$ is the frequency at which the two noise terms are equal. In designing high sensitivity optical preamplifiers, it is important to select the detectors, active devices and preamplifier topology in order to minimise the noise power spectral densities S_I and S_E . In particular, for wide band operation, S_2 should be minimised.

Personick actually solved equations 4.5 and 4.7 for a PCM system. In order to avoid intersymbol interference, he assumed a ‘raised cosine’ output pulse shape and evaluated equations 4.5 and 4.7 for several input pulse shapes. By a simple normalisation, Personick was able to express the noise in terms of the PCM bit-rate and the definite integrals I_2, I_3 . His contribution significantly eased the evaluation of the receiver sensitivity for PCM systems. However, his solution is inappropriate for digital PPM systems as the target output pulse shape is not a ‘raised cosine’.

4.4 Preamplifier structures

As the first stage in the receiver, it is the pre-amplifier that acts as the dominant noise source. Provided that the pre-amplifier has sufficiently high gain, then noise from subsequent stages can be ignored. The pre-amplifier configurations that have been proposed in the literature fall into three classifications [53,54]: low impedance, high impedance and transimpedance. Each of these will be considered and their respective limitations discussed.

4.4.1. Low impedance pre-amplifier

This is the simplest pre-amplifier structure in that the photodiode is terminated by a load resistor followed by a voltage amplifier, shown in Figure 4.2. The pre-amplifier bandwidth is then determined by the resulting RC time constant associated with the photodiode capacitance and terminating resistance. Although this configuration has a wide bandwidth and dynamic range it is at the cost of poor receiver sensitivity for direct detection systems. This can be attributed to the low terminating resistance giving rise to a high value of thermal noise. This structure therefore demands a trade-off between bandwidth and sensitivity which tends to make it impractical for long haul wideband optical communication systems.

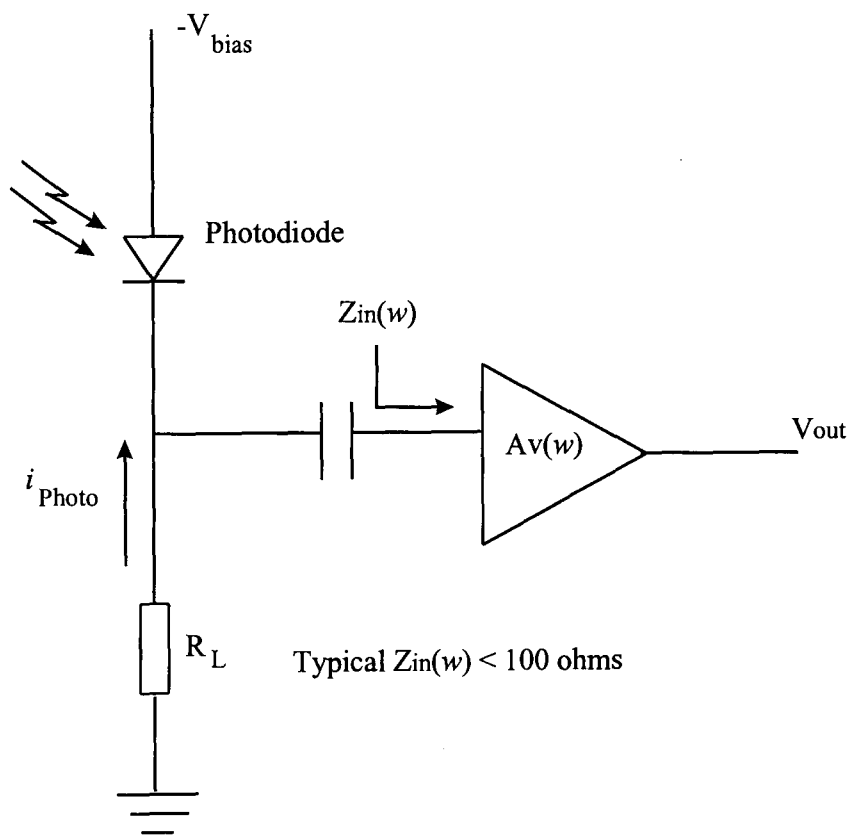


Figure 4.2 Low impedance pre-amplifier

4.4.2. High impedance pre-amplifier

In order to remedy the poor noise performance of the low impedance pre-amplifier, the input resistance can be increased leading to a reduced thermal noise contribution. However this reduces the bandwidth of the receiver until eventually it behaves as an integrator. This effect has led to this type of pre-amplifier becoming known as an integrating front-end. The signal shape can be restored by ensuring that the equaliser carries out the opposite process and differentiates the output of the pre-amplifier. The equalisation process results in the noise having a frequency squared spectral density which dominates in wideband high impedance receivers. Even so, the overall noise contribution is still less than that for a low impedance receiver. Although the most sensitive configuration, this type of pre-amplifier suffers from poor dynamic range and the added complexity of the requirement for a differentiating equaliser. Nevertheless, its excellent low noise performance has led to its widespread utilisation. Figure 4.3 shows a typical high impedance circuit configuration.

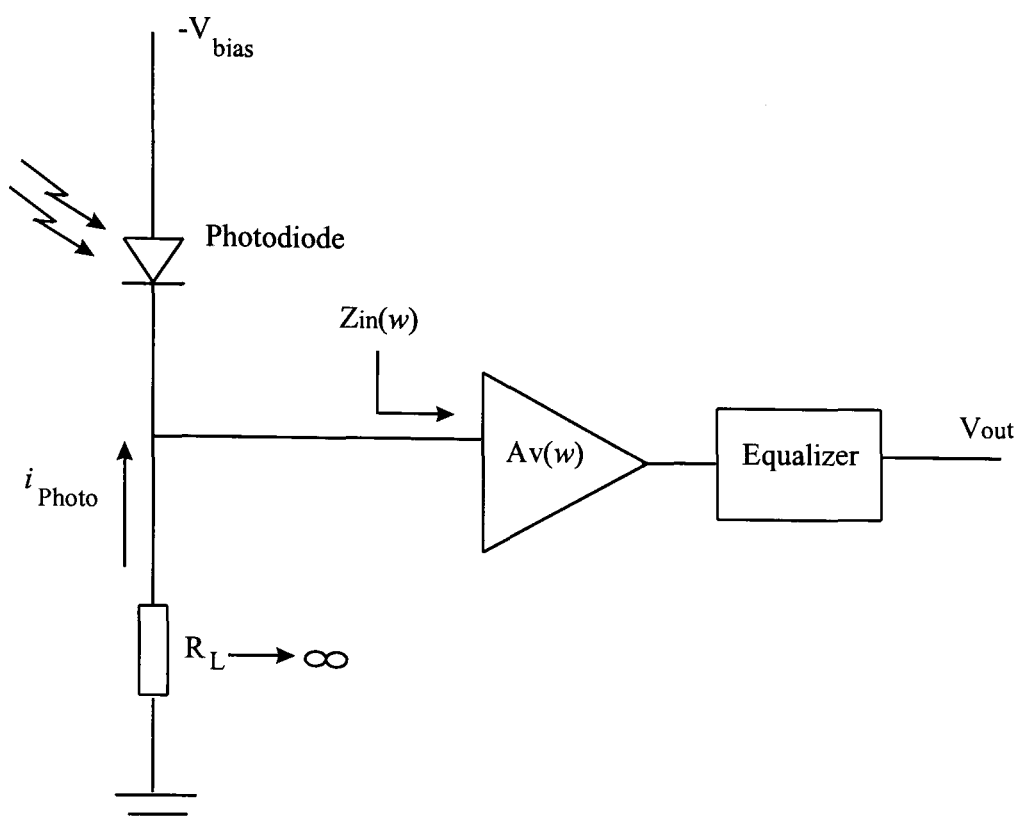


Figure 4.3 High impedance pre-amplifier

4.4.3. Transimpedance pre-amplifier

The transimpedance design offers a compromise between the wide bandwidth of the low impedance design and the low noise of the high impedance design. The typical circuit configuration of the transimpedance pre-amplifier is shown in Figure 4.4. In this configuration, shunt negative feedback is employed to reduce the effective input resistance of the amplifier. The load resistor is the element that is incorporated in the feedback loop of the amplifier and so its contribution to the input impedance is given by $R_f/(1+A)$. Provided that the gain is sufficiently large, the effective resistance is low leading to wider bandwidths than the high impedance designs.

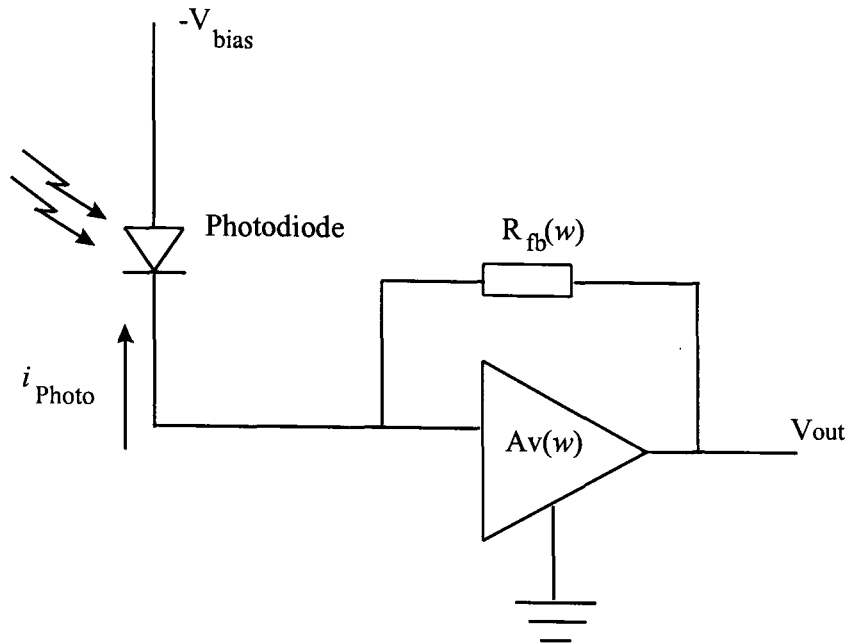


Figure 4.4 Transimpedance pre-amplifier

Hullet and Moui [55] have shown that the noise of the feedback resistor may be referred directly to the input of the preamplifier and so the noise contribution is merely that associated with the thermal noise of the resistor. This then becomes the dominant thermal noise source at the front end of the preamplifier and as the value of the resistor is considerably higher than that of the low impedance design, superior performance is achieved. Ideally, the feedback resistance should be the same as the resistance in a high impedance design in order to achieve the same noise performance. But in practice, this would require an extremely large amplifier gain in order to achieve the desired bandwidth. The maximum open loop gain is constrained by stability considerations and so this configuration always suffers a sensitivity penalty in comparison to the high impedance design but offers superior performance to the low impedance design.

From above discussion it can be seen that, the low impedance design can offer a high bandwidth but results in high preamplifier noise. The high impedance design can offer

a low noise but low bandwidth is the penalty. The transimpedance design can offer low noise and the bandwidth is between the low impedance and high impedance design. In our system we will choose the transimpedance design because it can offer the bandwidth we require and can result in low noise.

4.5 Preamplifier design

The receiver considered is composed of a preamplifier (PIN-BJT) followed by a matched filter, threshold detection then the PPM decoder. The instant the PPM pulse crosses the threshold level is used to determine which time slot contains the pulse. This requires a timing signal at the decoder [56].

The PIN-BJT receiver preamplifier is a self-biasing common collector common emitter transimpedance design as shown in Figure 4.5. The common collector first stage employs bootstrapping (incorporating capacitor C2) to reduce the effective capacitance of the large area PIN photodiode employed. The bootstrapped capacitance is given by

$$C_{bs} = [1 - A_{vcc}] C_d \quad (4.11)$$

where C_{bs} is the bootstrapped capacitance, C_d is the photodiode capacitance and $A_{vcc} = 0.97$ is the common collector gain. The preamplifier bandwidth is set by the

total input capacitance C_{in} and the total input resistance R_{in} . The preamplifier bandwidth is given by

$$\text{Bandwidth} = \frac{1}{2\pi R_{in} C_{in}} \quad (4.12)$$

where the total input resistance is given by

$$\begin{aligned} R_{in} &= (1 + \beta)R_3 // R_2 // \frac{R_f}{1 + A_{vcl}} \\ &= 1.49 \text{ k}\Omega \end{aligned} \quad (4.13)$$

and the total input capacitance is given by

$$\begin{aligned} C_{in} &= (C_d + C_\pi)(1 - A_{vcc}) + C_{cl} \\ &= 1.534 \text{ pF} \end{aligned} \quad (4.14)$$

where the C_π and C_{cl} are the hybrid π model transistor capacitances. Therefore the preamplifier bandwidth is 69.6 MHz.

The preamplifier transimpedance is shown in Figure 4.6(a) where the results have been obtained through a full circuit simulation. The circuit component values, transistor parameters and simulation program are given in Appendix 2. A bandwidth of about 70 MHz has been achieved with a transimpedance of 4.4 k Ω . This is in good agreement with the calculation results.

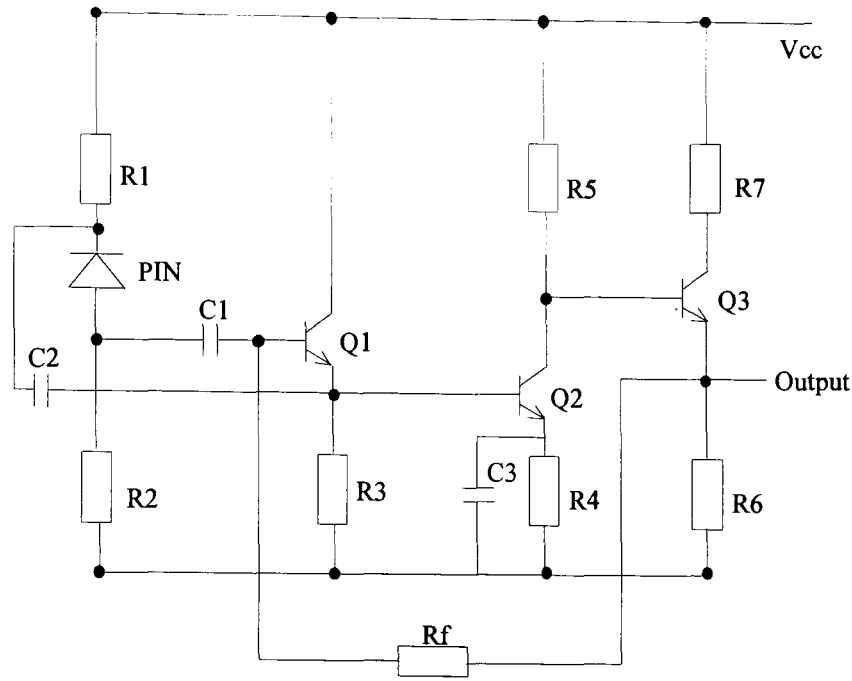


Figure 4.5. PIN-BJT transimpedance receiver

The dominant noise sources in the design of Figure 4.5 are associated with the first stage. Two of these noise sources are flat in nature and are due to the base shot noise and the thermal noise contribution of R_f . Two other noise sources have f^2 components (and flat components) and are attributed to the first stage collector shot noise and base spreading resistance thermal noise. The preamplifier overall noise can be expressed as (see appendix 3)

$$S(f) = 2qI_{b1} + \frac{4KT}{R_f} + \frac{2qI_{c1}}{g_{m1}^2} \left[\frac{1}{R_f} + \frac{1}{r_{\pi1}} + \frac{1}{R_2} \right]^2 + \frac{4KT r'_{bb1}}{R_{in}^2} + \frac{2qI_{c1}}{g_{m1}^2} \{2\pi f C_T\}^2 + 4KT r'_{bb1} \{2\pi f C_1\}^2 \quad (4.15)$$

where

$$2qI_{b1}$$

is the base current shot noise

$$\frac{4kT}{R_f}$$

is thermal noise due to the feedback resistor

$$4KT r'_{bb1} \left(\frac{1}{R_{in}^2} + (\omega C_1)^2 \right)$$

thermal noise due to the base spreading
resistance

$$\frac{2qI_{c1}}{g_{m1}^2} \left[\left(\frac{1}{R_f} + \frac{1}{r_{\pi1}} + \frac{1}{R_2} \right)^2 + (\omega C_T)^2 \right]$$

is collect current shot noise

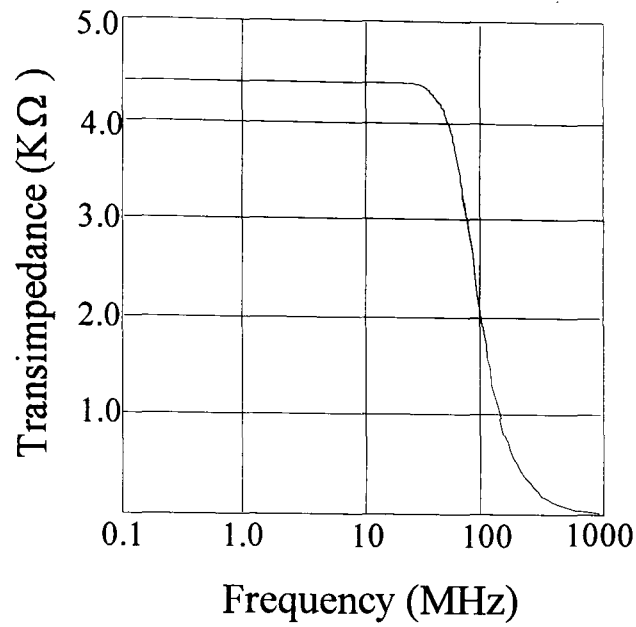
and

R_{in} is the input resistance,

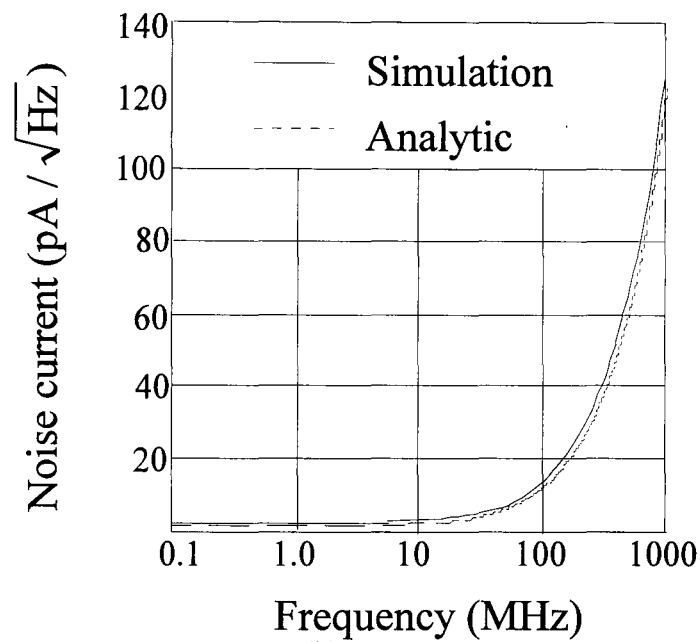
C_I is the PIN capacitance, stray capacitance and feedback capacitance and

C_T is the total capacitance (circuit and PIN).

The total preamplifier noise referred to the input is shown in Figure 4.6(b). Results were evaluated through a complete circuit simulation and through the use of (4.15). Good agreement is observed between the analytic and simulation results as depicted in Figure 4.6(b). The circuit simulation and the analytic result in (4.15) predict noise PSDs of $2.7 \text{ pA} / \sqrt{\text{Hz}}$ and $2.3 \text{ pA} / \sqrt{\text{Hz}}$ respectively. The difference may be attributed to the fact that (4.15) accounts only for the front end noise. The sensitivity calculations in section 5.4 will be based on a noise PSD of $2.7 \text{ pA} / \sqrt{\text{Hz}}$.



(a)



(b)

Figure 4.6 (a) Receiver transimpedance (b) noise performance

4.6 Summary

The noise sources that limit the performance of optical receivers have been identified and a general receiver noise model has been presented. Expressions have been derived for both the noise and signal voltage at the output of the receiver matched filter and

typical pre-amplifier structures have been discussed. A common collector common emitter bootstrapped PIN-BJT receiver design has been considered and shown to achieve a low noise current of $2.7 \text{ pA} / \sqrt{\text{Hz}}$ together with a bandwidth of 70 MHz.

Chapter 5 Optical Wireless PPM System

5.1 Introduction

Pulse Position Modulation has been widely studied [57-64]. Garrett suggested a PTM scheme for long haul point to point links over single-mode fibre [58-60]. This scheme uses the Pulse Position Modulation (PPM) format where the position of the received pulse in the PPM frame is used to convey the information. An M bit PCM word is represented in PPM by positioning a single high energy pulse in one of the 2^M discrete time slots and therefore a higher consumption of bandwidth is incurred than that required by PCM. Pierce [57] first suggested the use of PPM in optical channels for space communication using direct detection. In his work which was directed towards identifying modulation formats suitable for space communication links, Pierce presented an ideal channel model assuming no background light (or dark current) and assumed that the receiver is noiseless. Under his model the only error source will be that due to the quantum noise or the random arrival of photons at the photodetector which can only result in an erasure error. Under such assumptions Pierce demonstrated that a PPM system allowed unbounded transmission efficiency brought

about by the fact that a fixed number of photons is required to preserve the pulse energy and hence the system bit error rate. However, the PPM coding level in his channel is unbounded, so that the fixed pulse energy can be used to convey an unbounded amount of information by increasing the coding level. The increase in transmission efficiency is however at the cost of fast bandwidth expansion. In order to counter the effect of fast bandwidth expansion it has been proposed to alter the PPM format structure itself. This has led to several derivatives of Pierce's original PPM structure such as overlapping PPM (OPPM) [61], multiple PPM (MPPM) [62,63] and differential PPM (DPPM). Consideration has also been given to combining these modified PPM structures with coding to improve the throughput. The improvements are however achieved at the expense of increased coding complexity.

PPM gives power efficiency compared to OOK and therefore is suited for mobile terminals as it helps preserve battery life. The use of PPM also results in improved receiver sensitivity which is vital in this OW environment as the maximum transmitter power is limited by eye safety issues. PPM achieves these attractive features at the expense of bandwidth expansion. PPM has however been selected by the IrDA in 1995 [38] as the modulation format for their fast 4 Mbit/s links. The IrDA has however only considered 4-PPM.

In this chapter we begin by introducing the PPM model and error sources. The chapter also presents design details for a PPM coder and decoder. The PPM indoor infrared wireless system is then analysed and sensitivity results are presented and compared to OOK systems.

5.2 The PPM system

The general features of an optical wireless system employing digital pulse position modulation are shown in Figure 5.1. In the case of uncoded PPM, the PCM data is fed directly into the PCM/PPM coder where M bits at a time are coded into a set of symbols which are used to drive the laser driver circuit. At the receiver, the optical symbols are converted back into an electrical signal by a photodetector, amplified, filtered and converted into a set of symbols consisting of n pulse positions plus erasures. When Reed-Solomon error correction is incorporated, the PCM data is first fed into the Reed-Solomon encoder before being converted into digital PPM. Reed-Solomon codes have been shown to improve receiver sensitivity when employed with PPM [64]. These codes are suited for application in PPM systems since the loss of a PPM pulse results in losing a number of PCM bits, ie a burst error. Reed-Solomon codes are ideal under these conditions. A PCM source of information provides the input to the system. The PCM input comprises words of M bits in a frame of duration T_f . A PCM to PPM coder converts these M information bits into a single high energy pulse to be transmitted in one of $n = 2^M$ possible slots in a frame of the same duration T_f . A guard band is left at the end of each frame to allow for inter-frame interference due to pulse dispersion as well as for timing extraction purposes. The optical fibre PPM frame structure is shown in Figure 5.2. The ratio of the allowed band and the overall frame duration defines the modulation index, m . As a single PPM pulse is used to convey on average $\frac{M}{2}$ PCM bits the increase in sensitivity is evident, however the more important implication is that of the increased difficulty in synchronisation. The receiver is synchronised to the transmitter by a clock which may be derived from the

digital PPM stream [67]. At an instant t_d relative to this clock signal, the receiver output voltage $v_o(t)$ crosses a threshold level v_d with positive slope. The received symbol is determined by whichever of the n slots contains t_d . Due to receiver noise the received pulse shape may become distorted and cause an error in the threshold crossing which is denoted by e_k .

A laser driver circuit is used to transmit the PPM pulses and at the receiver direct detection can be carried out. The receiver comprises a PIN or APD photodetector followed by a preamplifier. Three preamplifier topologies have been shown to offer high sensitivity with PPM, these are PINFET [64], PINBJT [65], and APD [66] front ends. The post detection filter is a network optimised to estimate with minimum error the arrival time of a PPM pulse. This has been shown to be a matched filter in cascade with a proportional-derivative-delay network (PDD) [59,60].

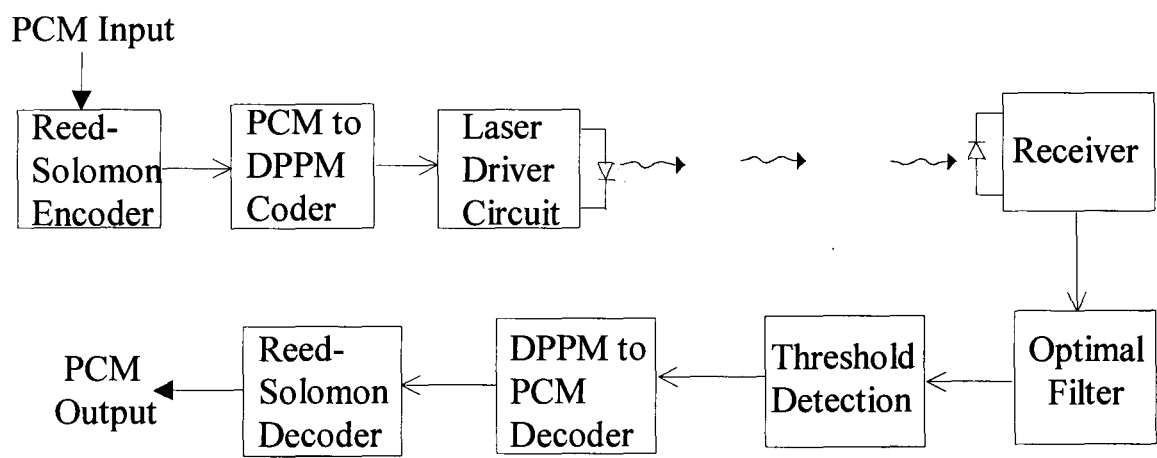


Figure 5.1 The digital wireless PPM system

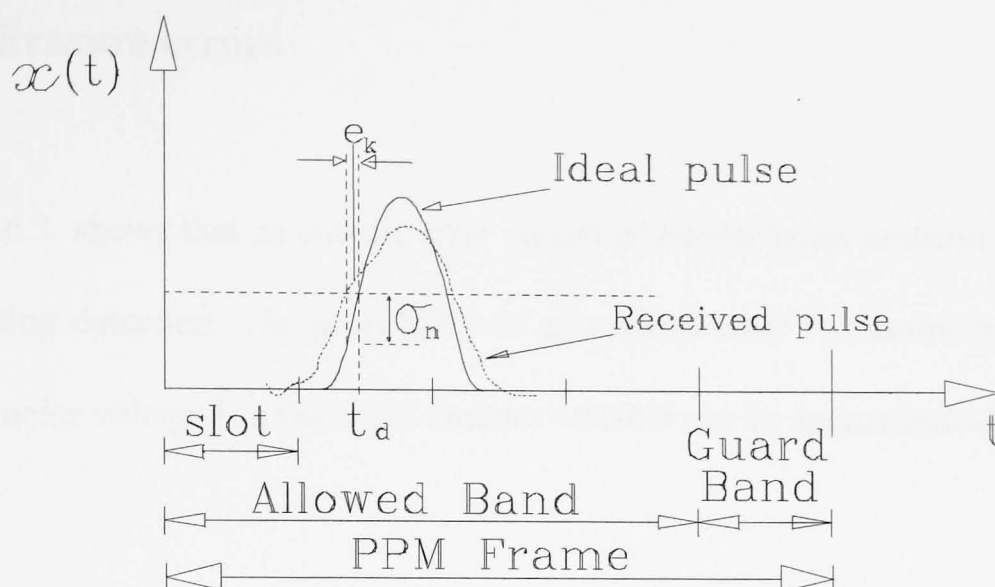


Figure 5.2 The PPM frame structure

5.3 Error sources

For a slightly dispersive channel the estimate y_i may differ from the true symbol x_i due to three main sources of error. These are erasure, wrong slot and false alarm errors [56,58].

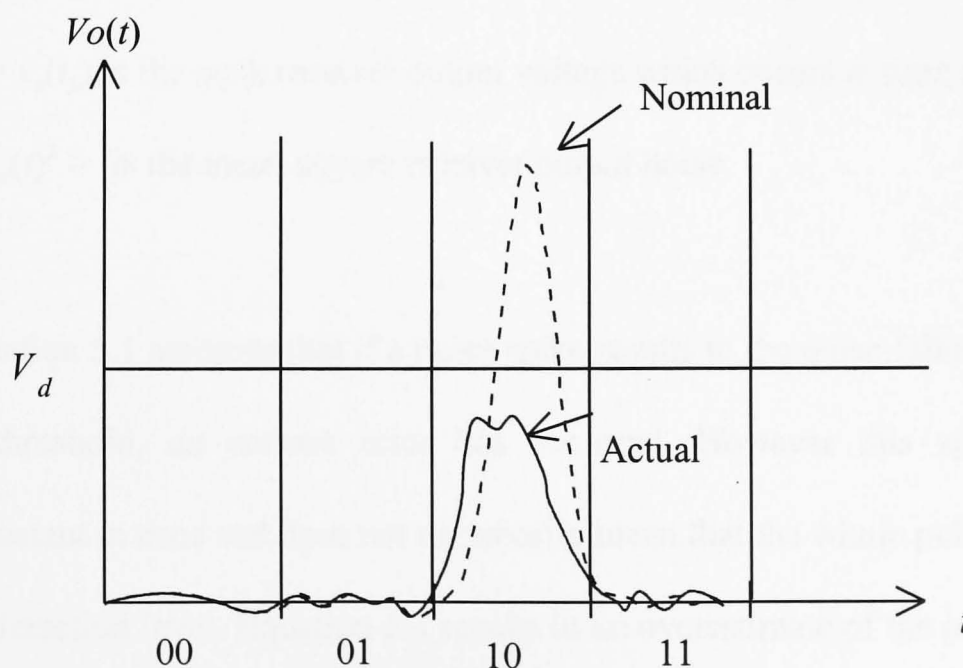


Figure 5.3 The erasure error

5.3.1 Erasure errors

Figure 6.3. shows that an erasure error occurs whenever noise destroys the pulse thus preventing detection. The probability of an erasure error P_r , assuming the receiver output noise voltage is a Gaussian random variable can be approximated by

$$P_r = 0.5\text{erfc}\left(\frac{Q_r}{\sqrt{2}}\right) \quad (5.1)$$

where

$$Q_r^2 = \frac{(v_p - v_d)^2}{\langle n_o(t)^2 \rangle} \quad (5.2)$$

and

$v_d = v_o(t_d)$ is the receiver output at the threshold crossing time.

$v_p = v_o(t_p)$ is the peak receiver output voltage which occurs at time t_p .

$\langle n_o(t)^2 \rangle$ is the mean square receiver output noise.

Use of Equation 5.1 assumes that if a noise spike results in the pulse falling below the detection threshold, an erasure error has occurred. However this applies for a particular instant in time and does not necessarily mean that the whole pulse has fallen below the detection level. Equation 5.1 results in an overestimate of the probability of an erasure, but is satisfactory in that the resulting sensitivity calculations are on the conservative side.

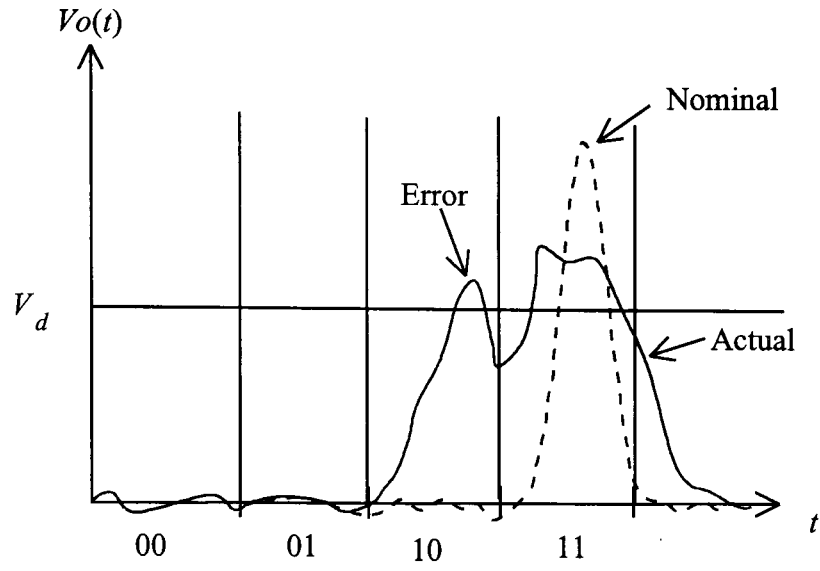


Figure 5.4 The wrong slot error

5.3.2 Wrong slot errors

The wrong slot error event is illustrated in Figure 5.4. It occurs when noise on the leading edge of the pulse produces a threshold crossing in the time slot immediately preceeding or following that containing the pulse. The probability of a wrong slot error, P_s is given by

$$P_s = \text{erfc}\left(\frac{Q_s}{\sqrt{2}}\right) \quad (5.3)$$

where

$$Q_s^2 = \left(\frac{mT_f}{2n}\right)^2 \frac{1}{\langle n_o(t)^2 \rangle} \left(\frac{dv_o}{dt}\bigg|_{t_d}\right)^2 \quad (5.4)$$

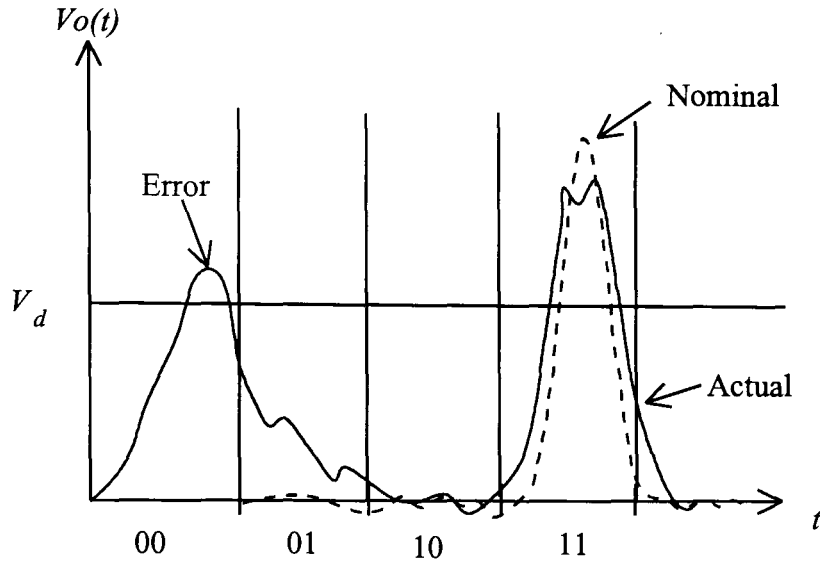


Figure 5.5 The false alarm error

5.3.3 False alarm errors

The false alarm or threshold violation error is illustrated in Figure 5.5. In the interval between the start of the frame and the arrival of the signal pulse, the receiver output voltage may cross the threshold due to noise with probability

$$P_t = 0.5\text{erfc}\left(\frac{Q_t}{\sqrt{2}}\right) \quad (5.5)$$

where

$$Q_t^2 = \frac{v_d^2}{\langle n_o(t)^2 \rangle} \quad (5.6)$$

The number of uncorrelated samples per time slot can be estimated in terms of the time τ_r at which the autocorrelation function of the receiver filter has become small, as

$(mT_f/ n\tau_r)$. The probability per time slot of a false alarm error is then approximated by:

$$P_f = \left(\frac{mT_f}{n\tau_r}\right)P_i \tag{5.7}$$

5.4 Sensitivity evaluation

The aim of this section is to compare OOK and PPM as modulation formats for the optical wireless system. As such receiver sensitivity calculations were performed for both formats. The receiver sensitivity is a measure of the minimum optical power level required at the receiver input so that it will operate reliably with a bit error rate less than a desired value. It is often given as the average optical power P required for a bit error rate of 10^{-9} . This receiver sensitivity representation is popular because it can be directly measured very accurately by simply monitoring the detected photocurrent.

Receiver bandwidth	70 MHz
Receiver noise PSD	2.7 pA / $\sqrt{\text{Hz}}$
Receiver Transimpedance	4.4 k Ω .
Bit rate	10 Mbit/s
Photodiode responsivity	0.5 A/W
Background noise	
Test room A	0.454 mW-0.8 μ W
Test room B	0.454 mw-0.2 μ W

Table 5.1 The PIN-BJT receiver parameters

In Chapters 2 and 3, we have discussed the three major obstacles to achieving high-speed indoor infrared communication (ie. background noise, multipath dispersion and high capacitance from large area photodiode). In this analysis, we have taken the effect of background noise and multipath dispersion into account. The background noise level and multipath dispersion parameters were shown in Chapter 3. The parameters associated with the PIN-BJT preamplifier are shown in Table 5.1.

5.4.1 Receiver performance analysis

The wireless PPM system was shown in Figure 5.1. The receiver consists of a PIN photodiode with quantum efficiency η followed by an electrical preamplifier, matched filter, threshold detector and the PPM to PCM decoder. The average signal power incident on the photodiode is given by

$$P_s = \frac{bh\nu}{T_s} \quad (5.8)$$

where $T_s = \frac{mT_f}{n}$ is the PPM slot duration, h is Planck's constant, ν is the optical frequency and b is the number of photons in the pulse. Under normal operating conditions, the signal power is negligible outside of the chosen slot and P_s is approximated by zero in the adjacent slots. Let the received pulse energy be ϵ and the pulse shape $h_p(t)$ such that

$$\int_{-\infty}^{\infty} h_p(t) dt = 1 \quad (5.9)$$

The resulting photocurrent input to the filter will be

$$i(t) = \frac{\eta q}{h\nu} \varepsilon h_p(t) \quad (5.10)$$

Equation 5.10 can be written in terms of the number of incident photons per pulse as

$$i(t) = b \eta q h_p(t) \quad (5.11)$$

where b is the number of photons per pulse. Chapter 3 has shown for the first time that the received pulses in the indoor diffuse environment can be approximated by a Gaussian pulse shape. Under this assumption the normalised Gaussian shape can then be defined as

$$h_p(t) = \frac{1}{\alpha \sqrt{2\pi}} e^{-\frac{t^2}{2\alpha^2}} \quad (5.12)$$

where α is

$$\alpha = \frac{0.2 T_f}{M CRB} \quad (5.13)$$

where T_f is the PPM frame duration, M is the number of information bits (OOK bits) per PPM frame and CRB is a normalisation parameter with $CRB=1$ indicating that the PPM system is consuming the same bandwidth as the OOK system, $CRB=2$ twice etc. Substituting Eq. 5.12 into Eq. 5.11 the resulting photocurrent input to the filter can be written as

$$i(t) = b\eta q \frac{1}{\alpha\sqrt{2\pi}} e^{-\frac{t^2}{2\alpha^2}} \quad (5.14)$$

The output current from the matched filter may now be expressed as

$$i(t) = \left(b\eta q \frac{1}{\alpha\sqrt{2\pi}} e^{-\frac{t^2}{2\alpha^2}} \right) \otimes g(t) \quad (5.15)$$

where \otimes denotes convolution between the input pulse shape and filter impulse response $g(t)$. For a Gaussian input pulse shape, the matched filter frequency response is given by (see Appendix 4).

$$G(f) = \int_{-\infty}^{\infty} h_p(t) e^{-j2\pi ft} dt = e^{-\frac{\omega^2 \alpha^2}{2}} \quad (5.16)$$

Also Eq. 5.15 can be written as (see Appendix 5)

$$\begin{aligned}
i_o(t) &= b\eta q \int_{-\infty}^{\infty} G(f)G(f)e^{j2\pi ft} df \\
&= b\eta q \frac{e^{-\frac{t^2}{4\alpha^2}}}{2\alpha\sqrt{\pi}}
\end{aligned} \tag{5.17}$$

Therefore, the current at the threshold crossing instant t_d can be defined by

$$i_{\text{det}} = b\eta q \frac{e^{-\frac{t_d^2}{4\alpha^2}}}{2\alpha\sqrt{\pi}} \tag{5.18}$$

and the peak received current, assuming $t_p = 0$, is given by

$$i_p = \frac{b\eta q}{2\alpha\sqrt{\pi}} \tag{5.19}$$

In order to evaluate the receiver performance, the noise at the output of the filter must be estimated. Assuming that the receiver is employed over the bandwidth region in which the noise is flat (see Figure 4.6(b)), then the noise at the output of the matched filter is

$$N_o = \frac{1}{2\pi} \int_{-\infty}^{\infty} S_o |G(\omega)|^2 d\omega \tag{5.20}$$

where S_o is the receiver flat noise component and $G(\omega)$ is the matched filter transfer function, hence (see appendix 6)

$$N_o = \frac{S_o}{2\alpha\sqrt{\pi}} \quad (5.21)$$

The false alarm error probability can be calculated using equations 5.5-5.7 together with equation 5.18 and 5.21. The erasure error probability can be evaluated using equation 5.1, 5.2, 5.18, 5.19 and 5.21. In order to calculate the probability of a wrong slot error, we calculate the rate of rise of the pulse at the threshold crossing time t_d

$$i'(t_d) = \left. \frac{di(t)}{dt} \right|_{t_d} = \frac{tbq\eta}{4\alpha^3\sqrt{\pi}} e^{-\frac{t_d^2}{4\alpha^2}} \quad (5.22)$$

Hence the wrong slot error probability can be estimated from equations 5.3 and 5.4 using the values given by equations 5.21 and 5.22. Note that signal and noise currents (as in this section) can be used instead of the voltages in forming the SNR expression in (5.2), (5.4) and (5.6)

5.4.2 Analytic results

The PPM system is subjected to the three error sources discussed in section 5.3. The receiver sensitivity was evaluated by using the following algorithm:

1. From knowledge of the received pulse shape and the receiver noise PSD, the system parameters i_p , i_d , t_d and $i'(t_d)$ are evaluated for a given pulse energy b and threshold detection time t_d or current i_d .
2. A numeric optimisation routine then searches in the $b>0$ and $0<i_d<i_p$ space for the smallest value of b that meets the performance criterion $\frac{n}{2(n-1)}\{P_r + P_s\} + \frac{nP_f}{4} - P_e = 0$, where $P_e = 10^{-9}$ is the error probability.
3. The receiver sensitivity in photons per information bit can be obtained by dividing b by M .

For LOS systems multipath dispersion does not effect the system performance (see Chapter 2). Therefore in the LOS system we will just consider background noise. In the diffuse system, we will examine both background noise and multipath dispersion and their effect on the system performance.

5.4.2.1 LOS system

For sensitivity evaluation purposes the system was specified to operate at an error rate of 10^{-9} . The sensitivity of the PIN-BJT PPM LOS system without the background noise is shown in Figure 5.6 as a function of the coding level M . As the coding level is increased, the single PPM pulse is used to convey more bits of information (M bits),

thus the sensitivity of the system improves. As the PPM coding level is increased, the PPM frame is continuously subdivided into finer subdivisions ($n=2^M$ slots). Accordingly the time slot duration decreases and the PPM probability of wrong slot errors increases. As a result the sensitivity degrades at large values of M . The system sensitivity improves as the channel and receiver bandwidth (CRB) increases as depicted in Figure 5.6. This is because with the large CRB values less dispersed PPM pulses can be accommodated. The system bit error rate performance is evaluated in Figure 5.7 at $CRB=3$ and at $CRB=10$. The equivalent PIN-BJT OOK system BER is also shown in Figure 5.7. The performance improvement achieved by using PPM rather than OOK is best illustrated by comparing the two systems (OOK and PPM) results in Figure 5.6. The best predicted sensitivity as depicted in Figure 5.6 is -50.5 dBm ($CRB=10$, $M=7$). The sensitivity of a comparable OOK PIN-BJT system using the same parameters and operating at 10 Mbit/s is -40.7 dBm. The PIN-BJT PPM system thus offers a 9.8 dB sensitivity improvement over the PIN-BJT OOK system.

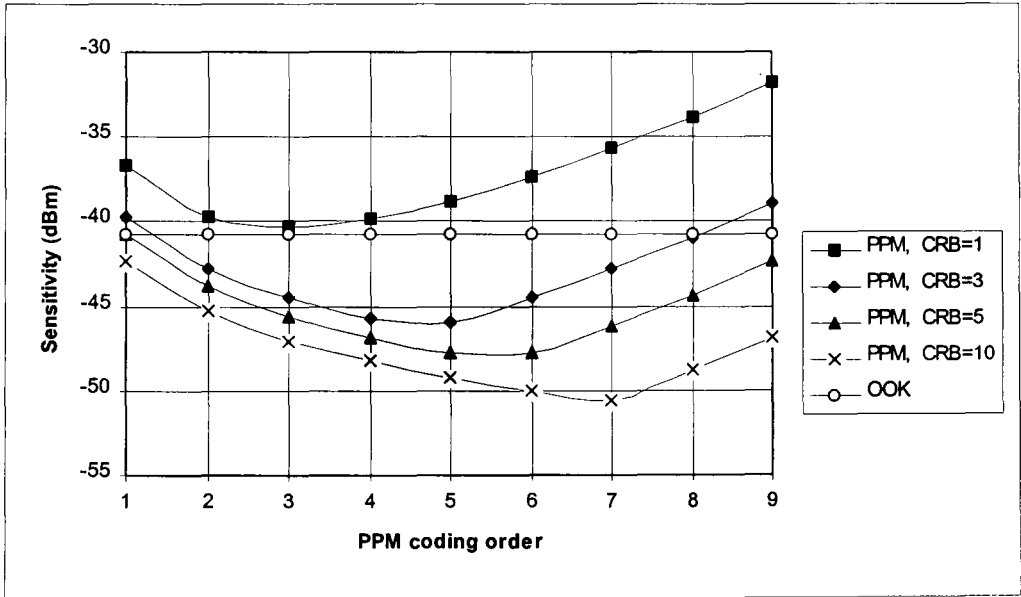


Figure 5.6 PIN-BJT PPM and OOK sensitivity

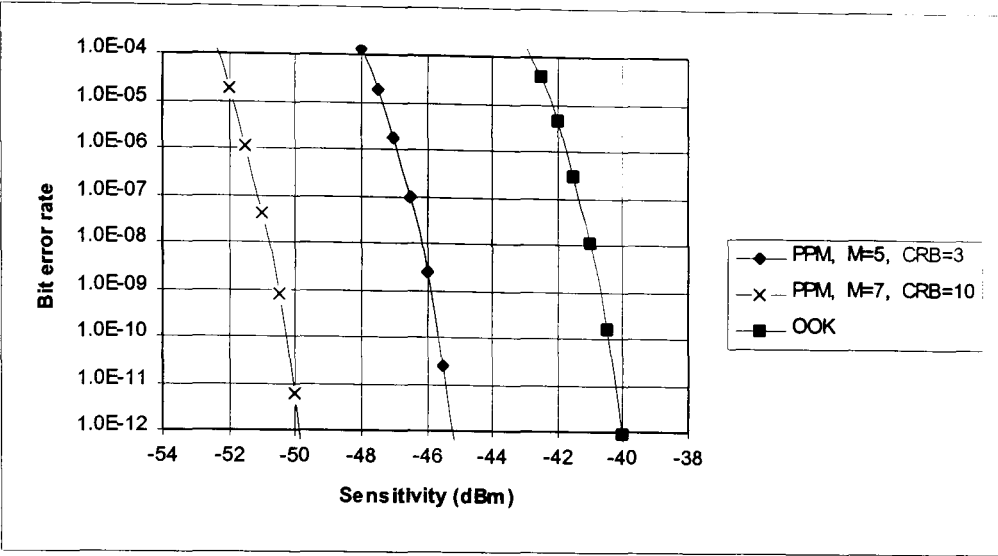


Figure 5.7 Bit error rate performance

Over more band limited channels, sensitivity improvement can still be achieved by using PPM rather than OOK. In fact, the results in Figure 5.6 indicate the set of PPM parameters and CRB values over which a sensitivity improvement is achieved. The portion of the ($CRB=3, 5$ and 10) PPM curves below the horizontal OOK line, represents sensitivity improvement. For example operating at $CRB=10$ calls for a 66 MHz bandwidth (determined using (5.13) and the Gaussian pulse shape) at 10 Mbit/s and offers a 9.8 dB sensitivity improvement. Operating at $CRB=3$ and $CRB=5$ calls for bandwidths of 20 MHz and 33 MHz respectively while offering sensitivity improvements of 5.2 dB and 7.1 dB respectively over OOK. Thus even with some more modest bandwidth expansion orders, a usable sensitivity improvement can be achieved by utilising the PPM format rather than OOK.

Next we will focus our attention on the impact of the OW environment and in particular in this section we will consider the effect of background radiation. There are three major light sources in the indoor environment: daylight, incandescent light and fluorescent light. Daylight and incandescent light represent essentially unmodulated sources [16] that can be received at an average power much larger than the desired

signal, even when optical filtering is employed (see Chapter 3). Therefore noise from background light must be taken into account when the system performance is analysed.

Experimental results have already been presented in Chapter 3 demonstrating that incandescent light produces higher levels of background current and it is therefore the major source of shot noise on the receiver photodiode. Therefore, in this analysis we have taken shot noise from incandescent light and evaluated the systems performance (ie. sensitivity and bit error rate). Therefore the system total noise current can be written as:

$$\sigma_T^2 = \sigma_{Rx}^2 + \sigma_d^2 \quad (5.23)$$

where σ_{Rx}^2 is receiver preamplifier noise and σ_d^2 is shot noise from background. The shot noise from background (incandescent) can be described by:

$$\sigma_d^2 = 2qRPB_T \quad (5.24)$$

where q is electronic charge, R is photodiode responsivity, P is optical power and B_T is bandwidth. In this analysis the optical power from the incandescent light is assumed to be 0.454mW and 1.42 μ W corresponding to the maximum and minimum expected levels respectively. Therefore the total noise current from the receiver and background noise is 8.94 pA/ \sqrt Hz when the optical power is 0.454 mW and 0.48pA/ \sqrt Hz when optical power is 1.42 μ W. Note that the receiver noise level is 2.7 pA/ \sqrt Hz. The

sensitivity performance under the background noise is shown in Figure 5.8. The results show that background noise has a significant effect on the sensitivity of the receiver. For the PPM system, the background noise effect reduces the receiver sensitivity by 5.2 dB when the receiver is placed directly under a spotlight and for the OOK system the penalty is 5.23 dB. It was found that ambient noise effects the sensitivity of the PPM format 0.03 dB less than the OOK scheme. The difference is very slight and does not impact OOK/PPM system choice with this (background noise) constraint in mind. Yet it should be remembered that under the same adverse conditions, PPM still offer about 9.8 dB better sensitivity compared to OOK.

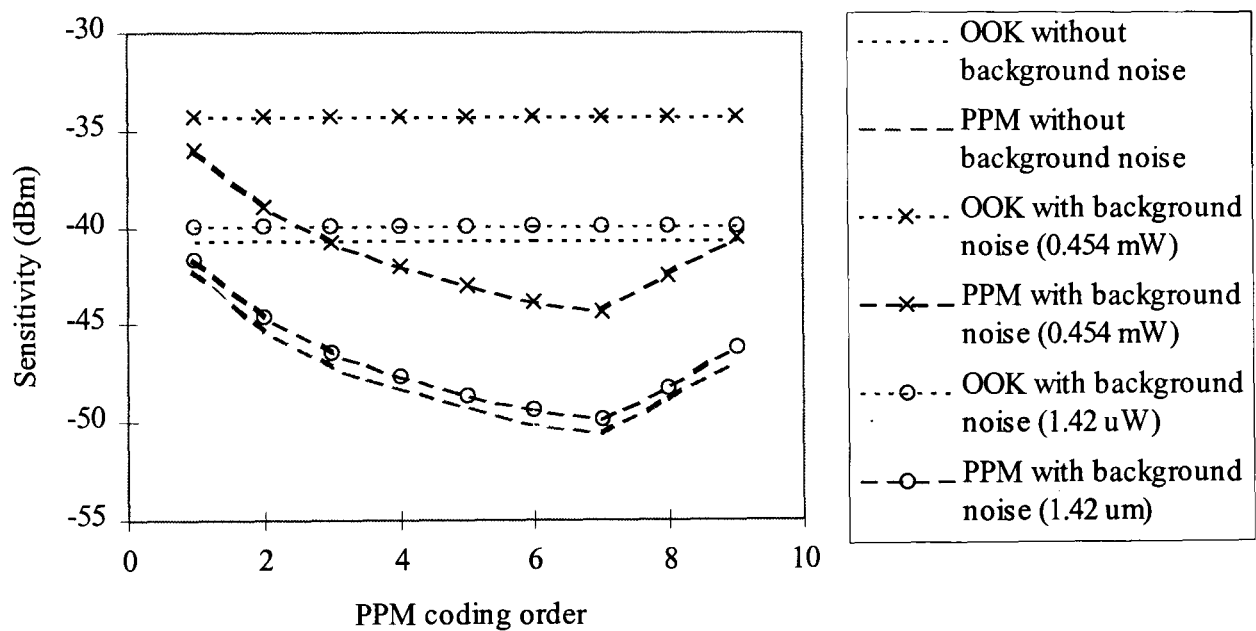


Figure 5.8: PIN-BJT and OOK sensitivity (Test room A) worst and best case scenario

5.4.2.2 Diffuse system

In Chapter 2, we have shown the diffuse link characteristics. The major limitations to the diffuse system sensitivity are multipath dispersion and background noise. In this section, we will evaluate the impact of multipath dispersion and background noise on the system.

The receiver sensitivity has been calculated at various points on the communication plane. The points have been chosen in such a way that sensitivity performance could be evaluated for points immediately under spotlights, in between spotlight, and immediately under the transmitter.

As mentioned before, the transmitter has been considered to emit the signal as a Lambertian source with $n = 1$. The system operated at a wavelength of 850 nm and a bit rate of 10 Mbit/s. Using this set-up and a diffuse configuration, it was found that the sensitivity equalled -49.47 dBm for PPM and -40.7 dBm for OOK. The PPM system transmitted 5 bits per frame and used a bandwidth of about 67 MHz. The OOK system utilised a bandwidth of 6.7 MHz. Under circumstances where there is no multipath dispersion and no background noise (receiver noise only); the sensitivity performance of the PPM scheme, hence, was found to be 8.77 dB better than OOK with a bandwidth expansion factor equal to 10. Note that the 9.8 dB sensitivity improvement quoted earlier corresponds to $M = 7$ bits per frame. Here $M = 5$ was used to ease the requirements on the channel bandwidth and the PPM slot clock resulting in 12.5 ns pulses. The propagation of such pulses was analysed in Section 3.4.

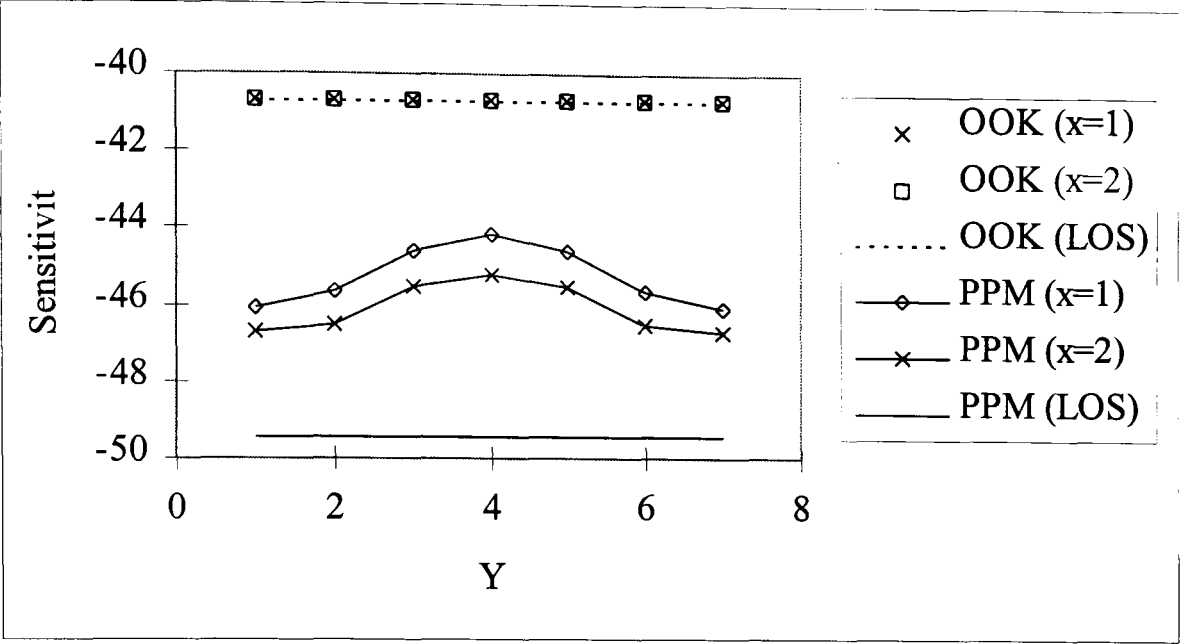


Figure 5.9 Sensitivity performance in a semi-dispersive environment (Room A)

Receiver Location (x,y,z)	OOK (LOS)	OOK (Diffuse)	PPM (LOS)	PPM (Diffuse)
(1,1,1), (1,7,1), (3,1,1), (3,7,1)	-40.7	-40.7	-49.47	-46.06 dB
(1,2,1), (1,6,1), (3,2,1), (3,6,1)	-40.7	-40.7	-49.47	-45.63 dB
(1,3,1), (1,5,1), (3,3,1), (3,5,1)	-40.7	-40.7	-49.47	-44.6 dB
(1,4,1), (3,4,1)	-40.7	-40.7	-49.47	-44.17 dB
(2,1,1), (2,7,1)	-40.7	-40.7	-49.47	-46.71 dB
(2,2,1), (2,6,1)	-40.7	-40.7	-49.47	-46.527 dB
(2,3,1), (2,5,1)	-40.7	-40.7	-49.47	-45.542 dB
(2,4,1)	-40.7	-40.7	-49.47	-45.213 dB

Table 5.2 Sensitivity performance in a semi-dispersive environment (room A)

Figure 5.9 and Table 5.2 display the sensitivity performance under the constraint of multipath dispersion only while Figure 5.10 and Table 5.3 show the impact of background noise coming from highly directive spotlights. The effect of both impairments is displayed in Figure 5.11. In all three figures, the values for x and y refer to the corresponding cartesian co-ordinates of the test room A (see Figure 3.2 (a)). Because of the symmetry of the test room, the results for $x = 3$ equal the results for $x = 1$.

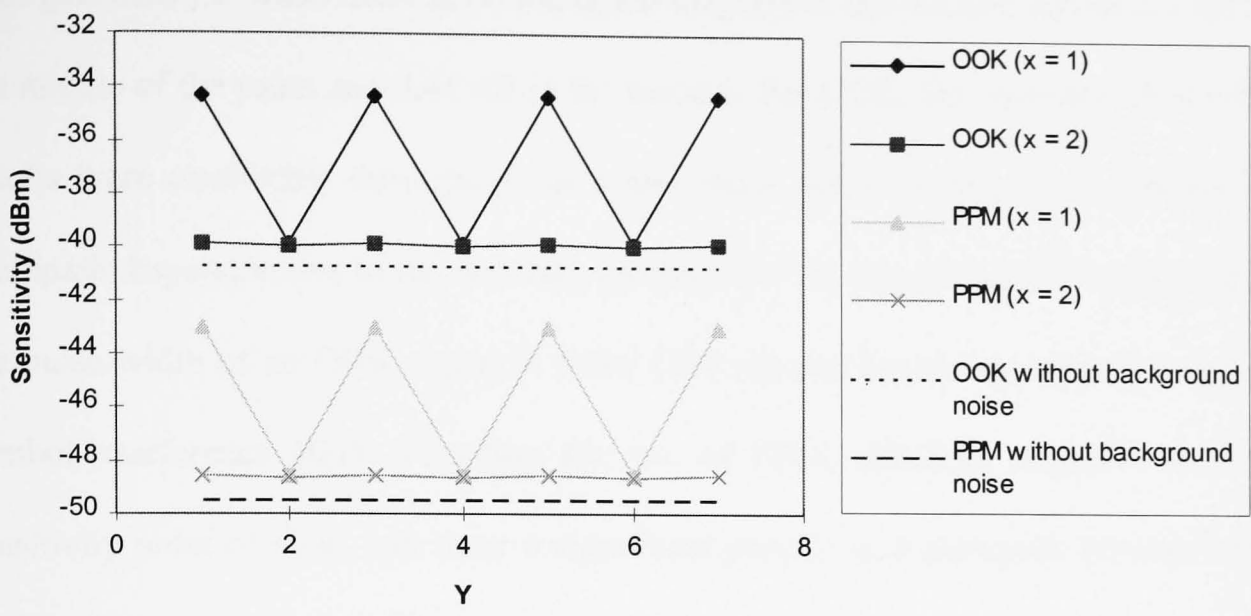


Figure 5.10 Sensitivity performance under highly directive spotlamps (room A)

Receiver Location (x,y,z)	OOK (LOS)	OOK (Diffuse)	PPM (LOS)	PPM (Diffuse)
(1,1,1), (1,7,1), (3,1,1), (3,7,1)	-35.47 dB	-35.47 dB	-44.27 dB	-44.27 dB
(1,2,1), (1,6,1), (3,2,1), (3,6,1)	-39.96 dB	-39.96 dB	-48.76 dB	-48.76 dB
(1,3,1), (1,5,1), (3,3,1), (3,5,1)	-35.47 dB	-35.47 dB	-44.27 dB	-44.27 dB
(1,4,1), (3,4,1)	-39.96 dB	-39.96 dB	-48.76 dB	-48.76 dB
(2,1,1), (2,7,1)	-39.96 dB	-39.96 dB	-48.76 dB	-48.76 dB
(2,2,1), (2,6,1)	-40.6 dB	-40.6 dB	-49.4 dB	-49.4 dB
(2,3,1), (2,5,1)	-39.96 dB	-39.96 dB	-48.76 dB	-48.76 dB
(2,4,1)	-40.6 dB	-40.6 dB	-49.4 dB	-49.4 dB

Table 5.3 Sensitivity performance under highly directive spotlamps

The results show that the sensitivity performance declines under the constraint of multipath dispersion. For PPM, and in the configuration where the transmitter was placed in the middle of the ceiling, the decline is highest in the middle of the communication plane and lowest in the corners. This is attributed to the fact that the difference between a direct ray and a reflected ray is maximum in the room’s centre, underneath the transmitter. The recorded sensitivity values were respectively -46.06 dBm (room corner) and -44.17 dBm (room centre). Compared to a LOS

configuration, i.e. when there is no multipath dispersion, the decline equals 5.3 dB in the middle of the room and 3.41 dB in the corners. For OOK, the recorded sensitivity results were unaffected throughout the entire room. OOK is thus less sensitive to multipath dispersion due to the fact that, for the same bit rate (10 Mbit/s in this case), the pulse width of an OOK signal is wider (100 ns) and hence less subject to inter-symbol-interference (ISI). Therefore the use of PPM, although attractive from a sensitivity point of view, can incur a significant penalty in a multipath environment. This has motivated the equalisation to be presented in Chapter 6.

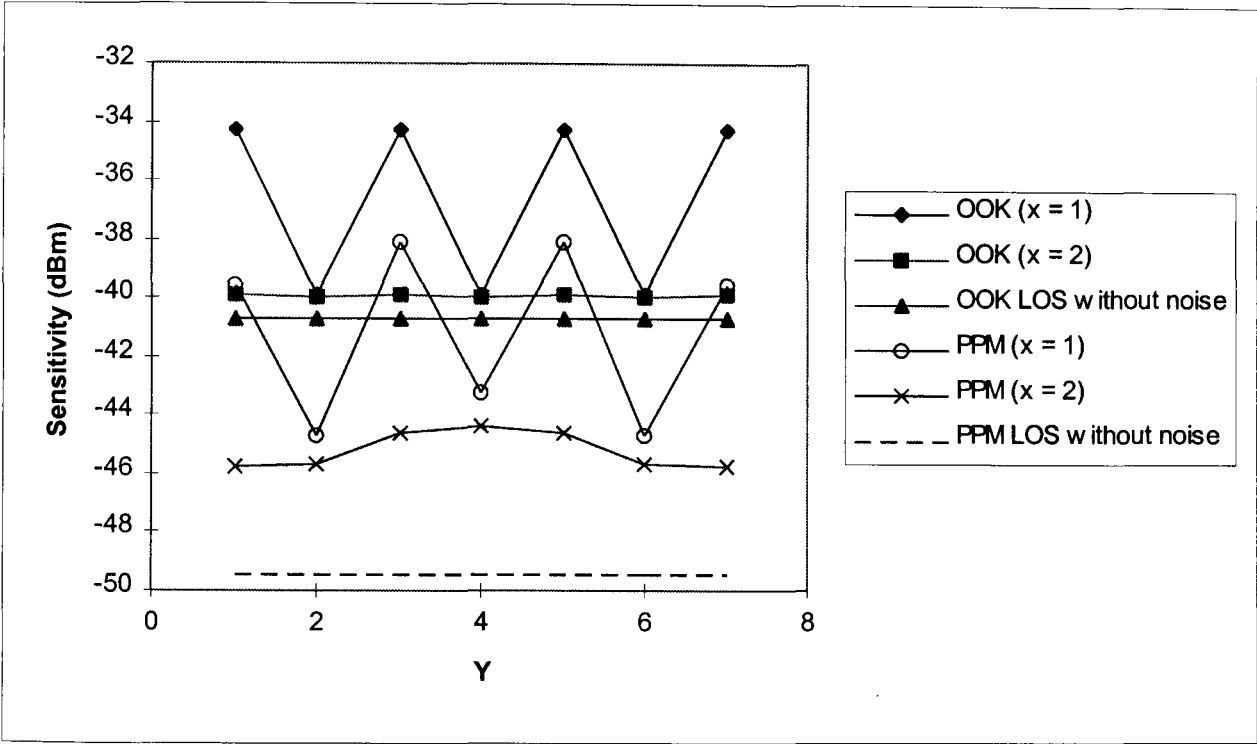


Figure 5.11 Sensitivity performance in a semi-dispersive environment and under highly directive spot lamps

Figure 5.10 shows that background noise has a significant effect on the sensitivity of the receiver. The impact is more devastating when the receiver is placed directly under a spotlight. The results show clearly the burn-out effect of spotlights. PPM and OOK are affected to almost the same extent. Figure 5.11 shows that the combined dispersion and multipath penalty varies between 10.07 dB and 3.01 dB for PPM, and

5.23 dB and 0.74 dB for OOK. With appropriate equalisation, it should be possible to reduce the effects of pulse dispersion and hence minimise the 10 dB PPM penalty to about 5 dB (residual due to background noise). As mentioned earlier, this will be further discussed in Chapter 6.

5.5 PPM coder design and experimental results

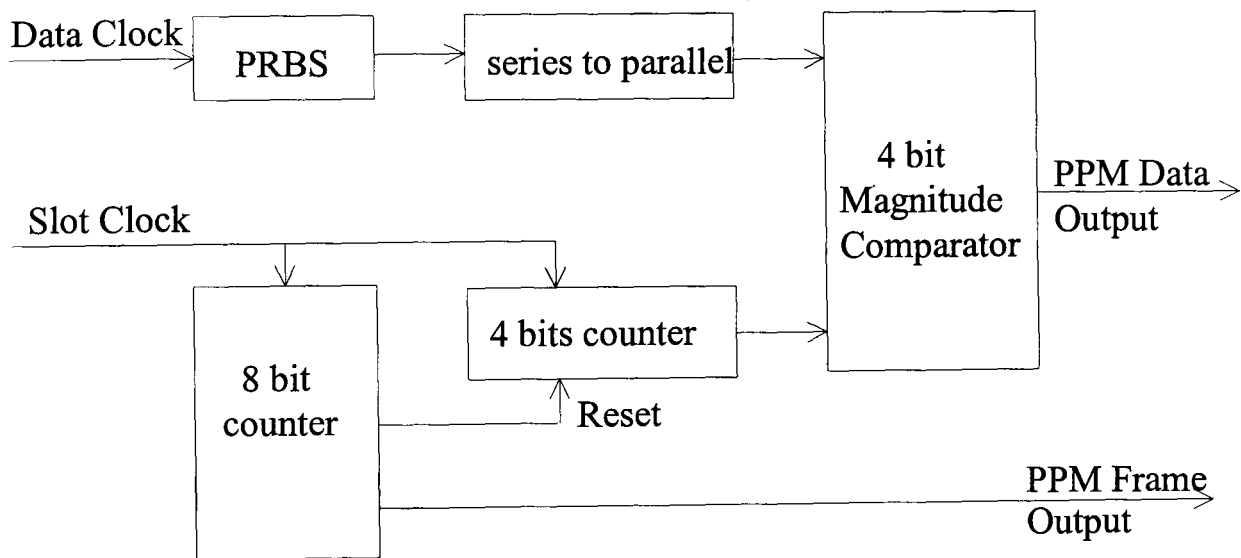


Figure 5.12 Binary source to digital PPM coder, designed to be employed with an optical wireless system

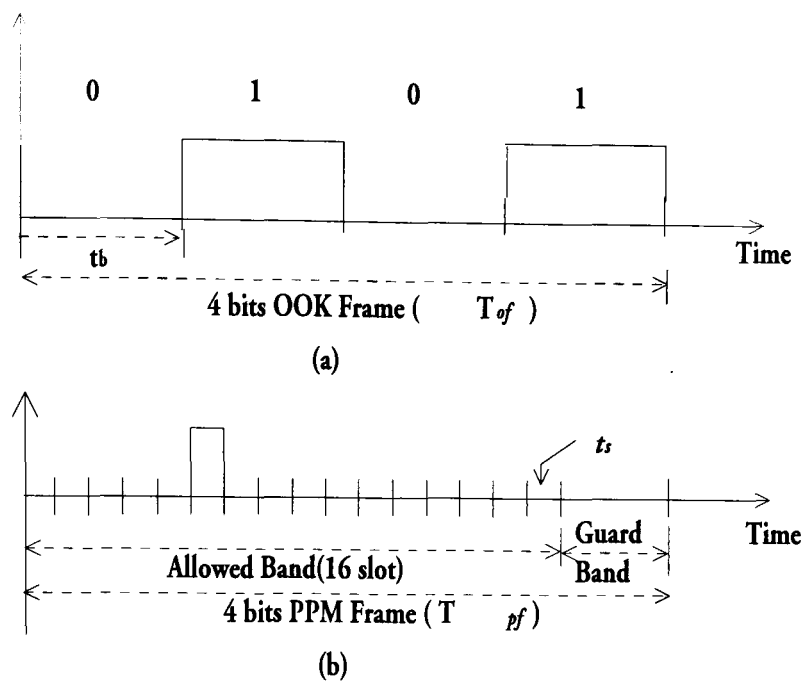


Figure 5.13 Frame timing diagram (a) OOK (b) PPM

This section describes the construction of a PPM coder and a PPM decoder. Although a complete OW PPM system has not been tested yet a description is given in this section for the system components which are additional to those found in a conventional OW OOK system. A block diagram illustrating the main features of the coder is shown in Figure 5.12. The purpose of the coder is to accept a binary source code either in serial or parallel format and then to furnish the equivalent PPM signal. The coder was designed with a fixed modulation index. In this case, we have set a modulation index (m) equal to 0.8. The frame and slots timing map of PPM and OOK are shown in Figure 5.13 which shows the timing information for PPM signals with reference to the OOK format. A 4 bit OOK frame structure is shown in which the OOK bit period is simply one quarter of the overall frame period. For a 10 Mbit/s system the corresponding bit period is $0.1 \mu\text{s}$ giving an overall OOK frame of $0.4 \mu\text{s}$ duration. The clock rate required in this case will be 10 MHz. For an equivalent PPM system such as that shown in Figure 5.13(b) the PPM frame consists of 16 slots plus

the guard band. The number of guard band slots is dependent on modulation index m . In this coder, the modulation index has been set equal to 0.8. So there are 4 slots in the guard band and thus the total number of slots in one frame is 20. The slot period becomes smaller than the OOK bit duration since the overall frame duration remains fixed as the bit rate has not changed. The PPM slot duration hence becomes $0.02 \mu\text{s}$ giving a clock requirement of 50 MHz.

In Figure 5.12, a pseudo random binary sequence (PRBS) circuit was used to generate a random sequence in four bits serial format. The output (of the PRBS) was fed in a controlled manner to one of the inputs of a four bit comparator. The required control was achieved by the use of a serial to parallel shift register, the purpose being to shift the data bits at the input of the comparator for the counter to identify the sequence. Two counters are used: a 4 bit counter and an 8 bit counter. The 4 bit counter is used to generate a parallel sequence that is fed into the comparator. The 8 bit counter is used to generate the PPM frame clock and to reset the 4 bit counter. The coder operation can be described as follows.

At the start of a new PPM frame, the serial to parallel counter furnishes a new 4 bit data word at one input of the comparator. The data word is held constant for the frame duration using a latch which together with a shift register make the serial to parallel counter. Also at the start of the PPM frame the 4 bits counter is initiated and caused to search sequentially for the stored word. Since both the input word and the counter have 16 permutations and since the counter searches sequentially, the stored word will be identified after i clock cycles where $0 \leq i \leq 15$. At the clock cycle in which the

binary source word is identified the comparator will give an output pulse placed at the i^{th} slot in the PPM frame. This satisfies the conversion requirement. Generally the 8 bit counter will be allowed to continue after the 16 cycles to provide extra slots that will serve as a guard band and also to provide the frame clock used to reset the 4 bit counter and enable the latch in the serial to parallel counter. The observed pulse stream at the output of this coder is shown in Figure 5.14. The upper trace is the frame waveform, with the high representing the allowed band and low representing the guard band. The lower trace is the PPM stream.

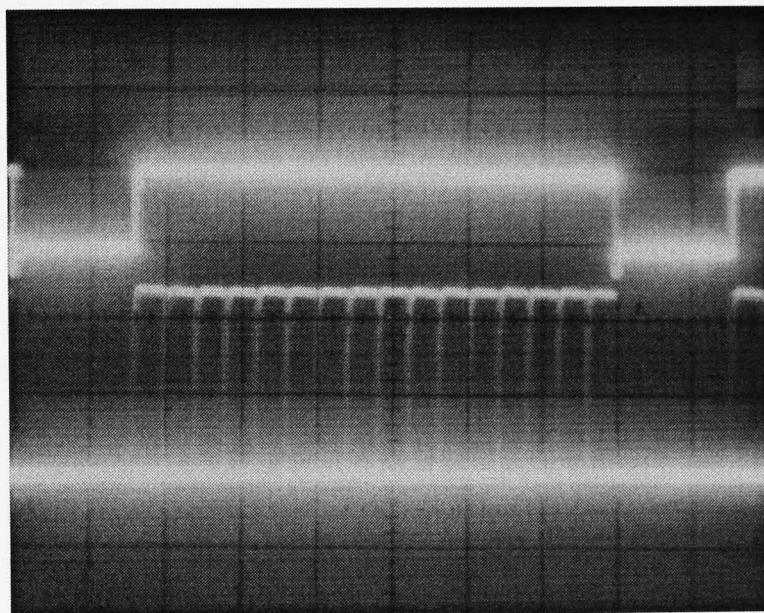


Figure 5.14 Observed PPM stream and the PPM frame at $n=16$ and $m=0.8$.

5.6 PPM decoder design

In this section, details of the PPM decoder are given. These are shown in Figure 5.15. The decoder comprises a 4 bit counter that is started in synchronism with the PPM frame by employing the frame clock available from the synchronisation subsystem.

The counter is caused to count at the PPM slot rate by employing the extracted slot frequency component. The count will continue until a PPM pulse is received at which point the counter is caused to stop and at the same time the output of the counter will be passed through latch 1. The output data will be stored in latch 2 until the new PPM frame starts. When the next PPM frame starts, the output data will be passed through latch 2 and the data is shifted to the output using the shift register.

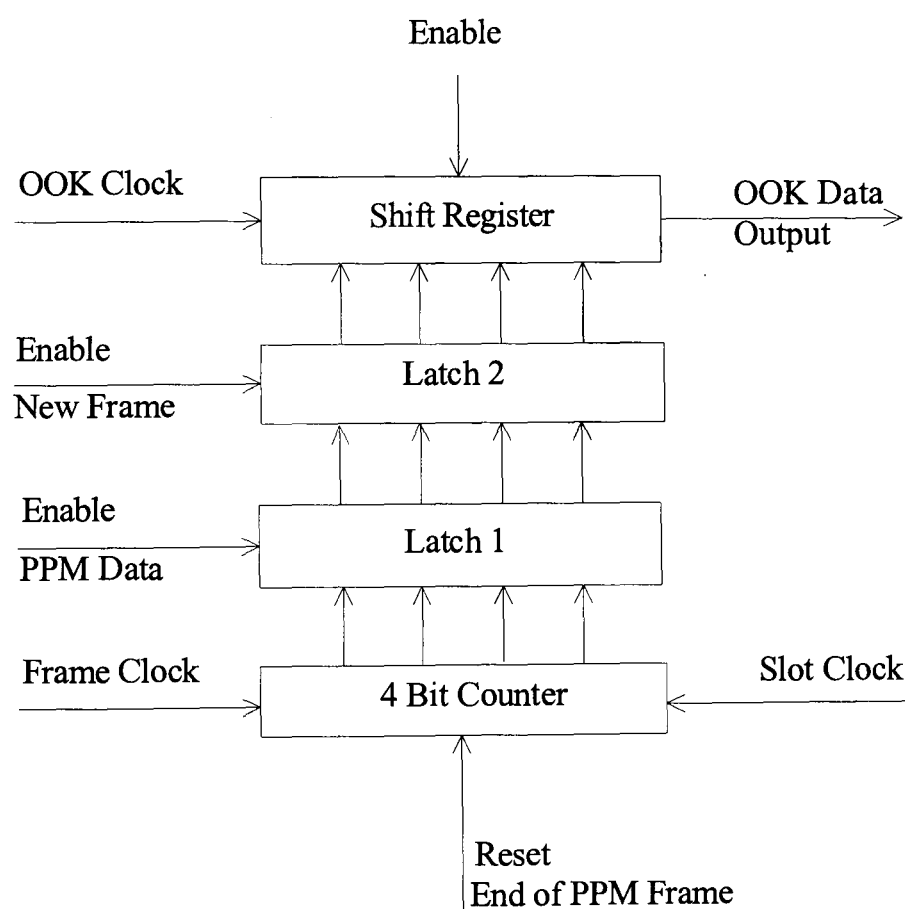


Figure 5.15 Details of the digital 16-PPM decoder

5.7 Summary

This chapter has described the PPM signal and its relation to the well known PCM format. The three error sources also cited with the PPM signal have been identified and expressions have been given to evaluate the associated error probabilities. The design of a PPM coder and decoder has been outlined and experimental results have been given for the generated PPM signal. A PPM optical wireless system has been presented and analysed. The results have shown that multipath dispersion and background noise can have serious impact on the system sensitivity. Moreover, it has been shown that PPM can offer up to 9.8 dB sensitivity improvement over a comparable OOK system. This benefit remains almost unaltered under the effect of ambient noise as both systems are affected to almost the same degree. However multipath dispersion has been shown to result in a higher penalty in PPM compared to OOK due to the narrow pulses used by PPM. The PPM penalty due to multipath effects was found to be in the order of 3-5 dB more than that associated with OOK. This has motivated the equalisation work to be presented in the next Chapter.

Chapter 6 Equalisation

6.1 Introduction

In Chapter 5, we have presented results for both LOS and diffuse systems which have shown that the PPM system is more vulnerable than OOK to multipath dispersion. The sensitivity penalty varied between 3.4 dB (at the corner of room A) to 5.3 dB (at centre of room A) in the indoor infrared wireless PPM diffuse system.

From the results obtained in Chapter 5, it can be seen that CRB has a profound effect on the system sensitivity. The higher the CRB value, the better the system sensitivity. The results showed that when CRB is equal to 3 (bandwidth = 20 MHz), the system sensitivity is -45.8 dB and when CRB equal to 10 (bandwidth = 67 MHz) the system sensitivity is -49.47 dB using 5-PPM (i.e. $M=5$). From Chapter 3, the impulse response results have shown that CRB is between 2.1 to 3 (depending on the receiver location) for a 10 Mbit/s 5-PPM system. In this chapter, we would like to design an equaliser that can compensate for the channel low pass function, thus improving CRB,

the received pulse shapes (reducing dispersion effect) and improving the sensitivity. The equaliser will employ a transversal filter.

A filter is essentially a system or network that selectively changes the wave-shape, amplitude-frequency or phase-frequency characteristic of a signal in a desired manner. A common filtering objective is to improve the quality of a signal. In this project a digital filter was used for the equaliser. Such a structure is very useful and suits the time varying optical wireless mobile environment. Moreover the filter response can easily be tuned to the required transfer function if the latter is variable.

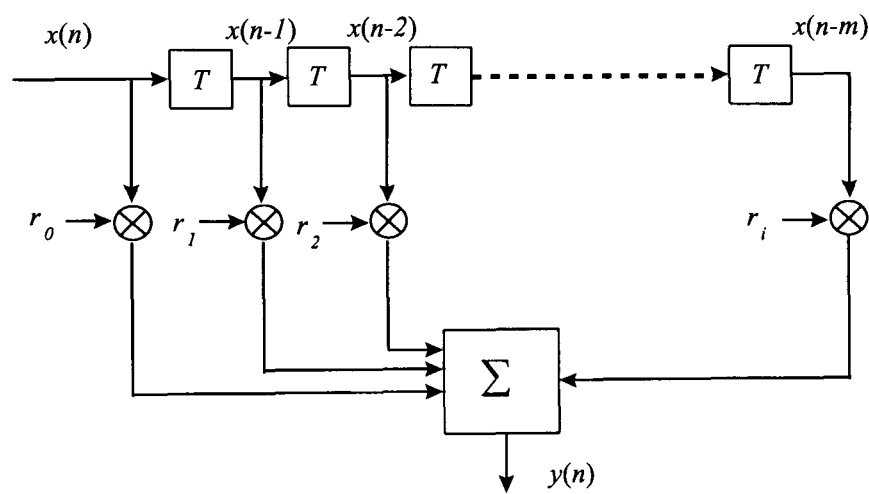


Figure 6.1 Transversal filter

In this project, we would like to design a transversal filter. Such filters are attractive since they are inherently stable, lend themselves to adaptive configurations and can easily be implemented. A transversal filter is shown in Figure 6.1, which consists of a delay line tapped at T second intervals. Each tap is connected through a variable gain device with tap coefficient r_i to a summing device. Intersymbol interference is reduced by filtering the input signal and by computing values for the tap coefficients which

minimize the peak ISI. This chapter begins by introducing the received pulse shapes, channel response and hence the equaliser design that minimises ISI. Next, the system performance, with the equaliser incorporated, is analysed. The chapter concludes by comparing the system performance to that of a system that does not include equalisation.

Receiver Location	Channel frequency response -3dB bandwidth	FWHM
r111	22 MHz	16.6 ns
r121	19.5 MHz	17.8 ns
r131	18 MHz	20.8 ns
r141	17.4 MHz	22.2 ns
r211	25 MHz	15 ns
r221	22.7 MHz	15.4 ns
r231	21.3 MHz	18 ns
r241	20.7 MHz	19 ns

Table 6.1 Channel bandwidth and received pulses FWHM

6.2 Range of received pulse shapes

Figure 6.2 shows the channel impulse response and frequency response in test room A (room parameters shown in Chapter 3). The shape of the received pulse depends on the location of the receiver in the room. Varying the location of the receiver will change the channel impulse response. Table 6.1 shows the channel bandwidth and the received pulses full width half maximum (FWHM). The results show that the channel bandwidth varies between 25 MHz and 17.4 MHz and the FWHM varies between 22.2 ns and 15 ns for the specified locations. An improvement in the system

sensitivity can be achieved if the pulse FWHM is reduced. The next section addresses the design of an equaliser that improves the channel bandwidth thus reducing the pulses FWHM.

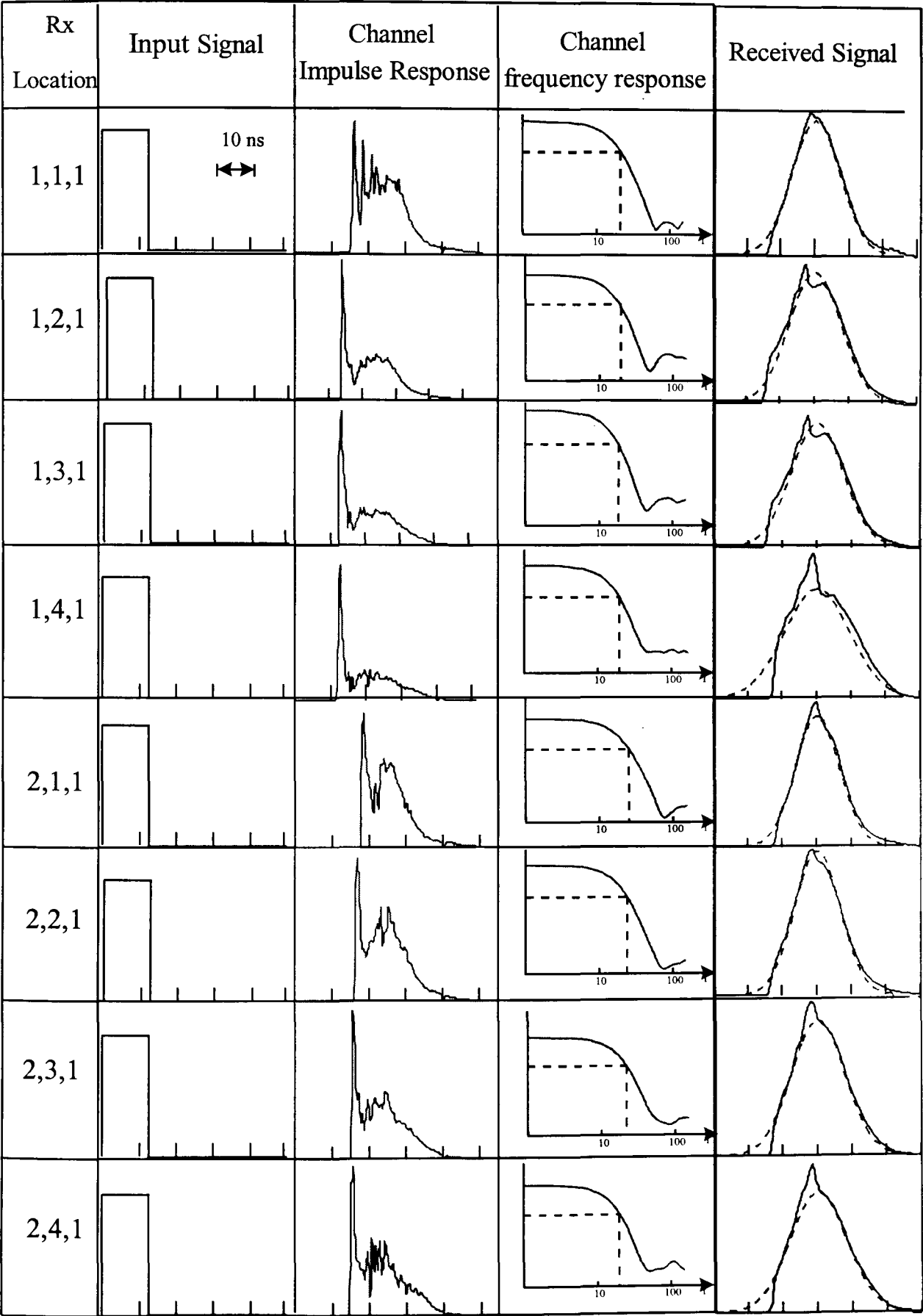


Figure 6.2 Channel impulse response and received pulse shape

6.3 Filter design

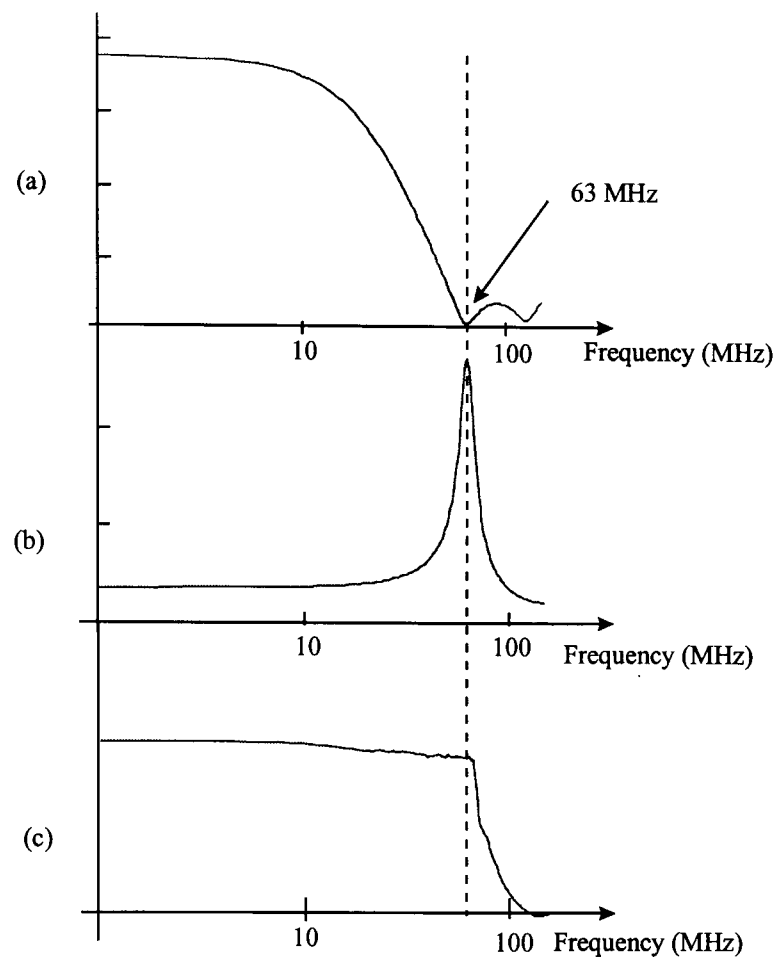


Figure 6.3 Frequency response (a) Channel (b) Equaliser (c) Channel and Equaliser

The received pulse shapes varied according to the receiver location. This in turn dictates a different channel. As an example, we chose the location (1,1,1) for the receiver. The channel frequency response at (1,1,1) is shown in the Figure 6.3 (a) which shows the bandwidth at the -3 dB point to be 22 MHz. In order to reduce multipath dispersion, it is necessary to increase the bandwidth at the -3 dB point. From Figure 6.3 (a) the channel frequency response exhibits a null at 63 MHz. The equaliser was designed to have a peak at this value and a response that compensates for the channel roll-off. Figure 6.3 (b) shows a filter frequency response ideal for this purpose. The combination of the channel and equaliser frequency response is shown in Figure 6.3 (c) which shows an improvement in the -3dB point, from 20 MHz to 65

MHz. The equaliser was designed with reference to the z-plane and the required pole-zero configuration. The normalised angular frequency in radians can be written as

$$\omega_1 = \frac{\omega_0}{f_s} \tag{6.1}$$

where the ω_0 is frequency of interest (the first null in this case) and f_s is the sampling frequency. From Figure 6.3 f_0 is 63 MHz and therefore a sampling frequency of 300 MHz was chosen giving an angular frequency on the unit circle of 0.42π . This sampling frequency is high, however it simplifies the filter design since the pole location (0.42π) is much smaller than π . A set of complex conjugate poles was therefore inserted at this frequency as shown in Figure 6.4. The resulting transfer function is given by

$$EQ(f) = \frac{1}{(e^{i2\pi fT_s} - r_1 e^{i\omega_0\pi})(e^{i2\pi fT_s} - r_1 e^{-i\omega_0\pi})} \tag{6.2}$$

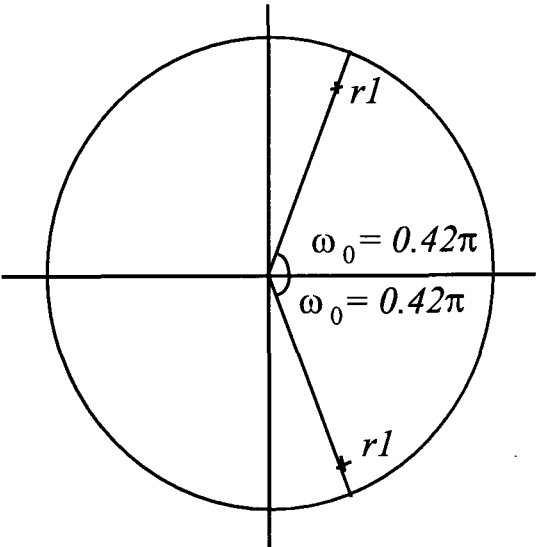


Figure 6.4 Z-plane pole-zero configuration

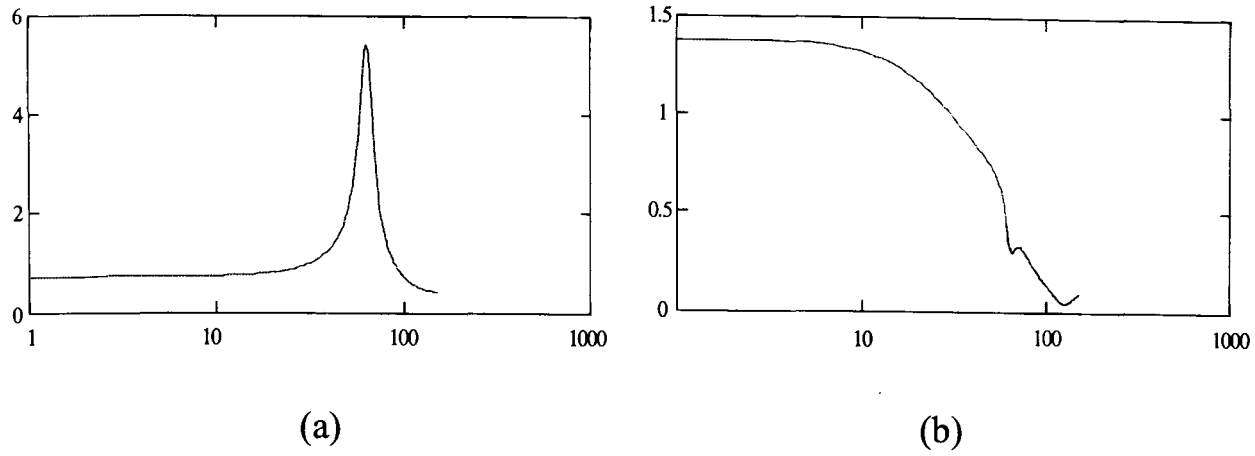


Figure 6.5 Frequency response (a)Equaliser (b) Total

Figure 6.5 shows the frequency response for the equaliser and the total frequency response (ie channel and equaliser). Figure 6.5 (b) shows that the -3dB point is equal to 33 MHz. Optimisation of the r_1 value does not lead to much improvement and therefore another set of poles was inserted at this frequency. The z-plane pole-zero configuration is shown in Figure 6.6. The equaliser transfer function now becomes

$$EQ(f) = \frac{1}{(e^{i2\pi fT_s} - r_1 e^{i\omega_0 \pi})(e^{i2\pi fT_s} - r_1 e^{-i\omega_0 \pi})} \times \frac{1}{(e^{i2\pi fT_s} - r_2 e^{i\omega_0 \pi})(e^{i2\pi fT_s} - r_2 e^{-i\omega_0 \pi})} \quad (6.3)$$

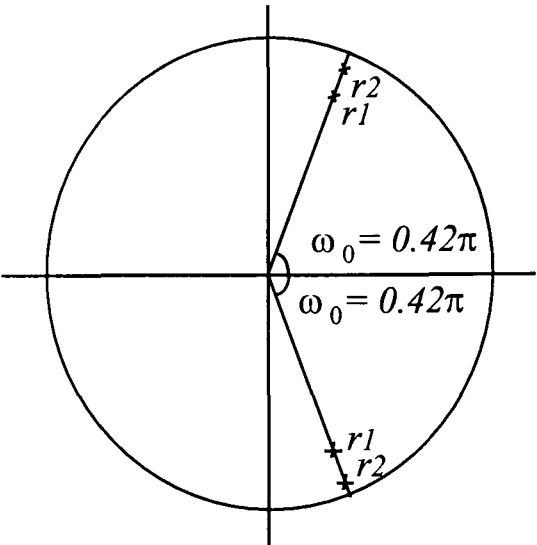


Figure 6.6 Z-plane pole-zero configuration

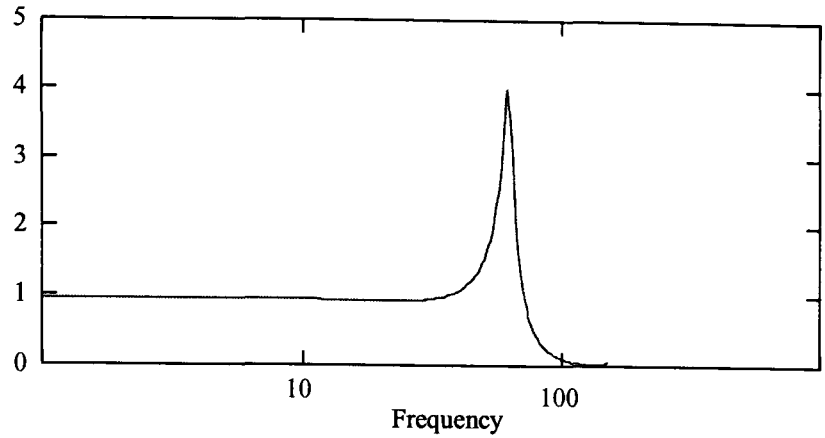


Figure 6.7 Total frequency response

The total frequency response is shown in Figure 6.7, which exhibits a large overshoot at the angular frequency ω_0 . Optimisation of the position of the new set of poles led to a reduction in the overshoot value but not complete elimination. To have complete control of the response prior and after the null, a new pole zero pair was introduced thus giving a controllable notch at the frequency ω_0 . The resultant Z-plane pole-zero configuration is shown in Figure 6.8 and the equaliser transfer function can be written as

$$EQ(f) = \frac{1}{(e^{i2\pi fT_s} - r1e^{i\omega_0\pi})(e^{i2\pi fT_s} - r1e^{-i\omega_0\pi})} \times \frac{1}{(e^{i2\pi fT_s} - r2e^{i\omega_0\pi})(e^{i2\pi fT_s} - r2e^{-i\omega_0\pi})} \times \frac{(e^{i2\pi fT_s} - rze^{i\omega_0\pi})(e^{i2\pi fT_s} - rze^{-i\omega_0\pi})}{(e^{i2\pi fT_s} - r3e^{i\omega_0\pi})(e^{i2\pi fT_s} - r3e^{-i\omega_0\pi})} \quad (6.5)$$

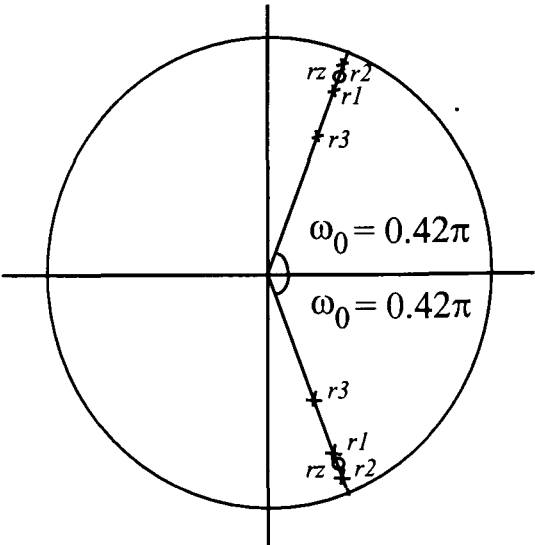


Figure 6.8 Z-plane pole-zero configuration

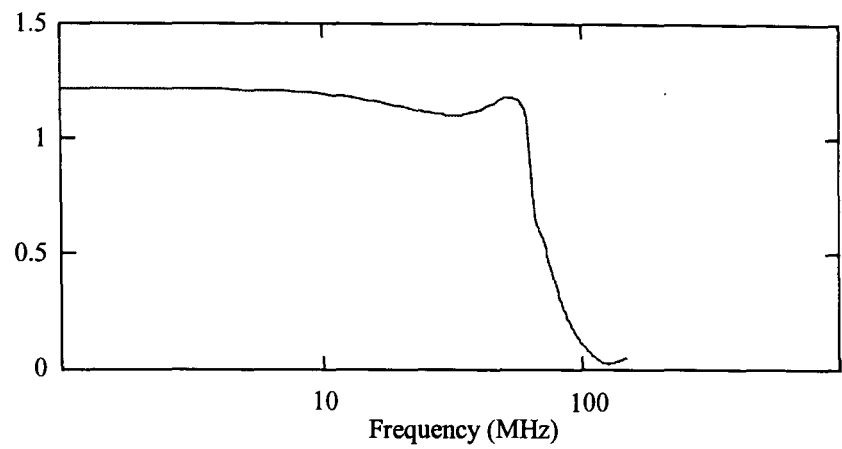


Figure 6.9 Total frequency response

The radii r_1 , r_2 , r_3 and r_z were then optimised using an LMS search for the best frequency response. The equalised response is shown in Figure 6.9 where the -3dB bandwidth is 64 MHz. This equaliser was then used to evaluate the system sensitivity in the same multipath environment.

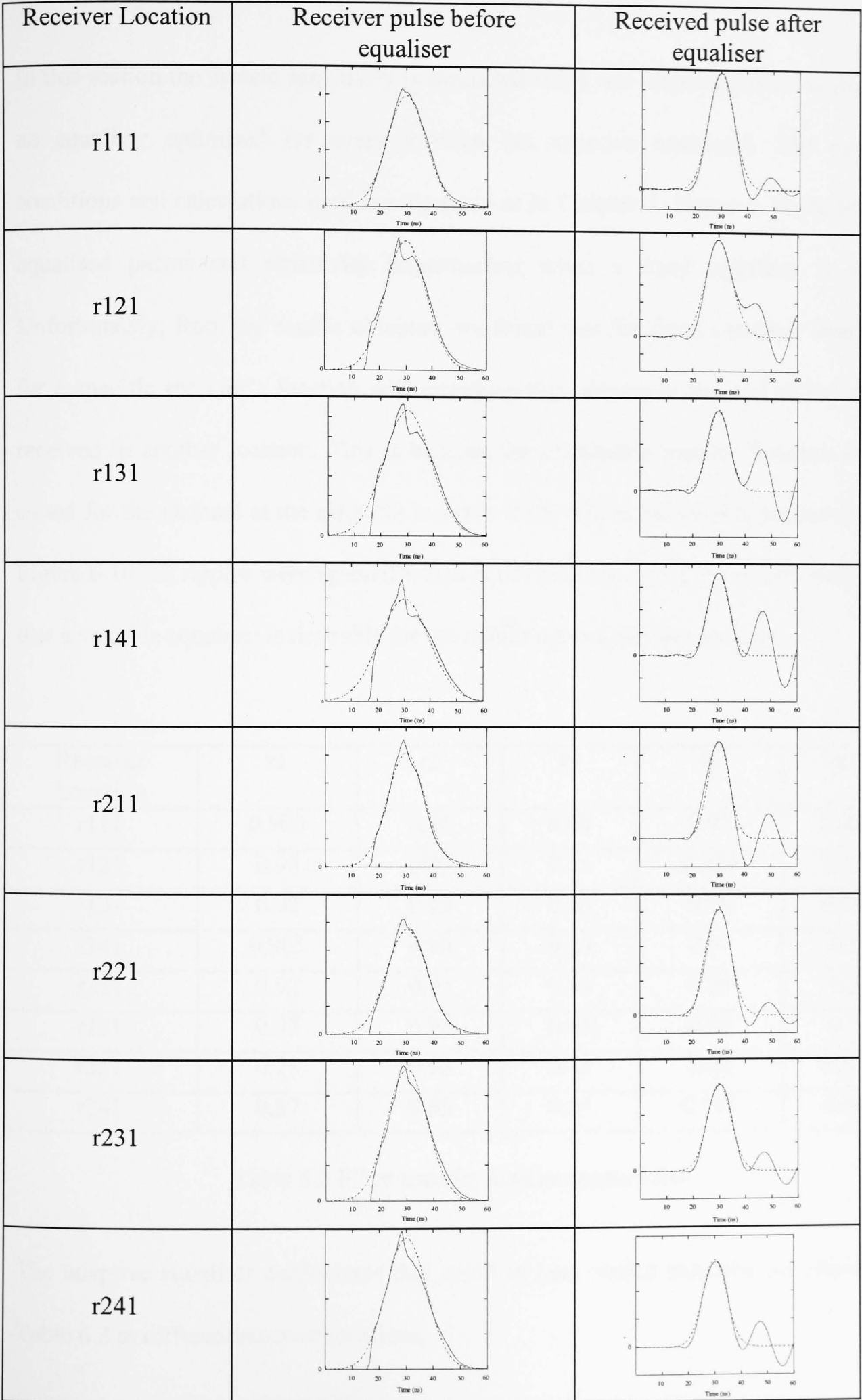


Figure 6.10 Received pulse before and after equaliser using fixed equaliser

6.4 Sensitivity evaluation

In this section the system sensitivity is evaluated using one fixed equaliser as well as an equaliser optimised for every location (an adaptive equaliser). The system conditions and calculations used are the same as in Chapter 5. Figure 6.10 shows the equalised pulses and sensitivity improvement when a fixed equaliser is used. Unfortunately, from the results obtained, we found that the fixed equaliser designed for a specific receiver’s location will introduce high ripples at the end of the pulse received in another location. This is because the equaliser’s transfer function is not suited for the channel at the different location. Note that in calculating sensitivities in Figure 6.10 the ripples were ignored which is not realistic. From the results we know that a variable equaliser is desirable for the indoor optical wireless system.

Receiver Location	r1	r2	r3	rz	$\omega 1$
r111	0.905	0.95	0.65	0.97	0.42
r121	0.93	0.95	0.65	0.955	0.32
r131	0.92	0.95	0.65	0.96	0.29
r141	0.905	0.95	0.65	0.97	0.3
r211	0.92	0.95	0.65	0.96	0.5
r221	0.92	0.95	0.65	0.96	0.5
r231	0.75	0.95	0.65	0.94	0.37
r241	0.87	0.95	0.65	0.955	0.34

Table 6.2 Filter transfer function parameters

The adaptive equaliser coefficients that result in best overall response are shown in Table 6.2 at different receiver locations.

Figure 6.11 shows the received pulses when a variable equaliser is used. The results show that the system sensitivity has improved between 1.69 dB to 3.81 dB. The results also show that the ripples at the end of the received pulses have been reduced when the variable adaptive equaliser is used.

Receiver Location	Before equaliser	Using fixed equaliser	Using variable equaliser
r111	-46.06 dB	-47.93 dB	-47.93 dB
r112	-45.63 dB	-47.85 dB	-47.85 dB
r113	-44.6 dB	-48.32 dB	-47.85 dB
r114	-44.17 dB	-48.38 dB	-47.98 dB
r211	-46.71 dB	-48.32 dB	-48.17 dB
r221	-46.53 dB	-48.07 dB	-47.89 dB
r231	-45.54 dB	-48.07 dB	-47.85 dB
r241	-45.21 dB	-48.07 dB	-47.85 dB

Table 6.3 System Sensitivity

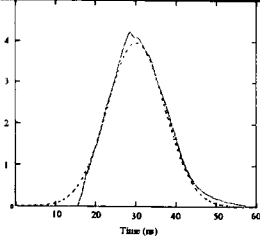
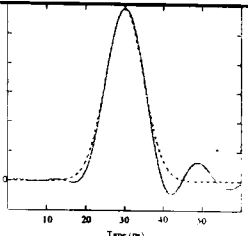
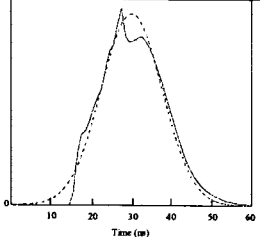
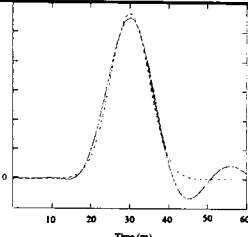
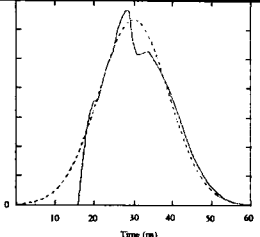
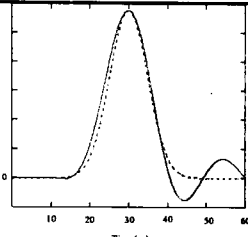
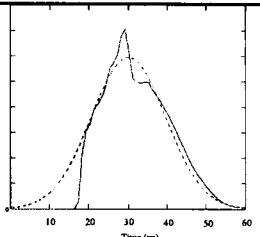
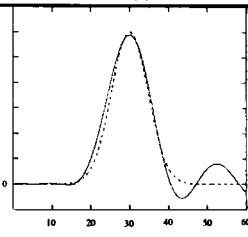
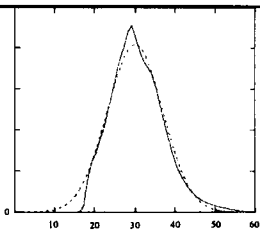
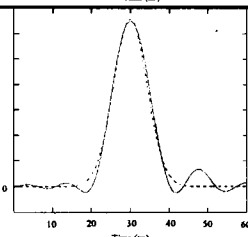
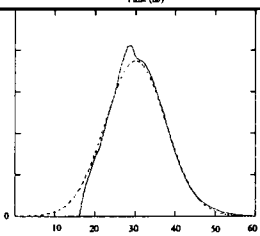
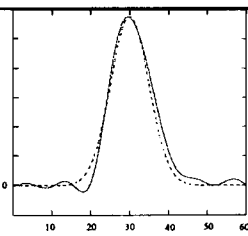
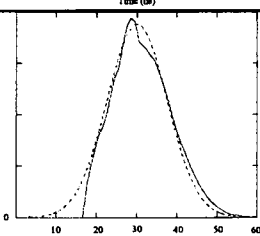
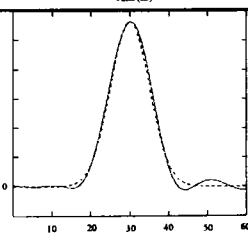
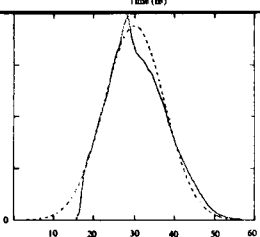
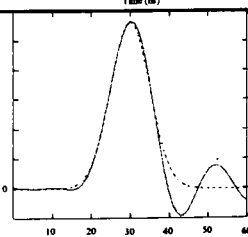
Receiver Location	Receiver pulse before equaliser	Received pulse after equaliser	Sensitivity improvement
r111			1.69 dB
r121			2.21 dB
r131			3.24 dB
r141			3.80 dB
r211			1.93 dB
r221			2.18 dB
r231			2.55dB
r241			2.79 dB

Figure 6.11 Received pulse before and after equaliser using variable equaliser

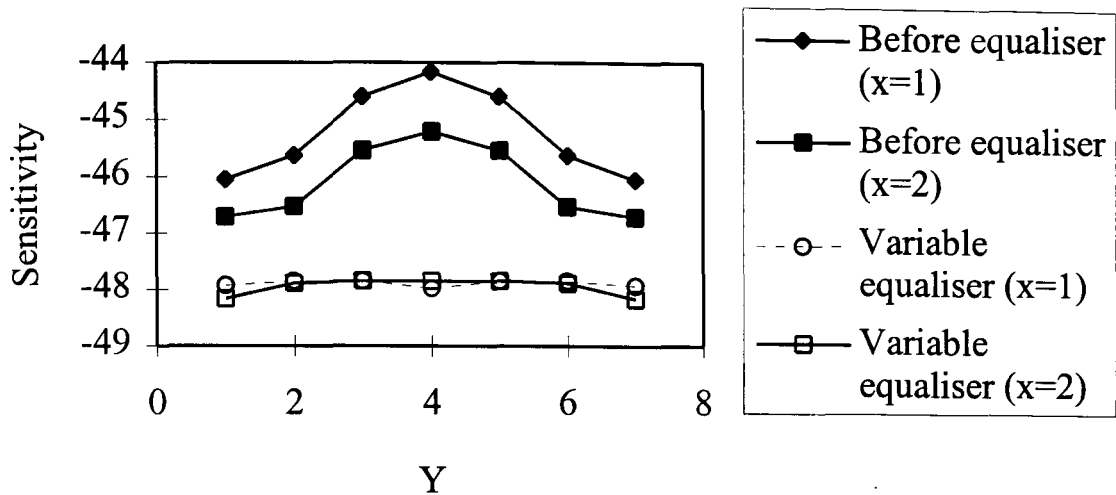


Figure 6.12 System sensitivity

Table 6.3 and Figure 6.12 show the system sensitivity before and after the equaliser. Before using the equaliser, the system has a sensitivity difference of 1.89 dB between the corner and the centre of test room A. After using the variable equaliser in the system the sensitivity difference is only 0.32 dB. Moreover using the equaliser a sensitivity improvement of up to 3.81 dB can be achieved.

6.5 Summary

In this chapter we have designed a new equaliser for indoor optical wireless systems to reduce the channel multipath dispersion. The results show that the system sensitivity can improve by up to 3.8 dB when a variable equaliser is used. This also results in minimum ripples in the received pulse shapes. The approach adopted in this chapter has been mainly concerned with demonstrating the benefits that can be achieved through the use of equalisation. Further work is needed in this area to examine non recursive (FIR) filter structures and adaptation algorithms for automatic

operation. The high sampling frequency used can also be reduced from 300 MHz to lower values in the order of 150 MHz with careful design. The benefit achievable (3.8 dBs) justifies the hardware investment.

Chapter 7 Optical Wireless PPM CDMA System

7.1 Introduction

Among various multiplexing schemes considered for use in local area networks (LAN's), Code Division Multiple Access (CDMA) techniques have recently received substantial attention. This is due to the development of large bandwidth optical communication channels which introduce several advantages over traditional networking [73-75]. CDMA fundamentally lends itself easily to asynchronous, randomly-originated transmission of data. There are very large numbers of channels available if one resorts to CDMA on a photonic data highway [76].

As is well known, in CDMA systems each user is assigned a sequence-code that serves as its address. In order for the receiver, in this case an optical correlator, to correctly recognize the active users, the employed codes must be orthogonal to one another. The usage of CDMA techniques has an advantage over synchronous multiple

access schemes such as Time Division Multiple Access (TDMA) because CDMA techniques do not require synchronization between the transmitters. Further, when compared to Frequency Division Multiple Access (FDMA), a version of CDMA with a tapped delay line and threshold detector in the receiver does not require any synchronization at all. Another aspect of CDMA systems of interest to optical wireless communications is that due to the asynchronous operation mode, they provide a natural choice for the bursty nature of the traffic in LANs. Moreover, in a CDMA system, the addition of new users is easy, since it requires only a new orthogonal code to serve as the address of new user.

A typical optical wireless code division multiple access (OW-CDMA) communication system is best represented by an information data source, followed by an optical encoder that maps each bit of the output information into a very high rate sequence, that is then transmitted into the wireless channel. At the receiver end of the OW-CDMA, the optical pulse sequence would be compared to a stored replica of itself and to a threshold level at the comparator for data recovery.

In OW-CDMA there are N such transmitter and receiver pairs. Figure 7.1 shows one such network in a diffuse configuration. The set of OW-CDMA optical pulse sequences essentially becomes a set of address codes or signature sequences for the network. To send information from user j to user k , the address code for receiver k is impressed upon the data by the encoder at the j th node. One of the primary goals of OW-CDMA is to extract data with the desired optical pulse sequence in the presence of all other user's optical pulse sequences. We therefore need to design sequences that

satisfy two conditions [74], namely: each sequence can easily be distinguished from a time shifted version of itself and each sequence can be easily distinguished from every other sequence in the set.

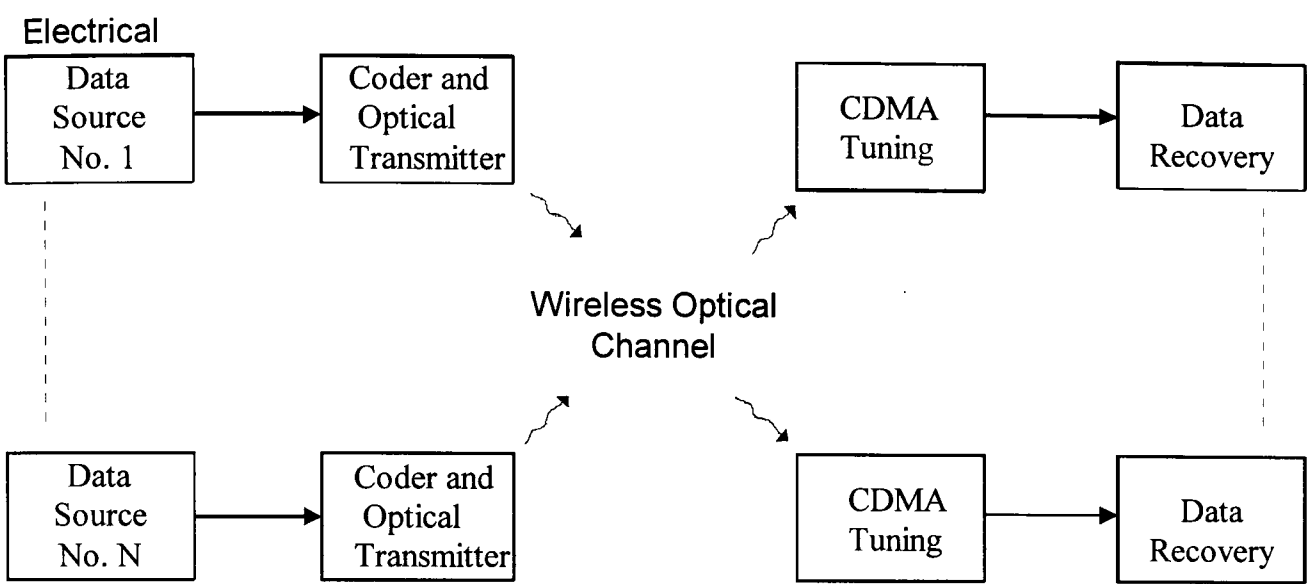


Figure 7.1 A schematic of an optical wireless code division multiple-access communication system with

Most work done on optical CDMA has concentrated on the binary transmission of data, e.g. ON OFF Keying (OOK). Very few suggested using M -ary transmission of data, e.g. Pulse Position Modulation (PPM) [75,77,78]. Lam and Hussain [75] suggested an M -ary system in which each symbol is represented by one of M mutually orthogonal sequences (signatures). Thus a total of MN code sequences are required, where N is the number of users. In this project, the reason we employ the PPM-CDMA technique is that PPM-CDMA gives a higher bit rate (at a given bandwidth) and results in less co-user interference compared to OOK CDMA as will be shown later. In the next section, we will analyse the PPM-CDMA system performance.

7.2 PPM-CDMA systems

In this project, two novel PPM CDMA systems have been considered and analysed.

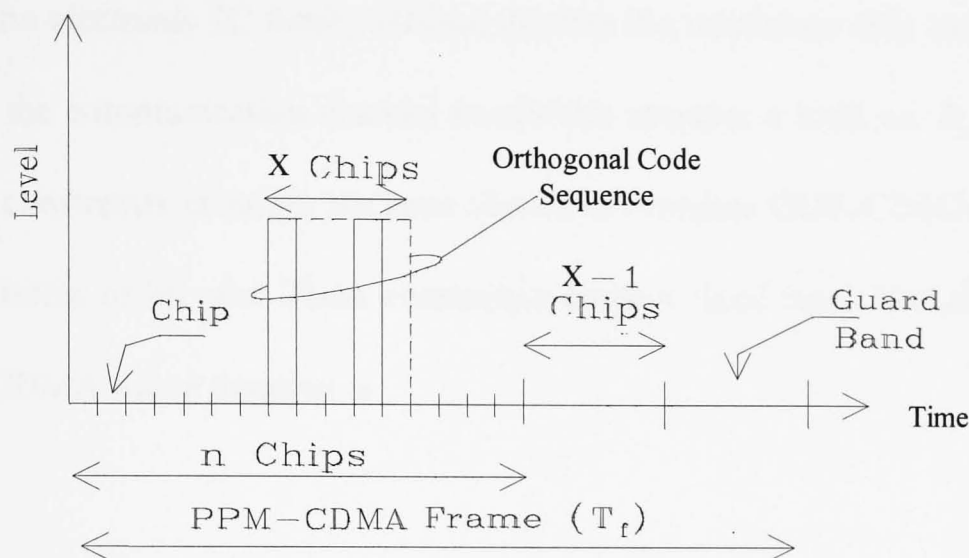


Figure 7.2 PPM CDMA system structure 1

Structure 1

The proposed transmission structure is shown in Figure 7.2. The time domain is subdivided into frames of duration T_f . Each frame has $n = 2^M$ allowed chip positions and as such conveys M bits of information. An orthogonal code of length X chips carries the destination address. The position of the sequence on the n chips determines the data word transmitted. The desired receiver auto-correlates its signature with the stream on the network, thus identifying the data sent to it. The transmission frame carries a reserved band of $X-1$ chips to avoid the event of the CDMA code protruding into the next frame when the n^{th} word is transmitted. Furthermore a guard band of

duration $(1-m)T_f$ (where $0 < m < 1$ is the modulation depth) serves to eliminate interframe interference (IFI) which would otherwise occur due to the pulse dispersion effects attributed to the channel and receiver limited bandwidth.

Typically the electronic IC family utilised dictates the maximum chip rate R_c . At the same time the communication channel bandwidth imposes a limit on R_c . Therefore with these constraints in mind, we have chosen to compare OOK-CDMA and PPM-CDMA in terms of bit rate. These constraints entail a fixed maximum chip rate R_c . The PPM CDMA frame duration is.

$$T_f = \left\{ \frac{n + X - 1}{m} \right\} \frac{1}{R_c} \quad (7.1)$$

and the PPM-CDMA bit rate is

$$R_{b1} = \left\{ \frac{m \log_2(n)}{n + X - 1} \right\} R_c \quad (7.2)$$

The OOK-CDMA system has to accommodate X chips per bit. Under the same chip rate R_c , the OOK-CDMA bit rate is

$$R_{boc} = \frac{R_c}{X} \quad (7.3)$$

A useful measure of performance can be established by considering the bit rate enhancement achieved (under bandwidth and electronic speed constraints) by using PPM-CDMA rather than OOK-CDMA. This bit rate enhancement can be expressed as

$$F_1 = \frac{R_{b1}}{R_{boc}} = \frac{X m \log_2(n)}{n + X - 1} \tag{7.4}$$

where F_1 is the bit rate enhancement factor. Results are presented in Figure 7.3 for F_1 at various PPM orders and orthogonal code lengths with $m=0.8$ (which is the modulation depth adopted throughout this study). The results indicate that for a given orthogonal code length X , there is an optimum PPM order that maximises the bit rate. Moreover, bit rate enhancement values corresponding to $F_1>1$ are depicted with a maximum enhancement of about $F_1=5.75$ (when $X = 2048$ and $n = 512$) over the range of parameters considered. This indicates that PPM-CDMA outperforms OOK-CDMA in this respect.

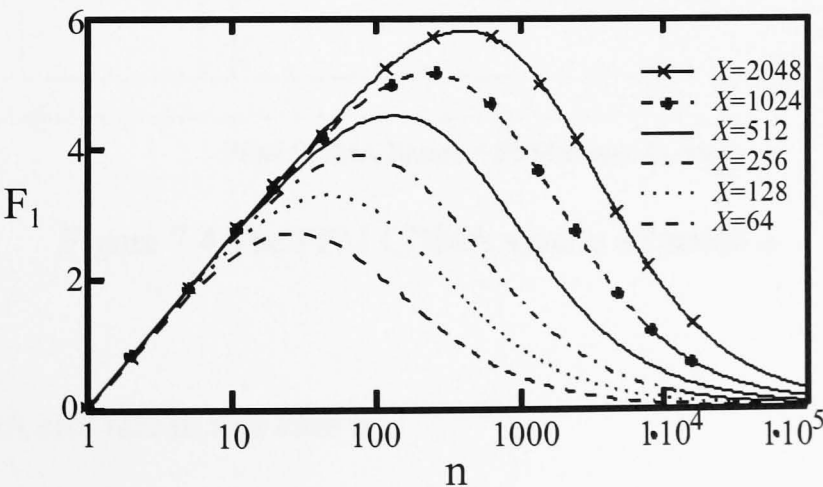


Figure 7.3 Bit rate enhancement for structure 1

Structure 2

The alternative transmission structure is shown in Figure 7.4. The main distinction is that the CDMA code is now inserted (accommodated) within one PPM slot. The code gives the destination address and its position on the frame conveys the information sent. The average power per frame is the same in both cases since the number of code pulses per frame is identical; moreover the energy per pulse (for a given noise environment and bit error rate) is constant (wide short pulses versus thin tall ones). Therefore a distinction needs to be made between the two structures based on bandwidth requirements and the achievable bit rate.

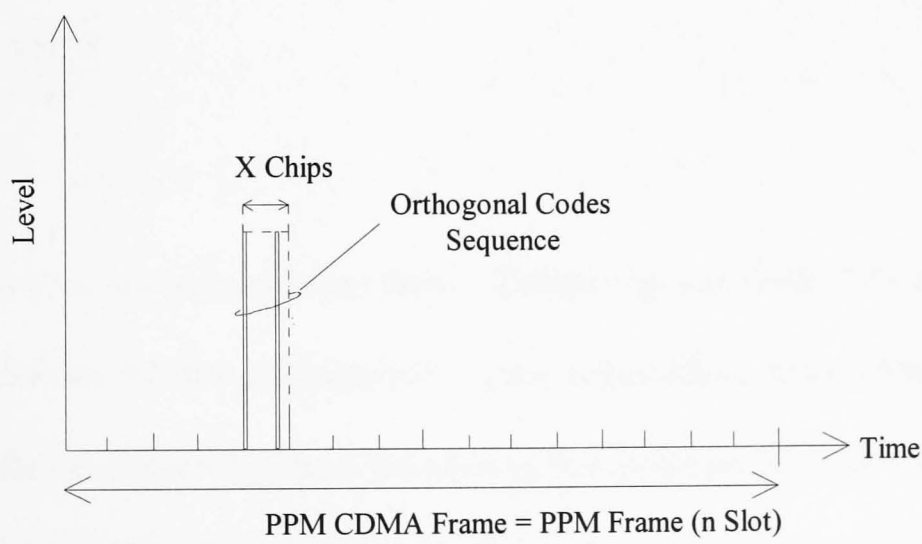


Figure 7.4 The PPM CDMA system structure 2

The PPM CDMA slot rate in this case is

$$R_s = \frac{R_c}{X} \tag{7.5}$$

and the PPM CDMA frame rate is

$$R_F = \frac{R_s}{n} \quad (7.6)$$

The PPM CDMA bit rate is

$$\begin{aligned} R_{b2} &= R_F \log_2 n \\ &= \frac{R_c}{X} \frac{1}{n} \log_2 n \end{aligned} \quad (7.7)$$

Then the bit rate enhancement can be expressed as

$$F_2 = \frac{R_{b2}}{R_{boc}} = \frac{\log_2 n}{n} \quad (7.8)$$

where F_2 is the bit rate enhancement factor. Comparing equations (7.8) and (7.4), it is to be noted that the bit rate enhancement is now independent of the code length. This result is implied in Figure 7.3 since the code in this structure is accommodated within a pulse as with OOK. Results are presented in Figure 7.5 for F_2 at various PPM orders. Bit rate enhancement values corresponding to $F_2 < 1$ are depicted with a maximum enhancement of about $F_2 = 0.55$ over the range of parameters considered. This indicates that structure 2 system performance is not better than OOK-CDMA. Further analysis in this project will concentrate on structure 1.

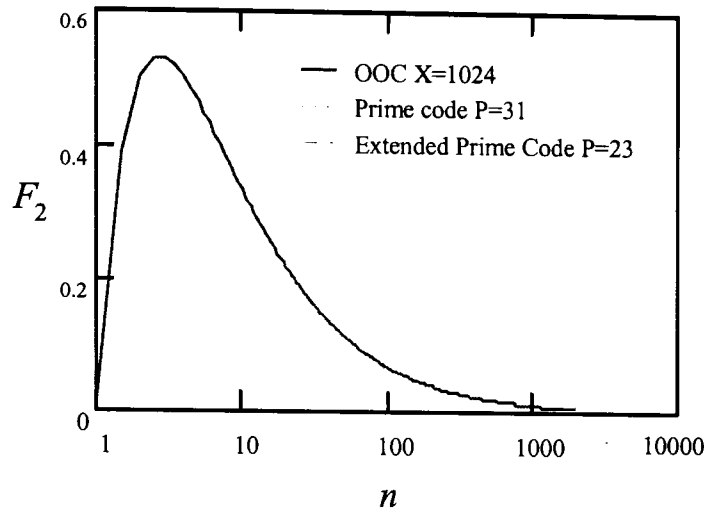


Figure 7.5 Bit rate Enhancement for Structure 2

7.3 Orthogonal coding schemes

Code division multiple access (CDMA) has been investigated extensively in the context of mobile radio communications and optical wireless networks [79,80]. It is an attractive multiple access scheme for optical wireless networks because it allows multiple users to access the same channel asynchronously with no delay or scheduling. CDMA is based upon the assignment of orthogonal codes to the address of each user, which substantially increases the bandwidth occupied by the transmitted signal. Conventional, CDMA applications have utilised pseudo noise (PN) sequences for signature. These rely on polar $\{-1,+1\}$ pulses to achieve the required auto- and cross-correlation properties. Optically, codes belonging to $\{0,1\}$ are desirable to avoid the complex coherent processing techniques.

In wireless networks low cross-correlation is a very important parameter which reduces the interference from unwanted signals. There are two types of optical address

codes that have widely been studied, namely, prime codes [81,82] and optical orthogonal codes (OOCs)[83]. OOCs are a family of $(0,1)$ sequences with good auto- and cross-correlation properties (i.e. maximum cross-correlation equal to 1). Prime codes have a maximum cross-correlation equal to 2 but they can be used to increase the number of users in the network. Although OOCs have better auto and cross correlation properties compared to prime codes, much more complex algorithms are required to produce/correlate the OOCs [84]. Yang and Kwong have presented a new code (extended prime code) to reduce the cross-correlation from 2 to 1 [85]. Therefore, extended prime codes appear more attractive than OOCs and prime codes (i.e. number of user, bit rate and error probability).

However another consideration when using such codes over optical wireless networks, is that of improving the system sensitivity. The receiver sensitivity is an important parameter in such networks due to the limitations imposed on transmitter power by eye safety [17]. Most of the work done on optical wireless CDMA networks has concentrated on the binary transmission of data, e.g. ON OFF Keying (OOK)[17]. Elmirghani et al [86] have shown that Pulse Position Modulation can be used to improve the system sensitivity, moreover the PPM low average power is suited for battery operation while its high peak power aids detection. In this chapter, the performance of OOCs, prime codes and extended prime codes is analysed with a PPM signal in the indoor wireless environment and the resulting performance is compared among the different codes.

7.3.1 Optical orthogonal codes

Central to any successful code division multiple access scheme, whether electrical or optical, is the choice of the signature sequences, on which the information bits of different users is mapped. In CDMA many asynchronous users occupy the same channel simultaneously. A desired user's receiver must be able to extract its signature sequence in the presence of other user's signature sequences. Therefore, a set of signature sequences that are distinguishable from time shifted versions of themselves and from other members of the family are needed. One such possible set is the set of optical orthogonal codes (OOC).

Optical orthogonal codes (OOCs) are a family of (0,1) sequences with good auto- and cross-correlation properties. The autocorrelation exhibits a high peak at zero shift and the crosscorrelation between any two sequences remains low throughout. The use of OOC's enables a large number of asynchronous users to transmit information efficiently and reliably. Let two periodic signals $x(t)$ and $y(t)$ be the sequences to be used as signature codes. These can be written as

$$x(t) = \frac{1}{T_c} \sum_{n=-\infty}^{\infty} x_n P_{T_c}(t - nT_c) \quad (7.9)$$

and

$$y(t) = \frac{1}{T_c} \sum_{n=-\infty}^{\infty} y_n P_{T_c}(t - nT_c) \quad (7.10)$$

where $P_{T_c}(t)$ is a unit rectangular pulse of duration T_c and $\{x_n, y_n\} \in \{0,1\}$. For $x(t)$ and $y(t)$ to be useful as signature sequences, they must possess a highly peaked autocorrelation and an extremely low cross correlation. In fact strict orthogonality necessitates a null crosscorrelation.

The theory of OOC has been rigorously formulated [74, 83, 87]. The requirements to be satisfied by the code sequence $x_n \in \{0,1\}$ can be summarized as

$$R_{xx}(l) = \left| \sum_{n=0}^{L-1} x_n x_{n+l} \right| = \begin{cases} k & \text{for } l = 0 \\ \leq \lambda_a & \text{for } 1 \leq l \leq L-1 \end{cases} \quad (7.11)$$

where L is the length of the code in bits. Equation (7.11) guarantees an autocorrelation with peak k and residue λ_a . Similarly, the cross correlation should be bound by a residue λ_c such that

$$R_{xy}(l) = \left| \sum_{i=0}^{L-1} x_i y_{i+l} \right| \leq \lambda_c \quad \text{for } 0 \leq l \leq L-1 \quad (7.12)$$

In general, for a given sequence of length L and weight k (number of pulses in L) with $\lambda_a = \lambda_c = 1$, the maximum number of OOC (Number of users) N is given by

$$N \leq \frac{L-1}{k(k-1)} \quad (7.13)$$

At a given chip rate R_c the PPM-CDMA bit rate is

$$R_b = \left\{ \frac{m \log_2(n)}{n + Nk(k-1)} \right\} R_c \quad (7.14)$$

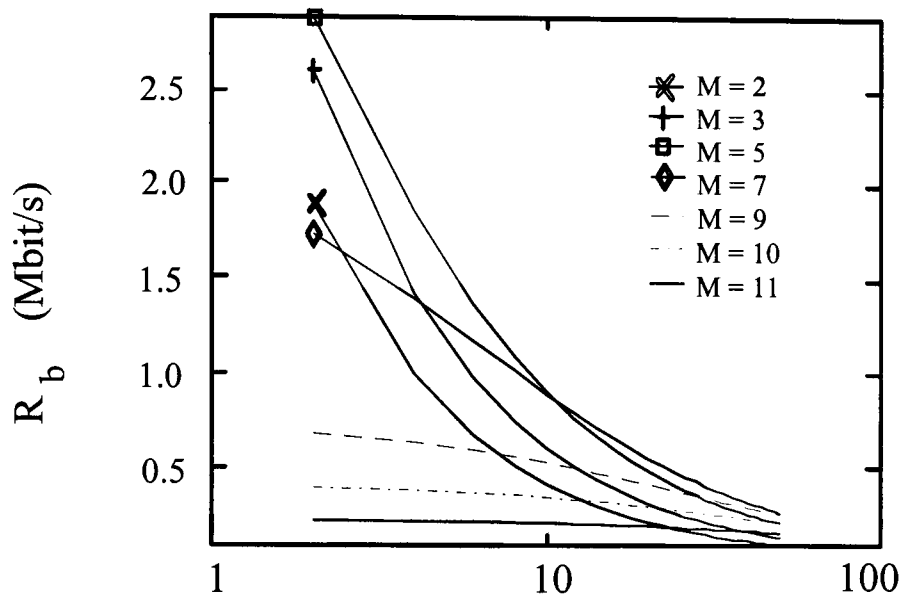


Figure 7.6: System bit rate at a given PPM order and number of users

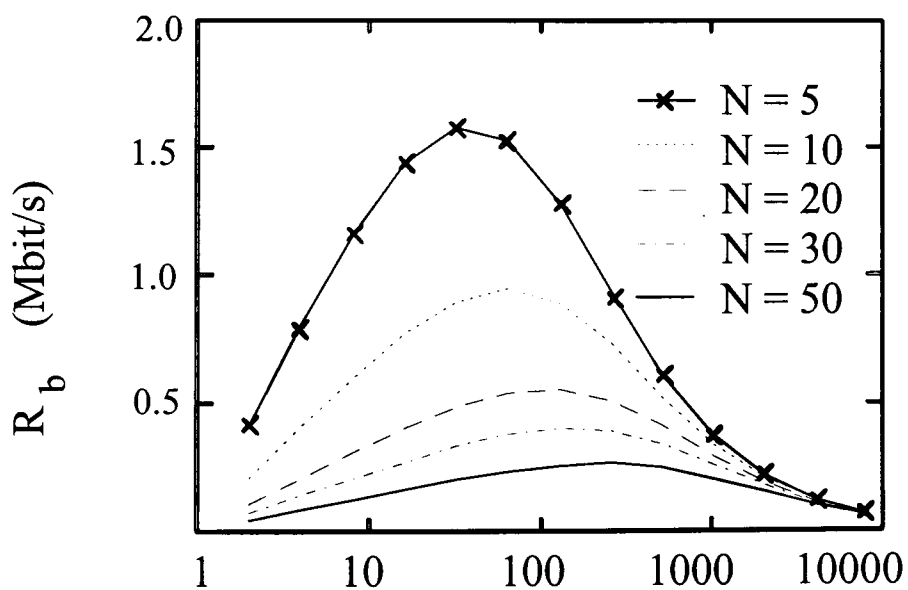


Figure 7.7 Optimum PPM order at a given number of user

The indoor diffuse infrared channel bandwidth has been shown to be limited by ISI when no equalisation is employed [3]. In particular, the channel bit rate distance product has been shown to be 260 Mbit/s [3]. Assuming a diameter of 5 meters (small room or one of many holographically defined cells [9]), a maximum $R_c=52$ Mbit/s can be defined. The results of Chapter 6 have illustrated that ISI can be greatly reduced through proper equalisation and hence R_c can be increased beyond 52Mbit/s. In this section we aim to establish the relationship between the system parameters. As such results are given at $R_c = 52$ Mbit/s. Results were obtained for the maximum number of users that can communicate at a given bit rate when a particular PPM order is considered. The results are depicted in Figure 7.6. It is apparent that there is a trade-off between increasing the number of users and the achievable bit rate. Moreover the achievable bit rate increases (at a given number of users) with increase in the PPM order (M) up to a given order then the performance deteriorates which indicates the presence of an optimum. This feature is explored in Figure 7.7 which demonstrates that there exists an optimum PPM order that maximises the achievable bit rate at a given number of users. The data of Figure 7.6 and 7.7 can be used by the system designer to select the optimum PPM order and number of users at a given bit rate.

The finite crosscorrelations due to the OOC give rise to a probability of threshold violation even in the absence of noise sources. The probability of a false alarm event is generally bound by [74]

$$P_{cf} = \frac{1}{2} \sum_{i=\text{Thr}}^{N-1} \binom{N-1}{i} \left(\frac{k^2}{2L} \right)^i \left(1 - \frac{k^2}{2L} \right)^{N-1-i} \quad (7.15)$$

where $1 \leq Thr \leq k$ is the detection threshold level. This error rate is depicted in Figure 7.8. at various threshold levels and code weights for $L = 2048$ and $N = 15$. This error probability is reduced by operating at threshold levels close to k (typical of false alarm errors) and by increasing the OOC weight.

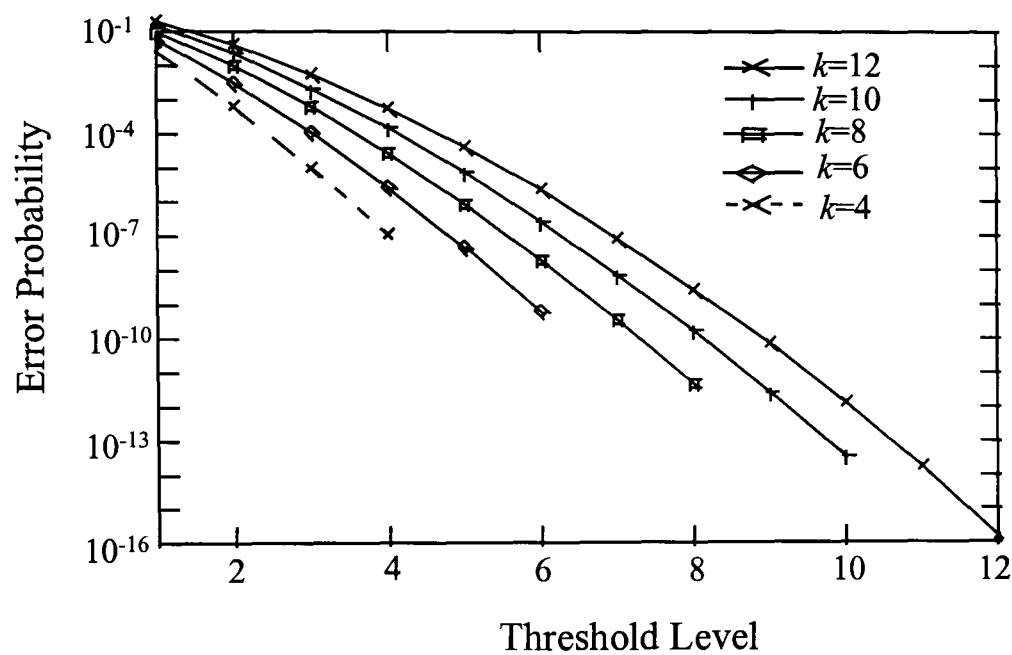


Figure 7.8 The OOC error rate

7.3.2 Prime codes and Extended Prime Codes

The construction of prime codes begins with the Galois field $GF(p)$ of a prime number p . A prime sequence $S_i = (s_{i,0}, s_{i,1}, \dots, s_{i,j}, \dots, s_{i,p-1})$ is constructed by $S_{i,j} = I \times j \pmod{p}$, where $i, j \in GF(p)$. Each prime sequence S_i is then mapped into a binary sequence $C_i = (c_{i,0}, c_{i,1}, \dots, c_{i,k}, \dots, c_{i,N-1})$ of length $X = p^2$, where C_i can be written as [82,88]

$$C_{i,k} = \begin{cases} 1, & \text{for } i = s_{i,j} + jp, \quad j = 0,1,\dots,p-1 \\ 0, & \text{otherwise} \end{cases} \tag{7.16}$$

Therefore, p code words, each of weight p and length p^2 are generated.

Quasi-optimum time mapped sequences can be produced by using the multiplication table of the elements of the Galois field $GF(p)$. The sequence set is constructed as follows:

1. Select a prime number p .
2. Write down the field elements in ascending or descending order.
3. Multiply this row by a field element modulo p .

An example for $p = 5$ is given in Table 7.1. Each element $S_{i,j}$ in the table is produced by the corresponding i and j modulo 5. The prime sequences are then mapped into a binary code sequence $C_x = (c_{x,0}, c_{x,1}, \dots, c_{x,p}, \dots, c_{x,N-1})$, by assigning ones in positions for $j = 0, 1, \dots, p-1$ and zeros in all the other positions.

GF(5) field elements in ascending order	0	1	2	3	4
Sequence S_0	0	0	0	0	0
Sequence S_1	0	1	2	3	4
Sequence S_2	0	2	4	1	3
Sequence S_3	0	3	1	4	2
Sequence S_4	0	4	3	2	1

Table 7.1 Family of prime sequences for $p = 5$

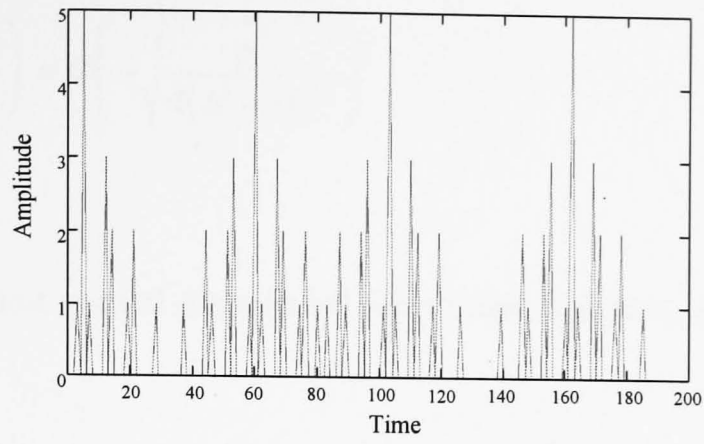
In effect, this requires that the code C_x be divided into p frames, each containing p chips. Within the j th frame, the chip shifted relative to the start of frame by S_{ij} is a one, all other chips being zero. The code C_x is therefore a time-mapped, binary version of sequence S_{ij} . To illustrate this, the set of prime codes for $p=5$ is shown in Table 7.2. Here the frames have been slightly separated for clarity. For example, prime sequence S_3 of table 7.2 would be mapped into the code sequence

$$C_3 = (1000000010010000000100100)$$

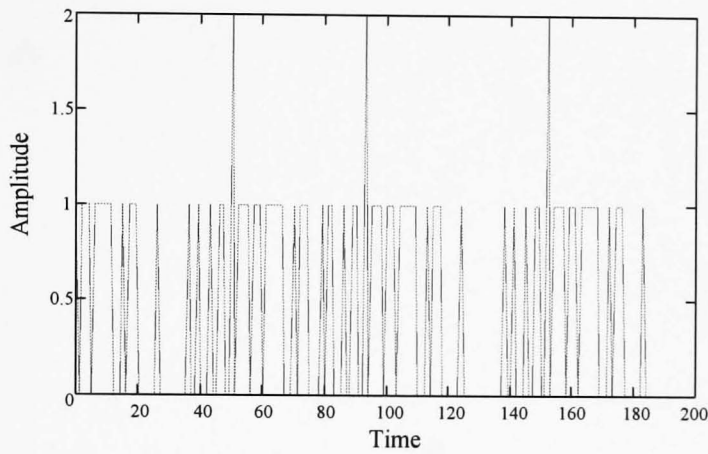
	frame 0	frame 1	frame 2	frame 3	frame 4
Code C_0	10000	10000	10000	10000	10000
Code C_1	10000	01000	00100	00010	00001
Code C_2	10000	00100	00001	01000	00010
Code C_3	10000	00010	01000	00001	00100
Code C_4	10000	00001	00010	00100	01000

Table 7.2 Family of prime codes for $p = 5$

For prime codes, the number of coincidences of 1's for all shifted version of any two code sequences is only one or two. The peak of the cross-correlation function is therefore at most two and the number of 1's per code sequence and the auto-correlation peak both equal p . Figure 7.9(a) shows the auto-correlation function of code sequence C_3 for the PPM data 5, 10, 3 and 12 (i.e. OOK data 0101, 1010, 0011 and 1100) when p is equal to 5. Figure 7.9(b) shows the cross-correlation of the code sequence C_3 with code sequence C_2 . The peak is equal to two. In the case of orthogonal codes used in optical CDMA with matched filter (correlator) detector, the general expression for SNR can be arrived at as follows [89]:



(a)



(b)

Figure 7.9 Prime Codes (a) Auto-correlation (b) Cross-correlation function

Assume that there are N users simultaneously accessing the channel. Out of these N users, one user can be considered to be the one destined for a particular receiver and the remaining $(N-1)$ can be considered as interferes. Then, with matched filter detectors at the receiver, the signal power is equal to the square of peak auto-correlation function, divided by product of noise power and variance of cross-correlation function (σ^2) between the one desired user and the remaining $(N-1)$ uncorrelated interferes. The value of the variance obtained is independent of noise power since the number of coincidences of 1's is independent of p . Therefore, using a Gaussian approximation, the probability of error P_{prime} at the receiver can be written as [90]

$$P_{prime} = \Phi\left(-\sqrt{\frac{SNR}{2}}\right) = \Phi\left(-\sqrt{\frac{p^2}{4(N-1)\sigma^2}}\right) \quad (7.17)$$

where $\Phi(x)$ is the unit normal cumulative distribution function, which can be written as:

$$\Phi(x) = \frac{1}{\sqrt{2\pi}} \int_{-\infty}^x e^{-\frac{y^2}{2}} dy \quad (7.18)$$

and

$$\sigma^2 = \sum_{m=0}^d \left(m - \sum_{m=0}^d m q_{d,m} \right)^2 q_{d,m} = \sum_{m=1}^d \sum_{n=0}^{m-1} (m-n)^2 q_{d,n} q_{d,m} \quad (7.19)$$

Note that $q_{d,m}$ denotes the probability that the cross-correlation value between any two codewords is m , where $m=\{0,1,...,d\}$ and d is the maximum cross-correlation value of the code. For the prime code over GF(p), the average probabilities $\overline{q_{2,m}}$ of having the cross-correlation value $m=\{0,1,2\}$ between any two codewords in the code set are

$$\begin{aligned} \overline{q_{2,2}} &= \left(\frac{(p+1)(p-2)}{12p^2} \right) \\ \overline{q_{2,1}} &= \left(\frac{2p^2 + p + 2}{6p^2} \right) \\ \overline{q_{2,0}} &= \left(\frac{7p^2 - p - 2}{12p^2} \right) \end{aligned} \quad (7.20)$$

The average variance $\overline{\sigma^2}$ of the prime code over GF(p) is then written as

$$\overline{\sigma^2} = \sum_{m=1}^2 \sum_{n=0}^{m-1} (m-n)^2 \overline{q_{2,n} q_{2,m}} = \frac{5p^2 - 2p - 4}{12p^2} \tag{7.21}$$

Therefore, for a sufficiently large p , the probability of error P_{prime} can be written as

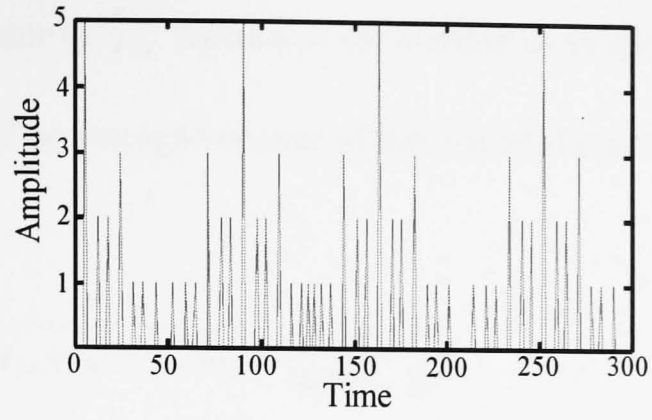
$$P_{prime} = \Phi\left(\frac{-p}{\sqrt{4(N-1)\overline{\sigma^2}}}\right) = \Phi\left(\frac{-p}{\sqrt{1.67(N-1)}}\right) \tag{7.22}$$

To reduce the maximum cross-correlation value from 2 to 1, each sub-block in the codewords of the prime code is now padded with $p-1$ or more trailing zeros [91]. An example of $p = 5$ is shown in Table 7.3.

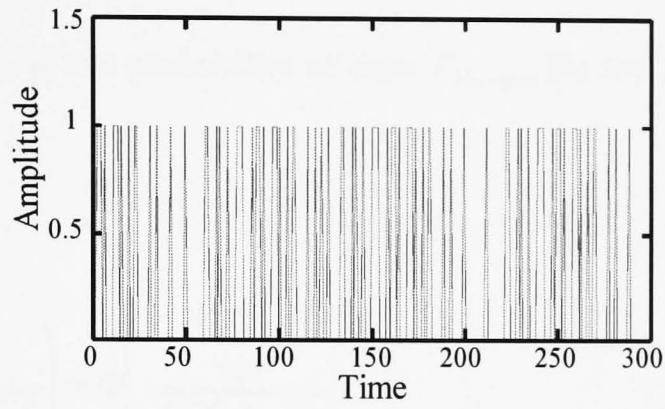
	frame 0	frame 1	frame 2	frame 3	frame 4
Code C_0	100000000	100000000	100000000	100000000	100000000
Code C_1	100000000	010000000	001000000	000100000	000010000
Code C_2	100000000	001000000	000010000	010000000	000100000
Code C_3	100000000	000100000	010000000	000010000	001000000
Code C_4	100000000	000010000	000100000	001000000	010000000

Table 7.3 Family of extended prime codes for $p = 5$

Figure 7.10 shows the extended prime code auto- and cross-correlation function. Although the extended prime code has the same cardinality and weight as the original one, its code length (i.e. $X=p^2+p(p-1)$) is longer.



(a)



(b)

Figure 7.10 Extend prime codes (a) Auto-correlation (b) Cross-correlation function

For the extended prime code, the average probabilities $\overline{q_{1,m}}$ of having the cross-correlation value $m=\{0,1\}$ between any two codewords in the code set are

$$\overline{q_{1,1}} = \frac{p^2}{2p(2p-1)} = \frac{p}{2(2p-1)} \quad (7.23)$$

and

$$\overline{q_{1,0}} = 1 - \overline{q_{1,1}} = \frac{(3p-2)}{2(2p-1)} \quad (7.24)$$

Note that the numerator in $\overline{q_{1,1}}$ represents the number of single overlaps in the cross-correlation function. The average variance of the extended prime code is then given by

$$\overline{\sigma^2} = \sum_{m=1}^1 \sum_{n=0}^{m-1} (m-n)^2 \overline{q_{1,n} q_{1,m}} = \overline{q_{1,0} q_{1,1}} = \frac{p(3p-2)}{4(2p-1)^2} \quad (7.25)$$

For a sufficiently large p , the probability of error $P_{Extended}$ for the extended prime code can be written as

$$P_{Extended} = \Phi\left(\frac{-p}{\sqrt{4(N-1)\overline{\sigma^2}}}\right) = \Phi\left(\frac{-p}{\sqrt{0.75(N-1)}}\right) \quad (7.26)$$

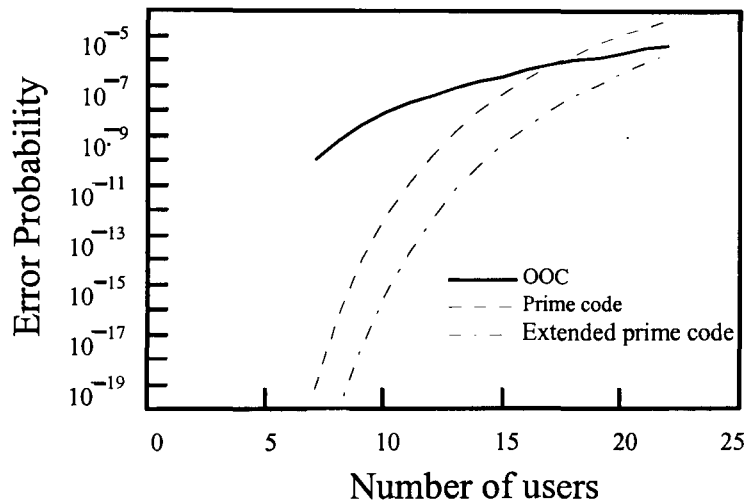


Figure 7.11 Probability of error versus number of user for OCs($X=1024$, $k=7$, $Thr=6$) Prime codes ($P=31$) and Extended prime codes ($P=23$)

Figure 7.11 compares the error probability of three different orthogonal codes, which is dramatically degraded as number of simultaneously user increases. From Figure 7.11, it is clear that OOCs can only support 8 simultaneous users in the network with bit error rate equal to 10^{-9} . But the prime codes have increased the number of simultaneous users to 12 and extended prime codes have increased the number of

simultaneous users to 16. In the context of PPM CDMA the overall error probability can now be written as

$$P_{system} = \frac{n}{2(n-1)} \{P_r + P_s\} + \frac{n}{4} \{P_f + P_{cf}\} \tag{7.27}$$

where P_r , P_s , and P_f are the known PPM erasure, wrong slot, and false alarm errors [82]. The contribution of the additional cross correlation false alarm error probability to the PPM CDMA error rate (P_{system} is shown in Figure 7.12 at various PPM orders). Careful selection of these parameters using the data of Figure 7.12 should result in an error rate lower than the system operating error rate (e.g., 10^{-9}).

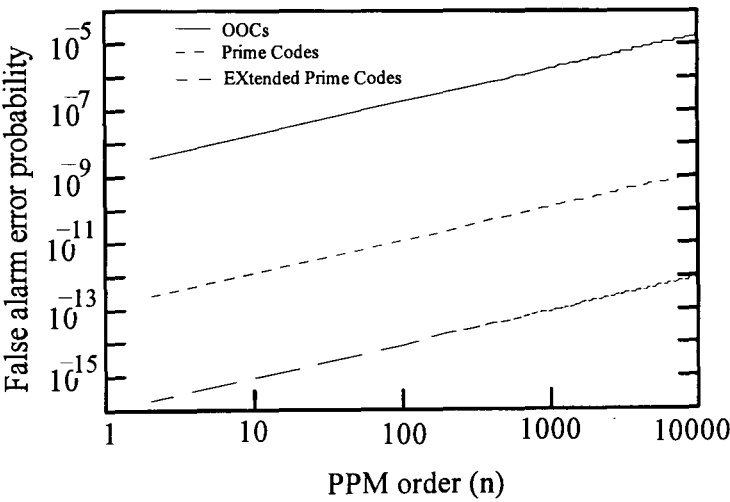


Figure 7.12 The additional PPM CDMA false alarm errors

7.4 PPM CDMA coder design

A coder has been designed and implemented to demonstrate the feasibility of the proposed structure. This section outlines the design details. To best illustrate the PPM CDMA structure we can refer to Figure 7.13 which shows the timing information for the PPM CDMA signal with reference to the PPM format as well as the OOK structure. A 4 bit OOK frame structure is shown in which the OOK bit period is simply one quarter of the overall OOK frame period. For a 10 Mbit/s system the corresponding bit period is $0.1 \mu\text{s}$ giving an overall OOK frame of $0.4 \mu\text{s}$ duration. The clock rate required in this case will be 10 MHz. For an equivalent PPM system such as that shown in Figure 7.13(b), the PPM frame consists of 16 slots plus the guard band. The slot period is smaller than the OOK bit duration since the overall frame duration remains fixed as the bit rate has not changed. The PPM slot duration hence becomes $0.02 \mu\text{s}$ assuming a modulation index $m = 0.8$ giving a clock requirement of 50 MHz.

Realising that the PPM signal consists of 4 bits of information (ie. 16 slots), then the PPM-CDMA also must have 16 chips for the information. In this system, we have selected $L = 32$, ie. a 32 bit OOC sequence. So the total PPM-CDMA frame duration (T_{pcf}) is equal to

$$T_{pcf} = \frac{(n + L - 1)}{m} \times T_c \quad (7.28)$$

where n is the number of chips reserved for data, L is the OOC sequence length, m is modulation depth and T_c is the chip duration. In this system we set n equal 16, L equal 32, $m \cong 0.8$ and use a total of 60 PPM-CDMA chips. Therefore $n+L-1 = 47$ slots and 13 slots are used as guard band.

The PPM CDMA structure is shown in Figure 7.13(c) and consists of the 16 PPM slots plus some 31 extra slots accomodating the optical orthogonal code which is required for user identification ($L = 32$ in this case). Therefore the total number of slots required in this case to give a modulation index of $m \cong 0.8$, having taken the requirement of the guard band into account is equal to 60. The number of slots has increased for the same frame duration resulting in the PPM CDMA slots becoming even smaller. The bandwidth requirement has increased further and a clock rate of 150 MHz is required.

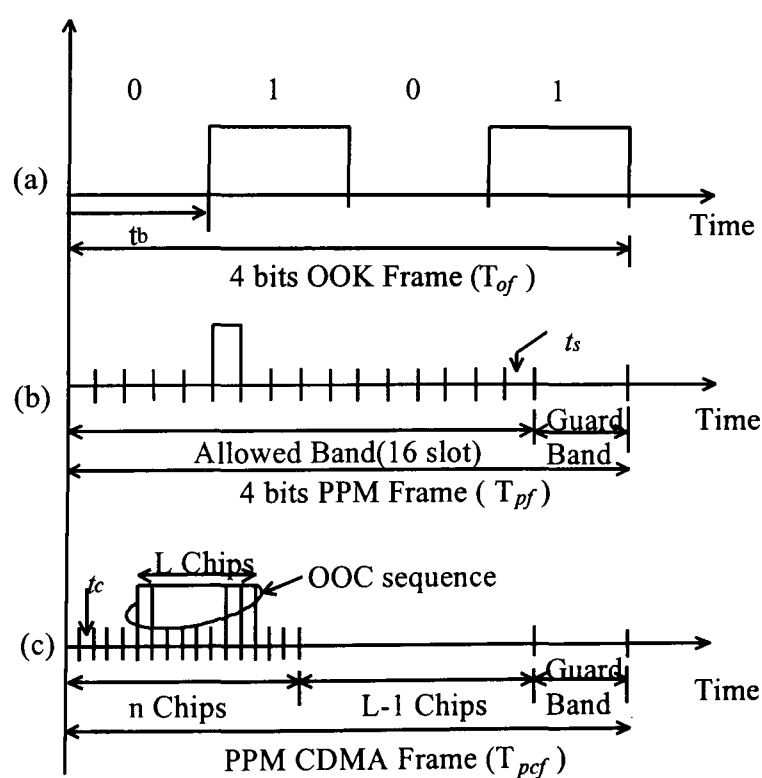


Figure 7.13 Frame timing diagram (a) OOK (b) PPM (c) PPM-CDMA

A block diagram illustrating the main features of the CDMA coder is shown in Figure 7.14. The purpose of the coder is to accept the input PPM pulse and a fixed OOC and then to furnish the equivalent PPM CDMA signal. From the frame structure timing diagram (Figure 7.12), it is clear that the PPM-CDMA frame duration (T_{pcf}) is equal to the frame duration of PPM (T_{pf}) and OOK (T_{of}). Also the OOK bit period (T_b) is equal to 5 times the PPM slot period ($5T_s$) and also equal 15 times the PPM-CDMA chip period ($15T_c$). The master clock was set equal to the PPM-CDMA chip clock and the master clock divided by 15 is OOK data clock. The master clock divided by 3 is the PPM slot clock.

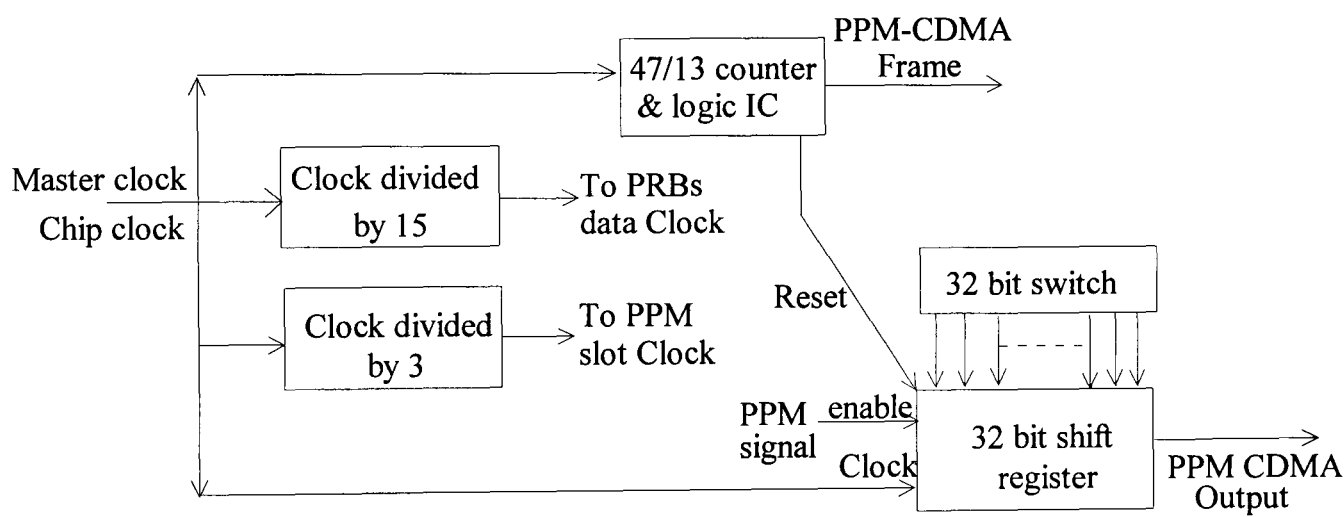


Figure 7.14 32 bit CDMA code-sequences coder, designed to be employed with an optical 16 bit PPM wireless system.

At the start of a new PPM-CDMA frame the shift register is reset to zero and the 32 bits OOC is loaded from the switches. When a PPM signal is received at the enable input, the shift register will start to shift the OOC to the output. The counter and shift register will be reset when the counter has counted to 60 clock pulses. The processes is then repeated for the next frame.

7.4 Summary

This chapter has introduced code division multiple access (CDMA) and has outlined the properties of these sequences. The performance of a PPM-CDMA system has been analysed in terms of the achievable bit rate over a band-limited channel. The results have indicated that PPM-CDMA can offer over 5 times the bit rate achievable using OOK-CDMA under the same bandwidth constraints.

A PPM CDMA transmission strategy has been presented and analysed with three different orthogonal codes. The strategy can find application in multi-user optical wireless networks. Original results were presented for the system error probability against the number of simultaneous users using the three different orthogonal codes. The results have shown that extended prime codes offer the best performance when utilised with PPM CDMA.

Chapter 8 Conclusions

This project has considered the development of a rigorous theoretical analysis and practical measurements for an indoor infrared wireless system. It has also considered multiple access techniques, channel characteristics, modulation techniques, and low noise receiver circuit design for an indoor optical wireless environment. The three major obstacles, high capacitance of large area photodiode, ambient light noise and multipath dispersion, to achieving high-speed indoor infrared communication were outlined in the Chapter 2. Moreover, optical safety limitations have been discussed in detail. In this project, pulse position modulation and code division multiple access were considered for application in the optical wireless environment.

Background light is the major noise source in the optical wireless environment. In Chapter 3 we have measured and analysed the noise associated with three different light sources, fluorescent light, incandescent light and halogen spotlight. New results have shown that incandescent and halogen light have the worst effect because their spectral peak overlaps that of GaAs and Si diodes. Moreover the results have shown that incandescent light source have a significant effect on the system sensitivity

resulting in a sensitivity penalty as high as 5.2 dB when the receiver is placed directly underneath a spotlight source. The results have also shown that the ambient light noise can be reduced by using an optical filter in front of photodiode.

A mathematical model for the optical wireless channel multipath dispersion has been presented in Chapter 3. The model has been used to evaluate the received pulse shapes when the transmitted pulse is rectangular NRZ. Original results have shown that the received pulse can be matched to a Gaussian shape with different pulse variances. This has led to a more tractable analysis leading to the evaluation of the optical wireless PPM system sensitivity. Sensitivity calculations have demonstrated that multipath dispersion can introduce a system sensitivity penalty of 5.3 dB in the middle of the room and 2.76 dB in the corners. The result have also shown that the impact of multipath dispersion depends on the receiver position within the communication environment.

A complete mathematical model of a common collector common emitter bootstrapped PIN-BJT receiver circuit has been presented. Simulation and analytic results were presented in Chapter 4. The receiver has been shown to achieve a low noise current of $2.7 \text{ pA} / \sqrt{\text{Hz}}$ together with a bandwidth of 70 MHz. The sensitivities of a PIN-BJT PPM LOS system and a PIN-BJT OOK LOS system have been evaluated demonstrating for the first time that the PPM system can offer 9.8 dB sensitivity improvement over the comparable OOK system. It has been shown that this sensitivity improvement is at the expense of bandwidth expansion (eg. 9.8 dB sensitivity improvement calls for a bandwidth of 66 MHz at 10 Mbit/s). However, it

has also been illustrated that even at modest bandwidth expansion, an appreciable sensitivity improvement can be achieved. For example bandwidth expansion factors of 3 and 5 (corresponding to 20 and 33 MHz bandwidth) result in 5.2 dB and 7.1 dB sensitivity improvement. The good sensitivity and low average power associated with the PPM format are important attributes that can integrate to make this format attractive over the optical wireless channel.

PPM signals offer improved receiver sensitivity. This is an attractive feature over the optical wireless channel where the maximum transmitter power is limited by safety issues. In Chapter 5 the three error sources associated with the PPM signal have been identified and expressions have been given to evaluate the associated error probabilities. A 16-PPM coder design has been outlined and experimental results have been given for the generated PPM signal.

In Chapter 6 we have designed a new equaliser for indoor optical wireless systems and used it to reduce the impact of the channel multipath dispersion. The results have shown that the system sensitivity have improved by up to 3.8 dB when using a variable. The results have also demonstrated that an adaptive filter is needed in the indoor optical wireless environment.

The provision of new multiple access facilities over the OW network has been considered in Chapter 7. Original results have been obtained for OOK CDMA and PPM CDMA with three different orthogonal codes. The performance of an indoor infrared wireless PPM CDMA system has been analysed in terms of the achievable bit

rate over a band-limited channel. The results have indicated that PPM CDMA can offer over 5 times the bit rate achievable using OOK CDMA under the same bandwidth constraints.

A PPM CDMA coder has been designed and its main features have been described. The coder is intended for use with a 16 slot PPM system and is capable of deploying up to 32 bit signature codes.

Chapter 9 Future Work

The work carried out to date has resulted in a number of original contributions to knowledge, however scope exists for further work in this area. This chapter outline some potential areas.

The mathematical model presented in Chapter 3 for simulating dispersion was simple to describe but not very efficient. The results presented in Chapter 3 included first and second order reflections. Future work may look into ways to speed up the simulation process and incorporate higher order reflections. The work can also benefit from some practical impulse response measurements in the indoor environment in order to compare the results and establish the effect (if any) of higher order reflections.

In the Chapter 4, we have designed and analysed a common collector common emitter bootstrapped PIN-BJT receiver. The results have shown that the receiver can achieve a low noise current of $2.7 \text{ pA}/\sqrt{\text{Hz}}$ together with a bandwidth of 70 MHz. Future work can include noise measurements and may explore the use of APD front ends in this environment.

A new equaliser has been designed and analysed for the indoor PPM optical wireless diffuse system. The results have shown that the fixed equaliser is not suitable for the mobile environment. An adaptive equaliser is needed to improve the system performance. Future work may look into the design of an adaptive equaliser to reduce the channel multipath dispersion. Future work may also look at diversity reception to improve the signal and to selectively reject the noise. Such a system also needs to be adaptive given the environment and the need for mobility.

The PPM CDMA system considered can benefit from further analysis into code design and the use/impact of correlators at the receiver. The use of soft or hard limiters with such correlators can be considered as a means of reducing the error rate. The practical demonstration of a full PPM CDMA network is also attractive and the system analysis can incorporate a full account of the environment as developed in this thesis.

References

1. J.E. Padgett, C.G. Gunther, and T. Hattori, "Overview of Wireless Personal Communications", IEEE Communications Magazine, pp. 28-41, Jan 1995.
2. J. L. Grubb, "The Traveller's Dream Come True", IEEE communications Magazine, pp. 48-52, Nov 1991.
3. F.R. Gfeller and U.H. Bapst, "Wireless in-house data communication via diffuse infrared radiation," Proc. IEEE, vol 67, No 11, pp.1474-1486, 1979.
4. O. Takahashi and T. Tougr, "Optical wireless Network for Office Communication," JARECT (Japan Electron Rev. Electron. Comput. Telecomm.), Vol. 20, pp. 217-228, 1985/1986.
5. C.S. Yen and R.D. Crawford "The use of Directed Optical Beams in Wireless Computer Communications" IEEE Globecom '85, pp. 1181-1184, Dec 2-5, 1985.
6. Y. Yamauchi, M. Sato and T. Namekawa, "In-House Wireless Optical Digital SSMA," Electronics and Communications in Japan, Part 1, Vol. 70, No. 6, pp. 87-101, 1987.
7. J.M. Kahn, W.J. Krause and J.B. Carruthers, "Experimental Characterisation of Non-Directed Indoor Infrared Channels," IEEE Transactions on Communications, Vol 43, No 2/3/4, pp. 1613-1623, Feb/Mar/Apr 1995.
8. A.Satoh and E. Ogawa, "Fundamental Characteristics of In-House Infrared Propagation and Environmental Noise," IEEE Antennas & Propagation Society Int Symp. pp. 205-208, 1986.
9. P.P. Smyth, M. McCullagh, D. Wisely, D. Wood, S. Ritchie, P. Eardley and S. Cassidy, "Optical Wireless Local Area Networks-enabling technologies" BT Technol. J. Vol 11, No 2, pp. 56-64, Apr. 1993.
10. J.R. Barry J.M. Kahn, W.J. Krause, E.A. Lee and D.G. Messerschmitt, "Simulation of Multipath Impulse Response for Indoor Wireless Optical Channels," IEEE Journal on Selected areas in Communications, Vol 11, No 3, pp.367-378, April 1993.
11. J.M.H. Elmirghani and R.A. Cryan, "New PPM-CDMA hybrid for indoor diffuse infrared channels," Electronics Letters , Vol 30, No 20, pp. 1646-1647, Sept. 1994.
12. J.R. Barry, J.M. Kahn, E.A. Lee and D.G. Messerschmitt, "High-Speed Nondirective Optical Communication for Wireless Networks," IEEE Network Magazine, pp. 44-53, Nov 1991.

13. S.D. Greaves, P.J. Nichols, D.R. Wisely, and R.T. Unwin, "Optical Wireless Video Distribution," The International Society for Optical Engineering Wireless Data Transmission Conference, Philadelphia, Pennsylvania, pp.280-285, 23-25 October 1995.
14. P. Nicholls, S.D. Greaves, and R.T. Unwin, "Optical Wireless Telepoint," IEE Colloquium on Optical Free Space Communication Links, pp. 4/1-4/7, London, February 1996.
15. Lee Goldbera, "Infrared Data Transmission: The Missing Link?," Electronic Design, pp. 47-64, April 17, 1995.
16. J.R. Barry, "Wireless infrared communications," Boston: Kluwer, 1994.
17. J.M. Kahn and J.R. Barry, "Wireless infrared communications," IEEE Proceedings, vol. 85, No.2, pp. 265-298, Feb. 1997.
18. 'Laser - Principles and Applications', Wilson and Hawkes, Prentic Hall, 1987.
19. P.P. Smyth, P.L. Eardley, K.T. Dalton, D.R. Wisely, P. McKee and D. Wood, "Optical Wireless - A Prognosis," The International Society for Optical Engineering Wireless Data Transmission Conference, Philadelphia, Pennsylvania, pp.212-224, 23-25 October 1995.
20. I.A. Parkin and J. Zic, "An Application of Infrared Communications," J. of Electrical and Electronic Engineering Australia, vol 4, No 4, pp. 331-336, Dec. 1984.
21. G.W. Marsh and J.M. Kahn, "50-Mb/s Diffuse Infrared Free-Space Link Using On-Off Keying With Decision-Feedback Equalization," IEEE Photonics Technology Letters, Vol. 6, No. 10, pp. 1268-1270, Oct. 1994.
22. M. D. Audeh, J.M. Kahn, "Performance Evaluation of Baseband OOK for Wireless Indoor Infrared LAN's Operating at 100Mb/s," IEEE Transactions on Communications, Vol. 43, No. 6, pp. 2085-2094, June 1995.
23. H.H. Chan, J.M.H. Elmirghani, and R.A. Cryan, "Performance Analysis of Indoor Infrared Wireless Networks Utilising PPM CDMA," Proc. IEEE The International Conference on Communications Systems, Vol. 3, pp. 1467-1471, Dallas, Texas USA, June 1996 (ICC'96).
24. P. Nicholls, R. T. Unwin, and K. T. Dalton, "A 10 MB/s Optical Wireless Ethernet - Practical Results," The International Society for Optical Engineering Wireless Data Transmission Conference, Philadelphia, Pennsylvania, pp.294-296, 23-25 October 1995.

25. M.D. Kotzin, "Short-range communications using diffusely scattered infrared radiation," Ph.D. dissertation, Northwestern University, Evanston, IL, June 1981.
26. M.D. Kotzin and A.P. van den Heuvel, "A duplex infrared system for in-building communications," IEEE Vehic. Technol. Conf. Proc., pp. 179-185, 1986.
27. D.B. Medved and Y. Azancot, "Wireless optical communication for FDDI, fast Ethernet and ATM connectivity," in Proc. SPIE Conf. On wireless communication, vol. 2556, San Diego, CA, pp. 294-304, July 1995.
28. N. Baran, "Wireless networking," BYTE, pp. 291-294, April 1992.
29. "Photolink User's Manual," Photonics Corp. San Jose, CA.
30. T. Minami, K. Yano, and T. Touge, "Optical wireless modem for office communication," National Computer Conference, pp. 721-728, 1983.
31. O. Takahashi and T. Touge, "Optical wireless Network for office communication," JARECT (Japan Electron. Rev. Electron. Comput. Telecomm.), vol. 20, pp. 217-228, 1985/1986.
32. Y. Nakata, J. Kashio, T. Kojima, and T. Noguchi, "In-house wireless communication system using infrared radiation," Proc. Of the International Conference on Computer Communication, pp. 333-337, 1984.
33. D.R. Pauluzzi, P.R. McConnell and R.L. Poulin, "Free space undirected infrared voice and data communication with a comparison to RF systems," Proc. IEEE International Conference on Selected Topics in Wireless Communications, Vancouver, pp. 279-285, June 1992.
34. R.L. Poulin, D.R. Pauluzzi and M.R. Walker, "A Multi-Channel Infrared telephony demonstration system for public access applications," Proc. IEEE International Conference on Selected Topics in wireless communication, pp. 286-291, June 1992.
35. IEC825-1: "Safety of laser products," part I: equipment classification, requirements and user's guide, 1993.
36. IEC825-2: "Safety of laser products," part II: Safety of optical fiber communication systems, 1993.
37. IrDA standard, "Serial infrared: Physical layer link specification," Version 1.2. November 1997.
38. IrDA standards can be obtained at <http://www.irda.org>.
39. Spectrix Corporation, "SpectrixLite™ System: Product specifications," 1997.

40. IBM web page, "<http://www.ibm.com>".
41. A.J.C. Moreira, R.T. Valadas and A.M. de Oliveira Duarte, "Performance of infrared transmission systems under ambient light interference," IEE Proc. Part J., vol 143, No. 6, pp. 339-346, Dece. 1996.
42. Kaveh Pahlavan and Allen H. Levesque, "Wireless information networks," Boston: Kluwer, 1995.
43. A.C. Boucouvalas, "Indoor ambient light noise and its effect on wireless optical links," IEE Proc. Part J., vol 143, No. 6, pp. 334-338, Dec. 1996.
44. A.M.R. Tavares, R.J.M.T. Valadas and A.M. de Oliveira Duarte, "Performance of an optical sectored receiver for indoor wireless communication systems in presence of artificial and natural noise sources," Proc. Of the SPIE conference on wireless data transmission, vol. 2601, pp. 264-273, Philadelphia, USA, October 1995.
45. McCullah and D.R. Wisely, "155 Mbit/s Optical Wireless Link Using a Bootstrapped Silicon APD Receiver," Electronics Letters, vol. 30, No. 5, pp. 430-432, March 1994.
46. P.J. Nicholls and R.T. Unwin, "The Design of Optical Receivers for Wireless LAN Applications," The International Society for Optical Engineering Wireless Data Transmission Conference, Philadelphia, Pennsylvania, pp.590-598, 23-25 October 1995.
47. Yun and M. Kavehrad, "Spot diffusing and fly-eye receivers for indoor infrared wireless communication," Proc. IEEE Int. Conf. on Selected Topics in Wireless Commun., pp. 262-265, 25-26 June 1992.
48. S.D. Personick, "Receiver Design for Digital Fiber Optical Communication System, Part I and II," Bell Syst. Tech. J., vol. 52, pp. 843-886, July-Aug. 1973.
49. R.G. Smith and S.D. Personick, "Receiver Design for Optical Fiber Communication Systems," in Semiconductor Devices for Optical Communication. New York: Springer-Verlag, 1980, Chapter 4.
50. D.R. Smith and I. Garrett, " A Simplified Approach to Digital Optical Receiver Design," Opt. Quantum Electron., vol. 10, pp 211-221, 1978.
51. T.V. Moui, J.L. Hullet, "Receiver for Multivel Digital Optical Fiber Systems," IEEE Trans. Commun., vol. Com-23, pp. 987-994, Sept. 1975.
52. Personick et al., "Detailed Comparison of Four Approaches to the Calculation of Sensitivity of Optical Fiber System Receivers," IEEE Trans. Commun., vol. com-25, pp. 541-548, May 1977.

53. J.J. O'Reilly, "High Performance Receivers for Optical Communications," *Elec. & Commun. Eng. J.*, pp. 129-137, 1989.
54. J. Senior, "Optical Fiber Communications: Principles and Practice, 2nd ed., Prentice Hall, 1992.
55. Hullet, and T.V. Muoi, "Referred Impedance Noise Analysis for Feedback Amplifiers," *Electron. Lett.*, 13, (13), pp. 387-389, 1977.
56. J.M.H. Elmirghani, R.A. Cryan and F.M. Clayton, "On the Spectral Estimation and Synchronisation of the Cyclostationary Optical Fiber PPM Process." *IEEE Trans. on Commun.*, vol com-43, No. 3, pp. 1001-1012, March 1995.
57. J.R. Pierce, "Optical Channels: Practical Limits with Photo Counting," *IEEE Trans. Commun.*, COM-26, pp. 1819-1821.
58. I. Garrett, "Digital Pulse Position Modulation for transmission over optical fiber channels with direct and heterodyne detection," *IEEE Trans.*, COM-31, pp. 518-527, 1983.
59. I. Garrett, "Digital pulse position over dispersive optical fiber channels," *Int. Workshop on Digital Communication*, Tirrenia, Italy, 1983.
60. I. Garrett, "Digital pulse position over slightly dispersive optical fiber channels," *Int. Symp. on Info. Theory*, St. Jovite, pp. 78-79, 1983.
61. I. Bar-David, G. Kaplan, "Information rates of photon limited overlapping pulse position modulation channels," *IEEE Trans. Info. Theory*, vol. IT-30, No. 3, pp.455-464, 1984.
62. G.M. Lee, G.W. Schroeder, "Optical pulse position modulation with multiple positions per pulsewidth," *IEEE Trans. Commun.*, COM-25, pp. 360-365, 1977.
63. H. Sugiyama, K. Hosu, "MPPM: A method of improving the band-utilization efficiency in optical PPM," *J. Lightwave Technol.*, vol. 7, No. 3, pp. 465-472, 1989.
64. R.A. Cryan and R.T. Unwin, "Reed-Solomon coded homodyne digital pulse position modulation," *Proce. IEE Pt. I*, vol. 139, No. 2, pp. 140-146, 1990.
65. R.A. Cryan, R.T. Unwin, I. Garrett, M.J.N. Sibley and N.M. Calvert. "Optical fibre digital pulse-position-modulation assuming a Gaussian received pulse shape," *IEE Proc.*, Pt. I, vol. 137, No. 2, pp. 89-96, 1990.
66. I.J.O. Pires and J.R.F. Da Rocha, "Digital pulse position over optical fibres with avalanch photodiode receivers," *IEE Proc. Pt. J*, vol. 133, No. 5, pp. 309-313, 1986.

67. J.M.H. Elmirghani, R.A. Cryan, and F.M. Clayton, "PPM phase bearing-events for direct frame phase extraction," *Elect. Lett.*, vol. 29, No. 9, pp. 775-777, April 1993.
68. R. Narasimhan, M.D. Audeh and J.M. Kahn, "Effect of electronic-ballast fluorescent lighting on wireless infrared links," *IEE Proc. Part J.*, vol.143, No. 6, pp. 347-354, Dec. 1996.
69. M.D. Audeh, J. M. Kahn and J.R. Barry, "Decision feedback equalization of pulse position modulation on measured non-directed indoor infrared channels," *IEEE Trans. Commun.*, June 1996.
70. H.H. Chan, J.M.H. Elmirghani, and R.A. Cryan, "An Equalisation Technique for Indoor IR Wireless LANs," *Microwave and Optical Technology Letters*, Vol. 10, No. 4, pp.235-238, NOV. 1995.
71. Paule A Lynn, "An introduction to the analysis and processing of signals," Third edition, Macmillan, 1989.
72. Emmanuel C. Ifeakor and Barrie W. Jervis, "Digital signal processing," Addison-Wesley, 1993.
73. J.Y. Hui, "Pattern code modulation and optical decoding - A novel code division multiplexing technique for multifiber networks," *IEEE J. Select. Areas Commun.*, vol. SAC-3, pp. 916-927, NOV. 1985.
74. A. Salehi, "Code division multiple-access techniques in optical fiber networks - part I: Fundamental principles," *IEEE Trans. on Commun*, vol. 37, No. 8, pp. 824-833, Aug. 1989.
75. A.W. Lam and A.M. Hussian, "Performance analysis of direct-detection optical CDMA communication system with avalanche photodiodes," *IEEE Trans. Commun.*, vol. COM-40, pp. 810-820, Apr. 1992.
76. N. Fujimoto, H. Rokvgawa, K. Yamaguch, S. Masuda and S. Yamakoshi, "Photonic Highway: borad-band ring subscriber loops using optical signal processing," *J. Lightwave Technol.*, vol. 7, No. 11, pp1798-1805, 1989.
77. H.H. Chan, J.M.H. Elmirghani, and R.A. Cryan, "Performance Analysis of Indoor Infrared Wireless Networks Utilising PPM CDMA," *IEEE Proc. The Internation Conference on Communications Systems*, Dallas, Texas USA, vol. 3/3, pp. 1467-1471, June 1996 (ICC'96).
78. J.M.H. Elmirghani and R.A. Cryan, "Hybrid PPM-CDMA systems utilizing optical orthogonal codes for indoor wireless infrared communication," *Microwave and Optical Technology Lett.*, vol. 8, No 1, pp. 44-47, January 1995.

79. K.S. Gihousen, I.M. Jacobs, R. Padovani, A.J. Viterbi, L.A. Weaver and C.E. Wheatley, "On the capacity of a cellular CDMA system," IEEE Trans. Veh. Technol., vol. 40, No. 2, pp-303-312, May 1991.
80. R. Steele, "Mobile radio communications," Pentech Press, London, 1992.
81. P.R. Prucnal, M.A. Santoro and T. R. Fan, "Spread spectrum fiber-optic local area network using optical processing," J. Lightwave Technol., vol. LT-4, pp. 547-554, May 1986.
82. A. S. Holmes and R. R. A. Syms, "All-optical CDMA using Quasi-prime codes," J. Lightwave Technol., vol. 10, No. 2, pp. 279-286, Feb. 1992.
83. Chung, J.A. Salehi and V.K. Wei, "Optical Orthogonal Codes: Design, Analysis, and Applications," IEEE Trans. on Infor. Theory, vol. 35, No. 3, pp.595-604, May 1989.
84. K. C. Ravindranathan and A. Selvarajan, "Code generation paradigms on optical orthogonal and other codes in a fiber optic CDMA LAN," J. of Scientific & Industrial Research, vol. 54, pp. 19-23, Jan. 1995.
85. C. Yang and W. C. Kwong, "Performance analysis of optical CDMA with prime codes," Electronics Letters, vol. 31, No. 7, pp. 569-570, March 1995.
86. J.M.H. Elmirghani, H.H. Chan, and R.A. Cryan, "Sensitivity evaluation of optical wireless PPM systems utilising PIN-BJT receives" IEE Proc. Pt. J., vol. 143, No. 6, pp. 355-359, Dec. 1996.
87. A. Salehi and C.A. Brackett, "Code division multiple-access techniques in optical fiber networks - part II: Systems performance analysis," IEEE Trans. on Commun, vol. 37, No. 8, pp. 834-842, Aug. 1989.
88. S.V. Maric, Z.I. Kostic and E.L. Titlebaum, "A New Family of Optical Code Sequences for use in Spread-Spectrum Fiber-Optic Local Area Networks," IEEE Trans. on Commun., vol. 41, No. 8, pp. 1217-1221, Aug. 1993.
89. C.L. Ho and C.Y. Wu, "Performance Analysis of CDMA Optical Communication Systems with Avalanche Photodiodes," IEEE J. of Lightwave Techn., vol. 12, No. 6, pp. 1062-1072, June 1994.
90. J.G. Zhang, W.C. Kwong and A.BV. Sharma, "Experiments on high speed all optical code division multiplexing (CDM) systems using a 2^n prime code," International Conference on Communication vol. 3, pp. 1294-1298, Atlanta USA, June 1998.
91. J.G. Zhang, W.C. Kwong and A.BV. Sharma, "All-optical 2^n extended prime codes for optical fiber code division multiple access applications," International Conference on Communication vol. 2, pp. 926-930, Atlanta USA, June 1998.

Appendix 1:

Background noise measurement results

Receiver Location	Ambient Noise (μW)
r111	454
r121	17.68
r131	454
r141	17.68
r211	17.68
r221	1.42
r231	17.68
r241	1.42

Table App1-1 Ambient noise in test room A

Receiver Location	Ambient Noise (μW)
r111	48.15
r121	48.19
r131	48.19
r141	48.15
r211	48.19
r221	48.23
r231	48.23
r241	48.19
r311	48.19
r321	48.23
r331	48.23
r341	48.19
r411	48.15
r421	48.19
r431	48.19
r441	48.15

Table App1-2 Ambient noise in test room B

Appendix 2:

PIN BJT receiver component values and circuit model

Appendix 2.1 Receiver circuit component values

R1	1k	Rf	7.5k
R2	7.5k	C1	0.1u
R3	1.8k	C2	0.1
R4	2.2k	C3	0.22
R5	240	Q1	BFR 520
R6	2.2k	Q2	BFR 520
R7	240	Q3	BFR 520
		PIN	

Table App2-1: Receiver components value

Appendix 2.2 Pspice simulation program for receiver bandwidth

```
Receiver circuit design
Vcc 1 0 5v
V1 11 3 sin(0 0.1 1000000 0 0)
R1 1 2 1k
R2 3 0 7.5K
R3 5 0 1.8k
R4 7 0 2.2k
R5 6 1 240
Rf 8 4 7.5k
R6 8 0 2.2k
R7 9 1 240
C1 3 4 0.1u
C2 5 2 0.1u
Cd 2 3 35p
C3 7 0 0.22u
* C B E
Q1 1 4 5 BFR520
Q2 6 5 7 BFR520
Q3 9 6 8 BFR520
.MODEL BFR520 NPN(BF=220.1 RB=10 RE=0.7753 RC=2.210 CJC=447.6f
+ CJE=1.245p MJC=0.07051 VJC=0.1892 TF=8.616p VTF=1.414 XTF=6.788
+ IKF=0.51 VAF=48.06 VAR=1.692 IS=1.016f NF=1 ISE=283f NE=2.035
BR=100.7
+NR=0.9881 IKR=2.352m ISC=24.48a NC=1.022 IRB=1.0u RBM=10 EG=1.11E
+XTI=3 VJE=0.6 MJE=0.2581 ITF=0.1103 PTF=45.01deg XCJC=0.13 TR=543.7p
+VJS=0.75 FC=0.7802)
```



```
.PROBE
.tran 100.000p 5.000u 0 0 ;
.END
```

Appendix 2.3 Pspice simulation program for receiver noises

Receiver circuit design

```
Vcc 1 0 5v
Iin 2 3 AC 1u
R1 1 2 1k
R2 3 0 7.5K
R3 5 0 1.8k
R4 7 0 2.2k
R5 6 1 240
Rf 8 4 7.5k
R6 8 0 2.2k
R7 9 1 240
C1 3 4 0.1u
C2 5 2 0.1u
Cd 2 3 35p
C3 7 0 0.22u
* C B E
Q1 1 4 5 BFR520
Q2 6 5 7 BFR520
Q3 9 6 8 BFR520
.MODEL BFR520 NPN(BF=220.1 RB=10 RE=0.7753 RC=2.210 CJC=447.6f
+ CJE=1.245p MJC=0.07051 VJC=0.1892 TF=8.616p VTF=1.414 XTF=6.788
+ IKF=0.51 VAF=48.06 VAR=1.692 IS=1.016f NF=1 ISE=283f NE=2.035
BR=100.7
+NR=0.9881 IKR=2.352m ISC=24.48a NC=1.022 IRB=1.0u RBM=10 EG=1.11E
+XTI=3 VJE=0.6 MJE=0.2581 ITF=0.1103 PTF=45.01deg XCJC=0.13 TR=543.7p
+VJS=0.75 FC=0.7802)
.PROBE
.NOISE V(3) IIN 10;
.AC DEC 10 100k 1.0G
.END
```

Appendix 2.4 BFR 520 transistor data sheet

NPN 9 GHz wideband transistor

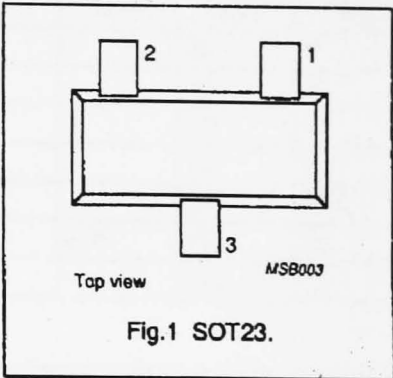


FEATURES

- High power gain
- Low noise figure
- High transition frequency
- Gold metalization ensures excellent reliability.

PINNING

PIN	DESCRIPTION
Code: N28	
1	base
2	emitter
3	collector



DESCRIPTION

The BFR520 is an npn silicon planar epitaxial transistor, intended for applications in the RF frontend in wideband applications in the GHz range, such as analog and digital cellular telephones, cordless telephones (CT1, CT2, DECT, etc.), radar detectors, pagers and satellite TV tuners (SATV) and repeater amplifiers in fibre-optic systems.

The transistor is encapsulated in a plastic SOT23 envelope.

QUICK REFERENCE DATA

SYMBOL	PARAMETER	CONDITIONS	MIN.	TYP.	MAX.	UNIT
V_{CBO}	collector-base voltage		—	—	20	V
V_{CES}	collector-emitter voltage	$R_{BE} = 0$	—	—	15	V
I_C	DC collector current		—	—	70	mA
P_{tot}	total power dissipation	up to $T_s = 72\text{ }^{\circ}\text{C}$ (note 1)	—	—	300	mW
h_{FE}	DC current gain	$I_C = 20\text{ mA}$; $V_{CE} = 6\text{ V}$	60	120	250	
C_{re}	feedback capacitance	$I_C = I_e = 0$; $V_{CB} = 6\text{ V}$; $f = 1\text{ MHz}$	—	0.4	—	pF
f_T	transition frequency	$I_C = 20\text{ mA}$; $V_{CE} = 6\text{ V}$; $f = 1\text{ GHz}$	—	9	—	GHz
G_{UM}	maximum unilateral power gain	$I_C = 20\text{ mA}$; $V_{CE} = 6\text{ V}$; $T_{amb} = 25\text{ }^{\circ}\text{C}$; $f = 900\text{ MHz}$	—	15	—	dB
		$I_C = 20\text{ mA}$; $V_{CE} = 6\text{ V}$; $T_{amb} = 25\text{ }^{\circ}\text{C}$; $f = 2\text{ GHz}$	—	9	—	dB
$ S_{21} ^2$	insertion power gain	$I_C = 20\text{ mA}$; $V_{CE} = 6\text{ V}$; $T_{amb} = 25\text{ }^{\circ}\text{C}$; $f = 900\text{ MHz}$	13	14	—	dB
F	noise figure	$\Gamma_s = \Gamma_{opt}$; $I_C = 5\text{ mA}$; $V_{CE} = 6\text{ V}$; $T_{amb} = 25\text{ }^{\circ}\text{C}$; $f = 900\text{ MHz}$	—	1.1	1.6	dB
		$\Gamma_s = \Gamma_{opt}$; $I_C = 20\text{ mA}$; $V_{CE} = 6\text{ V}$; $T_{amb} = 25\text{ }^{\circ}\text{C}$; $f = 900\text{ MHz}$	—	1.6	2.1	dB
		$\Gamma_s = \Gamma_{opt}$; $I_C = 5\text{ mA}$; $V_{CE} = 8\text{ V}$; $T_{amb} = 25\text{ }^{\circ}\text{C}$; $f = 2\text{ GHz}$	—	1.9	—	dB

Note

1. T_s is the temperature at the soldering point of the collector tab.

LIMITING VALUES

In accordance with the Absolute Maximum System (IEC 134).

SYMBOL	PARAMETER	CONDITIONS	MIN.	MAX.	UNIT
V_{CBO}	collector-base voltage	open emitter	–	20	V
V_{CES}	collector-emitter voltage	$R_{\theta E} = 0$	–	15	V
V_{EBO}	emitter-base voltage	open collector	–	2.5	V
I_C	DC collector current		–	70	mA
P_{tot}	total power dissipation	up to $T_s = 72\text{ °C}$ (note 1)	–	300	mW
T_{stg}	storage temperature		–65	150	°C
T_j	junction temperature		–	150	°C

THERMAL RESISTANCE

SYMBOL	PARAMETER	THERMAL RESISTANCE
$R_{th\ j-s}$	from junction to soldering point (note 1)	260 K/W

Note

1. T_s is the temperature at the soldering point of the collector tab.

CHARACTERISTICS

$T_j = 25\text{ °C}$ unless otherwise specified.

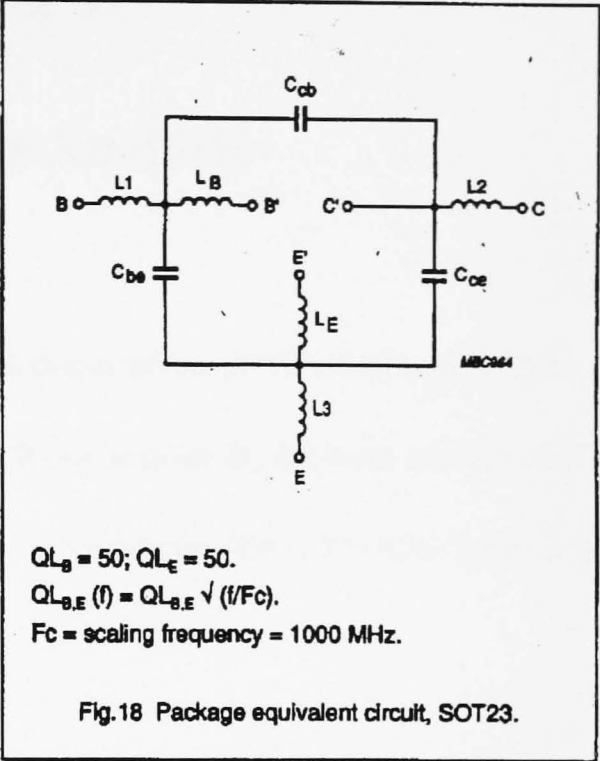
SYMBOL	PARAMETER	CONDITIONS	MIN.	TYP.	MAX.	UNIT
I_{CBO}	collector cut-off current	$I_E = 0; V_{CB} = 6\text{ V}$	–	–	50	nA
h_{FE}	DC current gain	$I_C = 20\text{ mA}; V_{CE} = 6\text{ V}$	60	120	250	
C_e	emitter capacitance	$I_C = I_E = 0; V_{EB} = 0.5\text{ V}; f = 1\text{ MHz}$	–	1	–	pF
C_o	collector capacitance	$I_E = I_C = 0; V_{CB} = 6\text{ V}; f = 1\text{ MHz}$	–	0.5	–	pF
C_{fb}	feedback capacitance	$I_C = 0; V_{CB} = 6\text{ V}; f = 1\text{ MHz}$	–	0.4	–	pF
f_T	transition frequency	$I_C = 20\text{ mA}; V_{CE} = 6\text{ V}; f = 1\text{ GHz}$	–	9	–	GHz
G_{UM}	maximum unilateral power gain (note 1)	$I_C = 20\text{ mA}; V_{CE} = 6\text{ V}; T_{amb} = 25\text{ °C}; f = 900\text{ MHz}$	–	15	–	dB
		$I_C = 20\text{ mA}; V_{CE} = 6\text{ V}; T_{amb} = 25\text{ °C}; f = 2\text{ GHz}$	–	9	–	dB
$ S_{21} ^2$	insertion power gain	$I_C = 20\text{ mA}; V_{CE} = 6\text{ V}; T_{amb} = 25\text{ °C}; f = 900\text{ MHz}$	13	14	–	dB
F	noise figure	$\Gamma_s = \Gamma_{opt}; I_C = 5\text{ mA}; V_{CE} = 6\text{ V}; T_{amb} = 25\text{ °C}; f = 900\text{ MHz}$	–	1.1	1.6	dB
		$\Gamma_s = \Gamma_{opt}; I_C = 20\text{ mA}; V_{CE} = 6\text{ V}; T_{amb} = 25\text{ °C}; f = 900\text{ MHz}$	–	1.6	2.1	dB
		$\Gamma_s = \Gamma_{opt}; I_C = 5\text{ mA}; V_{CE} = 6\text{ V}; T_{amb} = 25\text{ °C}; f = 2\text{ GHz}$	–	1.9	–	dB
P_{L1}	output power at 1 dB gain compression	$I_C = 20\text{ mA}; V_{CE} = 6\text{ V}; R_L = 50\text{ }\Omega; T_{amb} = 25\text{ °C}; f = 900\text{ MHz}$	–	17	–	dBm
ITO	third order intercept point	note 2	–	26	–	dBm

Notes

1. G_{UM} is the maximum unilateral power gain, assuming S_{12} is zero and $G_{UM} = 10 \log \frac{|S_{21}|^2}{(1 - |S_{11}|^2)(1 - |S_{22}|^2)}$ dB.
2. $I_C = 20\text{ mA}; V_{CE} = 6\text{ V}; R_L = 50\text{ }\Omega; T_{amb} = 25\text{ °C}; f_p = 900\text{ MHz}; f_q = 902\text{ MHz};$
measured at $f_{(2p-q)} = 898\text{ MHz}$ and $f_{(2q-p)} = 904\text{ MHz}.$

SPICE parameters for BFR520 crystal

1	IS = 1.016	fA
2	BF = 220.1	-
3	NF = 1.000	-
4	VAF = 48.06	V
5	IKF = 510.0	mA
6	ISE = 283.0	fA
7	NE = 2.035	-
8	BR = 100.7	-
9	NR = 988.1	m
10	VAR = 1.692	V
11	IKR = 2.352	mA
12	ISC = 24.48	αA
13	NC = 1.022	-
14	RB = 10.00	Ω
15	IRB = 1.000	μA
16	RBM = 10.00	Ω
17	RE = 775.3	mΩ
18	RC = 2.210	Ω
19 (note 1)	XTB = 0.000	-
20 (note 1)	EG = 1.110	EV
21 (note 1)	XTI = 3.000	-
22	CJE = 1.245	pF
23	VJE = 600.0	mV
24	MJE = 258.1	m
25	TF = 8.616	ps
26	XTF = 6.788	-
27	VTF = 1.414	V
28	ITF = 110.3	mA
29	PTF = 45.01	deg
30	CJC = 447.6	fF
31	VJC = 189.2	mV
32	MJC = 70.51	m
33	XCJC = 130.0	m
34	TR = 543.7	ps
35 (note 1)	CJS = 0.000	F
36 (note 1)	VJS = 750.0	mV
37 (note 1)	MJS = 0.000	-
38	FC = 780.2	m



List of components (see Fig.18)

DESIGNATION	VALUE
C _{be}	71 fF
C _{cb}	71 fF
C _{ce}	2 fF
L1	0.35 nH
L2	0.17 nH
L3	0.35 nH
L _B	0.40 nH
L _E	0.83 nH

Note

1. These parameters have not been extracted, the default values are shown.

Appendix 3:

Receiver Noise Analysis

The receiver circuit was shown in Fig. 4.5. The major noise sources associated with this circuit are the thermal noise due to the feedback resistor R_f , the base current shot noise, the collector current shot noise, and the thermal noise due to the base spreading resistance r'_{bb1} .

The shot noise of the base current is modelled as an equivalent shunt current source with a noise current spectral density given by

$$S_{ib1} = 2 q I_{b1} \quad (\text{App3-1})$$

Using the referred impedance method of Hullet and Muoi [55], then the thermal noise of the feedback resistor can also be modelled as an equivalent shunt current source

$$S_{R_f} = \frac{4kT}{R_f} \quad (\text{App3-2})$$

The noise associated with the base spreading resistance is modelled as a series voltage noise generator with a noise voltage spectral density $4KT r'_{bb1}$. Referring this to the input node as an equivalent current source

$$\begin{aligned}
S_{r_{bb}'} &= 4KT r_{bb1}' \left(\frac{1}{R_{in}^2} + (\omega C_1)^2 \right) \\
&= \frac{4KT r_{bb1}'}{R_{in}^2} + 4KT r_{bb1}' (2\pi f C_1)^2
\end{aligned}
\tag{App3-3}$$

where R_{in} is the input resistance

$$\begin{aligned}
R_{in} &= (1 + \beta)R_3 // R_2 // \frac{R_f}{(1 + A_{vcl})} \\
&= \frac{\frac{(1 + \beta)R_2 R_3}{(1 + \beta)R_3 + R_2} \frac{R_f}{(1 + A_{vcl})}}{\frac{(1 + \beta)R_2 R_3}{(1 + \beta)R_3 + R_2} + \frac{R_f}{(1 + A_{vcl})}}
\end{aligned}
\tag{App3-4}$$

and

$$C_1 = C_s + C_d + C_f \tag{App3-5}$$

The shot noise of the collector current is modelled as a shunt current source at the output with current spectral density $2qI_c$. This can be referred to the input as a series voltage source by dividing by g_m^2 and then converted to an input equivalent shunt current source by multiplying by $|Y_{in}|^2$ to give

$$S_{I_{c1}} = \frac{2qI_{c1}}{g_{m1}^2} \left[\left(\frac{1}{R_f} + \frac{1}{r_{\pi1}} + \frac{1}{R_2} \right)^2 + (\omega C_T)^2 \right] \tag{App3-6}$$

where $\omega = 2\pi f$

$$S_{I_{c1}} = \frac{2qI_{c1}}{g_{m1}^2} \left[\left(\frac{1}{R_f} + \frac{1}{r_{\pi1}} + \frac{1}{R_2} \right)^2 + (2\pi f C_T)^2 \right] \quad (\text{App3-7})$$

The preamplifier overall noise is

$$S(f) = S_{I_{b1}} + S_{I_{c1}} + S_{R_f} + S_{r_{bb}}, \quad (\text{App3-8})$$

Hence

$$S(f) = 2qI_{b1} + \frac{4KT}{R_f} + \frac{2qI_{c1}}{g_{m1}^2} \left[\frac{1}{R_f} + \frac{1}{r_{\pi1}} + \frac{1}{R_2} \right]^2 + \frac{4KT r'_{bb1}}{R_{in}^2} \\ + \frac{2qI_{c1}}{g_{m1}^2} \{2\pi f C_T\}^2 + 4KT r_{bb1} \{2\pi f C_1\}^2 \quad (\text{App3-9})$$

Appendix 4:

Matched filter transfer function assuming a Gaussian pulse shape

The incident pulse shape is given by

$$h_p(t) = \frac{1}{\alpha\sqrt{2\pi}} e^{-\frac{t^2}{2\alpha^2}} \quad (\text{App4-1})$$

Therefore the filter response is given by

$$G(f) = \int_{-\infty}^{\infty} h(t) e^{-j2\pi ft} dt \quad (\text{App4-2})$$

$$G(f) = \int_{-\infty}^{\infty} \frac{1}{\alpha\sqrt{2\pi}} e^{-\frac{t^2}{2\alpha^2}} e^{-j2\pi ft} dt \quad (\text{App4-3})$$

$$G(f) = \frac{1}{\alpha\sqrt{2\pi}} \int_{-\infty}^{\infty} e^{-\frac{t^2}{2\alpha^2} - j2\pi ft} dt \quad (\text{App4-4})$$

$$G(f) = \frac{1}{\alpha\sqrt{2\pi}} \int_{-\infty}^{\infty} e^{-\frac{1}{2\alpha^2}(t^2 + j4\pi\alpha^2 ft)} dt \quad (\text{App4-5})$$

$$\begin{aligned} t^2 + j4\pi\alpha^2 ft &= t^2 + 4j\pi\alpha^2 ft - 4\pi^2\alpha^4 f^2 + 4\pi^2\alpha^4 f^2 \\ &= (t + j2\pi\alpha^2 f)^2 + 4\pi^2\alpha^2 f^2 \end{aligned} \quad (\text{App4-6})$$

$$G(f) = \frac{1}{\alpha\sqrt{2\pi}} \int_{-\infty}^{\infty} e^{-\frac{1}{2\alpha^2}((t + j2\pi\alpha^2 f)^2 + 4\pi^2\alpha^4 f^2)} dt \quad (\text{App4-7})$$

$$G(f) = \frac{1}{\alpha\sqrt{2\pi}} \int_{-\infty}^{\infty} e^{-\frac{1}{2\alpha^2}((t + j2\pi\alpha^2 f)^2)} e^{-\frac{4\pi^2\alpha^4 f^2}{2\alpha^2}} dt \quad (\text{App4-8})$$

$$G(f) = \frac{1}{\alpha\sqrt{2\pi}} e^{-2\pi^2\alpha^2 f^2} \int_{-\infty}^{\infty} e^{-\left(\frac{1}{2\alpha^2}\right)^2 (t + j2\pi\alpha^2 f)^2} dt \quad (\text{App4-9})$$

Let $x = t + j2\pi\alpha^2 f^2$ then $dx = dt$

$$G(f) = \frac{1}{\alpha\sqrt{2\pi}} e^{-2\pi^2\alpha^2 f^2} \int_{-\infty}^{\infty} e^{-\left(\frac{1}{2\alpha^2}\right)^2 x^2} dx \quad (\text{App4-10})$$

However

$$\int_{-\infty}^{\infty} e^{-q^2 x^2} dx = \frac{\sqrt{\pi}}{q} \quad (\text{App4-11})$$

from equation (App4-10) $q = \frac{1}{\sqrt{2}\alpha}$

Therefore the matched filter response is given by

$$G(f) = \frac{1}{\alpha\sqrt{2\pi}} e^{-2\pi^2\alpha^2 f^2} \frac{\sqrt{\pi}}{\frac{1}{\sqrt{2}\alpha}} \quad (\text{App4-12})$$

$$G(f) = e^{-2\pi^2\alpha^2 f^2} = e^{-\frac{\omega^2\alpha^2}{2}} \quad (\text{App4-13})$$

Appendix 5:

Derivation of the output signal current of the matched filter assuming a Gaussian pulse shape

The output signal current of the matched filter is given by

$$i(t) = b \eta q \int_{-\infty}^{\infty} G(f) G(f) e^{2j\pi f t} df \quad (\text{App5-1})$$

Where $G(f) = e^{-\left(\frac{\omega^2 \alpha^2}{2}\right)}$

$$i(t) = b \eta q \int_{-\infty}^{\infty} \left(e^{-\frac{4\pi^2 f^2 \alpha^2}{2}} \right)^2 e^{2j\pi f t} df \quad (\text{App5-2})$$

$$i(t) = b \eta q \int_{-\infty}^{\infty} e^{-4\pi^2 f^2 \alpha^2} e^{2j\pi f t} df \quad (\text{App5-3})$$

$$i(t) = b \eta q \int_{-\infty}^{\infty} e^{-4\pi^2 \alpha^2 \left(f^2 - \frac{2j\pi f t}{4\pi^2 \alpha^2} \right)} df \quad (\text{App5-4})$$

where $f^2 - \frac{j2\pi f t}{4\pi^2 \alpha^2} = \left(f - \frac{j\pi t}{4\pi^2 \alpha^2} \right)^2 - \frac{j^2 \pi^2 t^2}{16\pi^4 \alpha^4}$

$$i(t) = b \eta q \int_{-\infty}^{\infty} e^{-4\pi^2 \alpha^2 \left(\left(f - \frac{j\pi t}{4\pi^2 \alpha^2} \right)^2 - \frac{j^2 \pi^2 t^2}{16\pi^4 \alpha^4} \right)} df \tag{App5-5}$$

$$i(t) = b \eta q \int_{-\infty}^{\infty} e^{-4\pi^2 \alpha^2 \left(f - \frac{j\pi t}{4\pi^2 \alpha^2} \right)^2} e^{\frac{j^2 \pi^2 t^2}{16\pi^4 \alpha^4}} df \tag{App5-6}$$

$$i(t) = b \eta q e^{-\frac{t^2}{4\alpha^2}} \int_{-\infty}^{\infty} e^{-(2\pi\alpha)^2 \left(f - \frac{j\pi t}{4\alpha^2 \pi^2} \right)^2} df \tag{App5-7}$$

$$\text{let } x = f - \frac{j\pi t}{4\alpha^2 \pi^2} \text{ therefore } df = dx$$

$$i(t) = b \eta q e^{-\frac{t^2}{4\alpha^2}} \int_{-\infty}^{\infty} e^{-a^2 x^2} df \tag{App5-8}$$

$$\text{where } a = 2\pi\alpha \text{ and } \int_{-\infty}^{\infty} e^{-a^2 x^2} dx = \frac{\sqrt{\pi}}{a}$$

$$i(t) = b \eta q e^{-\frac{t^2}{4\alpha^2}} \frac{\sqrt{\pi}}{2\pi\alpha} \tag{App 5-9}$$

$$i(t) = b \eta q \frac{e^{-\frac{t^2}{4\alpha^2}}}{2\sqrt{\pi}\alpha} \tag{App5-10}$$

Appendix 6:

Noise equivalent bandwidth of the receiver assuming a Gaussian pulse shape

The noise current on the output of the matched filter is given by

$$N_o = \frac{1}{2\pi} \int_{-\infty}^{\infty} S_o |G(\omega)|^2 d\omega \quad (\text{App6-1})$$

where $G(\omega) = e^{-\frac{(\alpha\omega)^2}{2}}$

$$\begin{aligned} N_o &= \frac{S_o}{2\pi} \int_{-\infty}^{\infty} e^{-\left(\frac{\alpha^2\omega^2}{2}\right)} d\omega \\ &= \frac{S_o}{2\pi} \int_{-\infty}^{\infty} e^{-\alpha^2\omega^2} d\omega \end{aligned} \quad (\text{App6-2})$$

but

$$\int e^{-q^2x^2} dx = \frac{\sqrt{\pi}}{q} \quad (\text{App6-3})$$

Therefore

$$N_o = \frac{S_o}{2\pi} \frac{\sqrt{\pi}}{\alpha} = \frac{S_o}{2\sqrt{\pi}\alpha}$$

(App6-4)